SYNTHESIS AND PROPERTIES OF MAGNETORHEOLOGICAL (MR) FLUIDS

by

Seval Genç

B.S. in Physics Education, Marmara University, Turkey, 1991

M.S. in Physics, Bogazici University, Turkey, 1994

Submitted to the Graduate Faculty

of School of Engineering in partial fulfillment

of the requirements for the degree of

Doctor of Philosophy

University of Pittsburgh

2002

UNIVERSITY OF PITTSBURGH

SCHOOL OF ENGINEERING

This dissertation was presented

by

Seval Genç

It was defended 0n

July 18, 2002

and approved by

Dr. Donald J. Plazek, Professor, Materials Science and Engineering

Dr. Ian Nettleship, Associate Profeesor, Materials Science and Engineering

Dr. Nicholas Eror, Professor, Materials Science and Engineering

Dr. William W. Clark, Associate Profeesor, Mechanical Engineering

Dr. John M. Ginder, Ford Motor Company

Dr. Pradeep P. Phulé (Dissertation Director), Professor, Materials Science and Engineering

ABSTRACT

Seval Genç

University of Pittsburgh, 2002

SYNTHESIS AND PROPERTIES OF MAGNETORHEOLOGICAL (MR) FLUIDS:

Magnetorheological (MR) fluids are dispersions of fine (~ 0.05-10 μm) magnetically soft, multi-domain particles. The apparent yield strength of these fluids can be changed significantly within milliseconds by the application of an external magnetic field. MR fluid devices are being used and developed for shock absorbers, clutches, brakes, and seismic dampers. The major goals of this research were to advance the science of MR fluids. More specifically, the goals were: (a) influence of interparticle forces on stability and redispersibility of MR fluids and (b) factors affecting the "on" and "off" state rheological properties of MR fluids. In first part, the influence of the remnant magnetization ($\mu_0 M_r$) of soft magnetic particulates on the redispersibility of MR fluids was investigated. The ratio of magnetic dipole interaction energies to thermal energy (V_{mag}/k_BT) for 33 vol% iron based MR fluids (average particle size ~6μm), manganese zinc ferrite (average particle size ~2.3μm) and nickel zinc ferrite (average particle size ~2.1μm) were calculated as -161000, -6400, and -3900. Our calculations showed that even small levels of remnant magnetization levels in the magnetic particles introduce significant dipole-dipole interparticle interactions. These can lead MR fluids to show a tendency to undergo agglomeration. The second part of this study was concerned with the magnetic properties of the dispersed phase and "on-state" rheological behavior. The effects of dispersed phase saturation magnetization ($\mu_0 M_s$) and applied magnetic fields (H) on the "on-state" apparent yield stress of

MR fluids was investigated. Rheological measurements were conducted on MR fluids based on two different grades of carbonyl iron powder. Grade A (average size 7-9μm, $\mu_0 M_s \sim 2.03$T) and Grade B (average size ~2μm, $\mu_0 M_s \sim 1.89$T). The yield stresses of 33 and 40 vol% Grade A were 100 ± 3 and 124 ± 3 kPa, respectively at 0.8 ± 0.1T. The yield stress values of MR fluids were based on finer particles (Grade B) were consistently smaller. For example, the yield stresses for 33 and 40 vol% Grade B based MR fluid were 80 ± 8 and 102 ± 2 kPa respectively at 0.8 ± 0.1T. These experimental results were in good agreement with the analytical models developed by Ginder and co-workers. The decrease in the apparent yield strength of MR fluids based on smaller particles was attributed to the smaller saturation magnetization of these particles.

The third part of this research was directed to better elucidate the "off-state" rheological behavior of MR fluids. MR fluids composed of 40 vol% Grade B and 100 cSt silicone oil exhibited shear thinning behavior with a viscosity of 199±52 and 1.9±0.3 Pa-s at a shear rate of 0.1 and 100 s^{-1} respectively at 25 ^{0}C. One of the major findings of this study was establishment the existence a measurement of a critical yield *strain*. The creep-recovery measurements revealed multiple yielding in the MR fluid where the first yield strain occurred between 0.01 and 0.02 strain values at stress levels between 10-120 Pa and the second yielding occurred at larger strains ranging from 0.08-20. This research shows that rheologically MR fluids exhibit a time and shear dependent behavior. Further research is needed to fully understand the rheological behavior of these complex materials. The effects of resting and shearing periods on the yielding were also investigated. Finally, in an effort to address issues concerning durability of MR fluids, the effect of exposing MR fluids to higher temperatures was investigated. MR fluids were exposed to high temperatures (175 ^{0}C) for 24 hours. The "on" state apparent yield stress did not show any decrease, however the "off" state apparent viscosity showed an increase at shear rates

> 15 s^{-1}. The viscosity at a shear rate of $50s^{-1}$ was 3.9 Pa-s and the yield strain increased ~10 times the first yield strain observed in the MR fluids without heat treatment.

DESCRIPTORS

Coercivity	Magnetic Interaction Energy
Redispersiblity	Remnant Magnetization
Rheology	Rheometry
Shear Thinning	Soft Magnetic Materials
Thixotropy	van der Waals Energy
Yield Strain	Yield Stress

ACKNOWLEDGEMENTS

I wish to thank my dissertation advisor, Dr. Pradeep P. Phulé, for his patience, guidance, and encouragement throughout this thesis. I am grateful Dr. Donald J. Plazek for all his help, interest and discussions. This thesis was made possible with all their help.

I would like to thank my committee members; Dr. N. Eror, Dr. I. Nettleship, Dr. W. Clark, and Dr. Ginder from Ford Motor Company for their interest and discussions.

I would like to acknowledge Marmara University, School of Engineering for the financial support and Dr. Omer Z. Cebeci for all his help and support.

University of Pittsburgh, Department of Mechanical Engineering is also acknowledged for letting us use their TA Rheometer.

I am thankful to Dr. Deepa Godbolé for all her help, support, assistance and friendship. Sincere gratitude is also extended to George McManus, Al Stewart, Seunghyun Ra, Heather Shirey for their help and support.

Partial financial support for this research was provided by the National Science Foundation (NSF) through grant CMS 9817578. This support is also acknowledged.

I want to dedicate this work to my mother Elcin and my father Ugur and my sisters Sibel and Selin for their inspiration, patience, and encouragement throughout my Ph.D study.

TABLE OF CONTENTS

LIST OF TABLES

Table Number **Page**

LIST OF FIGURES

Figure Number **Page**

1.0 INTRODUCTION

1.1 Magnetorheological Fluids

Magnetorheology is a branch of rheology that deals with the flow and deformation of the materials under an applied magnetic field. The discovery of MR fluids is credited to Jacob Rabinow [1, 2] in 1949. Magnetorheological (MR) fluids are suspensions of non-colloidal (~0.05-10 μm), multi-domain, and magnetically soft particles in organic or aqueous liquids. Many different ceramic metals and alloys have been described and can be used to prepare MR fluids as long as the particles are magnetically multi-domain and exhibit low levels of magnetic coercivity. Particle size, shape, density, particle size distribution, saturation magnetization and coercive field are important characteristics of the magnetically active dispersed phase. Other than magnetic particles, the base fluids, surfactants, anticorrosion additives are important factors that affect the rheological properties, stability and redispersibility of the MR fluid.

In the "off" state, in terms of their consistency, MR fluids appear similar to liquid paints and exhibit comparable levels of apparent viscosity (0.1 to 1 Pa-s at low shear rates) [3]. Their apparent viscosity changes significantly (10^5 - 10^6 times) within a few milliseconds when the magnetic field is applied. The change in the viscosity is completely reversible when the magnetic field is removed. Once the magnetic field is applied, it induces a dipole in each of the magnetic particles.

The inert-particle forces originating from the magnetic interactions lead to a material with higher apparent viscosity. This dipolar interaction is responsible for the chain like formation of the particles in the direction of the field (**Figure 1-1**).

*Parenthetical references superior to the line of text to the bibliography

It is also believed that in addition to magnetic interactions between two particles, the formation of the particles contribute to a certain level to the increase in the apparent viscosity. Particles held together by magnetic field and the chains of the particles resist to a certain level of shear stress without breaking which make them behave like a solid. When this shear stress exceeds a critical value, the structure breaks and the material starts to flow. MR fluid effect is often characterized by Bingham Plastic model which will be discussed in the proceeding sections in this thesis [4]. The critical value of the shear stress necessary to break the structure is the "apparent yield stress" of the material. Phulé and Ginder reported a yield stress of ~100 kPa at a flux density of 1 T for 40 vol% Fe based fluids [5]. Weiss and co-workers reported the yield stress of MR fluids with an unknown concentration as 90-100kPa for 30 kOe (3 T) of magnetic field [6]. A table of conversion for magnetic measurements is given in Appendix A.

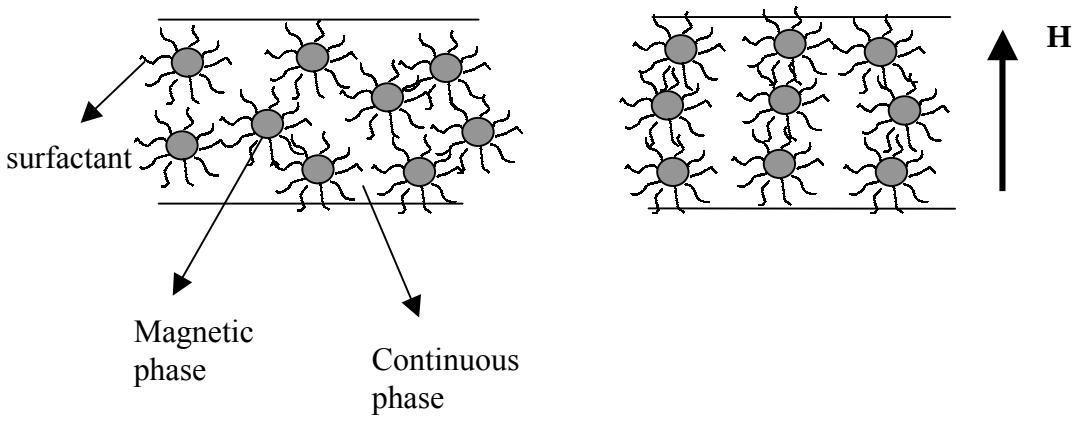

Figure 1.1 Schematic of the formation of chain-like formation of magnetic particles in MR fluids in the direction of an applied magnetic field.

1.2 Electrorheological (ER) Fluids

ER fluids are suspensions of electrically polarizable particles dispersed in an electrically insulating oil [7]. The ER fluid is typically composed of 0.5 to 100 μm particles of cornstarch, silica, barium titanate or semiconductors [8]. For particles such as silica, polyelectrolytes need to be added to cause the adsorption of water onto the particulate material to enhance the ER effect, thus increasing the electrostatic force of attraction between the particles. The water also creates a conductive layer on the surface of the particles in which the ions in the water can drift in response to an electric field [9]. These materials are called extrinsically polarizable materials in which the ER effect results from interfacial polarization. The ER effect decreases as the amount of water absorbed decreases. Therefore, at temperatures of ~50 ^{0}C, the ER activity decreases significantly and thus the temperature instability limits the potential use of the ER fluids. Materials such as ferroelectrics, inorganics, semiconductor polymers, metals, coated conductors and liquid crystals has also been reported as producing water-free ER suspensions [9] and these materials are called intrinsically polarizable materials and they function by bulk polarization or interfacial polarization. They have lower thermal coefficient of yield stress which may help expanding the temperature range of ER activity.

Similar to MR fluids, upon the application of electric field, particles become polarized and the local electric field is distorted. The polarizability of the particles is increased by the migration of the mobile charges to areas with greatest field concentration. This gives rise to larger dipole moments that attract one another and cause the particles to form chain in the direction of the field. ER fluid is characterized by the Bingham Plastic Model in which the change in viscosity from particle chain interactions under shear corresponds to the yield stress. This model will be discussed in Section 2. Weiss and co-workers reported a yield stress value of 3.5 kPa for

4kV/mm of electric field for one of the Lord Corporation's ER fluids (VersaFlo ER 200) [6]. ER fluids were mostly developed for valves, mounts, clutches, brakes, and dampers. However, not much progress has been made in their commercialization.

1.3 Ferrofluids

Ferrofluids also known as magnetic liquids that are colloidal suspensions of ultra-fine (typically 5-10 nm), single domain magnetic particles such as iron oxides (γFe_2O_3, Fe_3O_4), Mn-Zn ferrites [10], Fe and Co in either aqueous or non-aqueous liquids. Since the particle size of the magnetic phase is very small, under ordinary field strengths, thermal agitation gives rise to Brownian forces that can overcome the alignment of the dipoles. Thus, MR fluids are based on ferromagnetic or ferromagnetic particles and ferrofluids are based on superparamagnetic materials. Instead, ferrofluids experience a body force on the entire material that is proportional to the magnetic field gradient. Ferro-fluids exhibit field dependent viscosity but they exhibit no yield stress (τ_y=0) under magnetic fields. Ferro-fluids are used in rotary seals, magnetic bearings, and motor dampers [11, 12]

Another family of the ferrofluids is *inverse* ferrofluids, also known as magnetic holes. These are suspensions of non-magnetic materials that are usually one or more orders of magnitude larger than the magnetic particles in ferrofluids. Therefore, the non-magnetic particles experience a medium that is magnetically continuous [13, 14].

1.4 Comparison of Field Responsive Fluids

More recently MR fluids have gained considerably more attention than their electric analogue electrorheological (ER) fluids which where discovered by Winslow in 1948 [15, 16].

One of the advantages of MR fluids is the higher yield stress value than ER fluids. The reason for having higher yield stress for MR fluids is the higher magnetostatic energy density, $\mu_0 H_0^2$, of MR fluids compared to electrostatic energy density, $\varepsilon_0 E_0^2$ of ER fluids. Low voltage power supplies for MR fluids and relative temperature stability between –40 and +150 ^{0}C make them more attractive materials than ER fluids. Ferrofluids do not exhibit yield stress, but show an increase in the viscosity. The viscosity under an applied magnetic field increases almost twice as much as the viscosity when there is no magnetic field applied. Since ferrofluids are synthesized by colloidal magnetic particles, these fluids are more stable than MR fluids which are based on non-colloidal magnetic particles. The comparison of MR, ER fluids, and ferrofluids is summarized in **Table 1-1.**

Table 1. 1 Comparison of some of the properties of MR, ER and Ferrofluids [17]

	MR Fluids	**ER Fluids**	**Ferrofluids**
Particulate Material	Iron, ferrites, etc	Zeolites, Polymers, SiO_2, $BaTiO_3$	Ceramics, Ferrites, iron, cobalt, etc.
Particle size	0.1-10μm	0.1-10μm	2-10 nm
Suspending fluid	Nonpolar oils, polar liquids, water and other	Oils	Oils, Water
Density (g/cc)	3-5	1-2	1-2
Off viscosity (mPa-s)	100-1000	50-1000	2-500
Required field	~ 3 kOe	3kV/mm	~1 kOe
Field Induced changes	τ_y (B)~100kPa	τ_y (E)~ 10 kPa	$\frac{\Delta\eta(B)}{\eta(0)} \approx 2$
Device excitation	Electromagnets or permanent magnets	High voltage	Permanent magnet

1.5 Applications of MR fluids

In the marketplace today state-of-the-art MR fluids are becoming increasingly important in applications concerning active control of vibrations or torque transfer. Shock absorbers, vibration dampers, seismic vibration dampers, clutches and seals are the most exciting applications of MR fluid [18-21]. For these applications, rheological properties of fluids, working mode of the device, design of the magnetic circuit, flux guide and coil configuration are crucial parameters for the operation of the actuators and devices [22, 23]. One of the most important and recent development in MR fluid applications has been developed by Delphi Automotive Systems. Delphi and Cadillac developed MagneRide^{TM} Semi active Suspension System which adjusts damping levels with the combination of MR fluid based struts and shock absorbers [24].

Optical polishing, which was first initiated by Kordonski and co-workers, is another promising application of MR fluids [25, 26]. MR fluid contains a nonmagnetic polishing abrasive. Under high shear the flow of non-magnetic abrasive particles cause material removal. The most commonly used polishing abrasive/carrier liquid combination for optical polishing for all optical glasses and crystals is cerium oxide/water combination. Abrasives like alumina and diamond are used for materials other than glasses.

The Lord Corporation has currently manufactured MR fluid devices for commercial applications including heavy-duty vehicle seat suspensions, rotary brakes that provide a tunable resistance for exercise equipment and vibration dampers for various industrial applications such as dampers for washing machines [27]. The damper that contains MR fluids for commercial applications such as seat suspensions is presented in **Figure 1-2**.

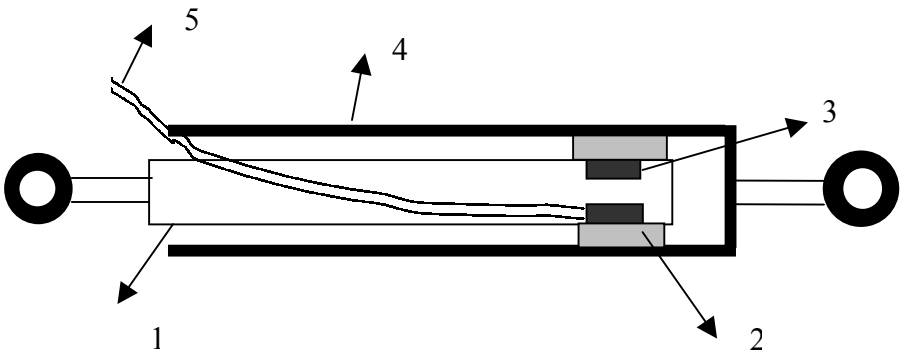

Figure 1. 2 MR fluid damper [13] 1) Plastic shaft, 2) Sponge saturated with MR fluid, 3) Coil, 4) Steel tube, 5) Wire supplying current.

1.6 Challenges in MR Technology

The biggest challenge of MR fluid is to have high turn up ratio, temperature stability and durability. The second biggest challenge of MR fluids is the materials science oriented studies such as surface chemistry, polymer physics, in synthesizing stable and redispersible MR fluids. To our knowledge there are not many systematic published studies on this aspect of MR fluid technology. Making durable MR fluids is also another challenge. There have been temperature studies in determining the yield stress of MR fluids at different temperatures and these studies revealed the temperature stability of MR fluids. However, there are not many studies conducted by exposing the MR fluid to high and low temperatures and high shearing stresses and then conducting experiments at room temperature.

Although the "off-state" viscosity of MR fluids is a crucial parameter for having a high MR effect, it has not been investigated in detail. The rheology of MR fluids in their off state is also worth studying.

1.7 Research Objectives

The overall objective of this research was to initiate and develop materials science based approach for developing MR fluids. Although MR fluids have been investigated thoroughly since they were first discovered, very little research has been performed on the synthesis of stable redispersible and durable MR fluids. More specifically, the objectives of this research were:

A. To investigate the influence of interparticle forces on stability and redispersibility of MR fluids. The influence of remnant magnetization of soft magnetic particulates on the redispersibility of MR fluids is investigated.

B. To investigate the on state rheological properties of MR fluids. The dependence of yield stress on the average particle size and magnetic properties of particles was investigated

C. To investigate the off state, when no magnetic field was applied, rheological properties of MR fluids. There is not much research reported on the off state viscosity of MR fluids. The apparent viscosity of MR fluids was investigated. The yielding properties of MR fluids was investigated by creep-recovery experiments

D. In an effort to address durability of MR fluids, the effect of high temperature exposures for 24 hours on the "on" and "off" state rheological properties of MR fluids was investigated.

1.8 Outline of the Ph.D. Dissertation

The remainder of this dissertation is organized as follows: The theoretical background and literature review concerning the magnetic materials, rheology of suspensions and magnetorheological (MR) fluids, and stability of MR fluids are presented in Section 2.0. Following this, the experimental procedures used in conducting the proposed research are discussed in Section 3.0. The results and discussions of the experiments are presented in Section 4.0 and the conclusion of this research is discussed and summarized in Section 5.0. The last section (Section 6.0) contains suggestions for the future work. The appendices at the end contain unit conversion of magnetic and rheological properties.

2.0 BACKGROUND

2.1 Magnetic Properties of Materials

The magnetization, M is the total magnetic moment of dipoles per unit volume in units of $A.m^2$ per m^3. Magnetic induction or magnetic flux density B is the flux per area expressed in units of Wb/m^2 or Tesla (T). In free space the induction is [28]

$$B = \mu_0 H \tag{2-1}$$

where μ_0 is the permeability of free space (4π x 10^{-7} H/m). If the space is filled with any magnetic substance in which the induced magnetization is $\mu_0 M$, so the total induction becomes [28]

$$B = \mu_0 (H + M) \tag{2-2}$$

Figure 2-1 shows the for B-H and M-H hysteresis curves for ferromagnetic and ferromagnetic materials. The curve with the dash line reaches a constant value of B-Hμ_0 which is B_s. From Equation 2.2 it can be seen that $B_s = M_s \mu_0$.

Magnetic response of various materials is compared with their susceptibility and permeability values **(Table 2-1)**. Susceptibility is defines as [28]

$$\chi = \frac{M}{H} \tag{2.3}$$

and permeability is defined as [28]

$$\mu = \frac{B}{H} \tag{2.4}$$

The ratio between the permeability of the material and the vacuum is called **relative permeability** μ_r and given by μ/μ_0.

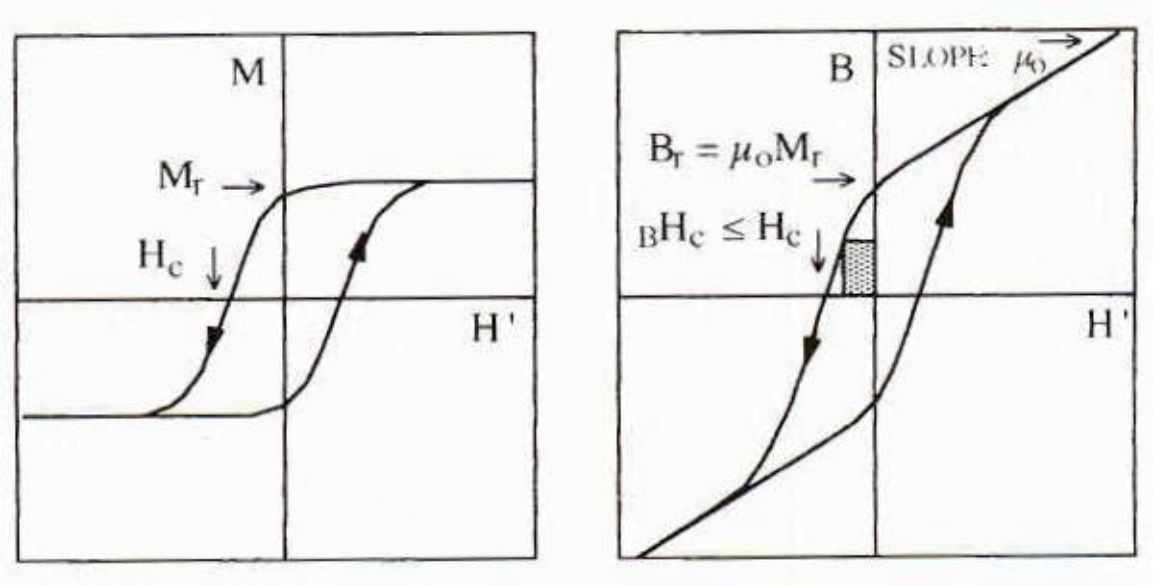

Figure 2. 1Typical hysteresis loops for M-H and B-H curves [29].

Table 2. 1 Comparison between these different kinds of magnetism in terms of susceptibility and relative permeability [30]

	Diamagnetism	*Paramagnetism*	*Ferro- or ferri-magnetism*
Susceptibility, χ	< 0	≥ 0	$>> 0$
Relative permeability, μ	< 1	≥ 1	$>> 1$

2.2 Origin of Magnetism

There are two kinds of electron motion, orbital and spin, and each has a magnetic moment associated with it. The magnetic moment of the atom is the vector sum of all its electronic moments. The magnetic moments of the electrons are oriented in such a way that they cancel each other out and the atom as a whole has no net magnetic moment or the cancellation of the electronic moments occurs partially and the atom is left with a net magnetic moment. According to the electron motion and canceling of the dipoles, magnetic particles take different forms of magnetism.

Diamagnetism exhibits negative magnetization and it is entirely due to the orbital motion of the electrons. Electrons which constitute a closed shell in an atom usually have their spin and orbital moments so oriented that the atoms as a whole has no net moment. Even though a diamagnetic substance composed of atoms which have no net magnetic moment, it reacts to the applied magnetic field in a particular way causing the magnetization to be less than zero. Cu, Ag, Au. Be, Zn, Cd, In, Hg, Pb, and Bi are diamagnetic [28].

Paramagnetism occurs when each atom is carrying a magnetic moment, but the atomic moments point in all directions, therefore generating no net magnetization. The complete disorder of atomic moments occurs because there is no magnetic interaction between neighboring atoms as well as the thermal agitation causing the moments to be aligned randomly. Alkali metals (Li, Na, K and Rb) and all transition metals except Fe, Ni and Co are paramagnetic materials [30].

The magnetization in ferromagnetic materials is caused by the unfilled energy levels in the 3d level. The dipoles easily line up with the applied magnetic fields due to exchange interaction. Ferromagnetism was first postulated by Weiss [31]. His postulate was based on two assumptions:

1) spontaneous magnetization, 2) domains. A ferromagnetic material in the demagnetized state is divided into a number of small regions called domains. Each domain is spontaneously magnetized but the direction of magnetization is such that the magnetic domains cancel out each other and as a result there is no net magnetization. Upon the application of the magnetic field, domain walls start to move and the domains with the magnetization parallel to the applied field grow while the domains not parallel to the field shrink.

Ferrimagnetic materials, like ferromagnetics, consist of self saturated domains. Ferrimagnetism was first credited to Neél. He made the assumption that the exchange force acting between an ion on A site and an ion on B site was negative. Thus, the lattice of A ions was spontaneously magnetized in one direction and the lattice of B ions magnetized in the opposite direction. However the strength of the dipoles is not equal, the magnetic moments do not cancel out each other, and a net magnetization results.

In multi-domain magnetic particles, the magnetization mechanism is controlled by (1) wall motion and (2) rotation, whereas in a single domain material magnetization changes occur through the usually high field process of rotation of the total magnetic moment of the particle. The x-axis shows the applied magnetic field. When the magnetic field is reduced to zero, the magnetization will decrease to a value called **residual magnetization, $\mathbf{M_r}$**. If the applied field is reversed, the magnetization will decrease to zero and the field at this zero magnetization is called **intrinsic coercivity**, $\mathbf{H_c}$.

When there is an applied magnetic field, the material develops a net magnetic moment and this increases the inter-particle magnetic attraction that is known as magnetostatic energy and it is given by [31]

$$U = \frac{-m^2}{4\pi\mu_0 a^3}(3\cos^2\theta - 1) \qquad (2\text{-}5)$$

where **m** is the magnetic dipole, μ_0 is the permeability of the free space ($4\pi*10^{-7}$ H/m) and **a** is the inter-particle separation between particles (**Figure 2-2**). The angle between the dipole moment, **m** and the inter-particle, **a** separation is given by θ. The energy is minimum and attractive when $\theta = 0$ and the particles are in contact. It then follows that [31]

$$U = \frac{-m}{2\pi a^3 \mu_0} \tag{2-6}$$

where in this case **a** is the diameter of the particle. The particles will attract each other only if the coupling constant, λ representing the ratio of dipole-dipole energy to thermal energy, kT, is greater than unity [32].

$$\lambda = \frac{m^2}{4\pi\mu_0 a^3 kT} > 1 \tag{2.7}$$

2.2.1 Soft and Hard Magnetic Materials

Coercivity which is described as the resistance of the material to the magnetization reversal, is the most important criterion for differentiating between a soft and hard magnetic material as well as the energy product B_rH_C, required to demagnetize the magnetic material where B_r is the remnance and H_c is the coercivity. It is a microstructure sensitive property. Materials with coercivity values less than 50 Oe are considered magnetically soft and those with the values greater than 100 Oe are considered magnetically hard materials [30].

The coercivity of fine particles has a strong dependence on their sizes. As the particle size decreases, the coercivity increases, therefore the coercivity of multi-domain particles is smaller than that of the single domain particles since the rotation of the magnetic moment in multi-domain particles occur easily from motion of domain walls. As the particle size gets smaller, the

coercivity goes through a maximum and then decreases to zero, such particles are called superparamagnetic. The magnetic properties of magnetic elements and alloys are presented in **Figure 2-3.**

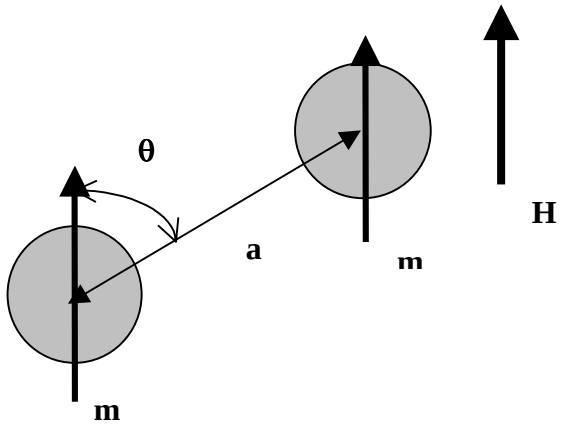

Figure 2. 2 Schematic of magnetic dipole-dipole interaction energy [28].

The magnetic hardness of most fine materials can also occur due to the forces of shape or crystal anisotropy. Shape anisotropy is due to magnetostatic fields external to the particle whereas crystal anisotropy is more due to the spin-orbit coupling. Spherical particles eliminate shape anisotropy and elongated particles have low or zero crystal anisotropy. If the fine magnetic particles must be compacted, the *packing fraction, p* is an important variable in determining what kind of anisotropy is present. This packing fraction is defined as the volume fraction of magnetic

particles in the assembly. If shape anisotropy prevails, then the coercivity decreases as p increases. The relation between the coercivity and packing factor can be given as [28]

$$H_{ci}(p) = H_{ci}(0)(1-p) \tag{2-8}$$

where $H_{ci}(0)$ is coercivity of the isolated particle. When crystal anisotropy prevails, the coercivity is independent of the packing fraction, p.

The imperfections in the crystals, such as impurity atoms, can act as barriers to the movement of domain boundaries. This domain wall pinning increases the coercivity of the material.

Other than low coercivity, high saturation magnetization, high permeability, small remnance, small hysteresis loop, and high electrical resistivity are other characteristics of soft magnetic materials. On the other hand, hard magnetic materials have high remanence, high coercive field large hysteresis loop, and high permeability.

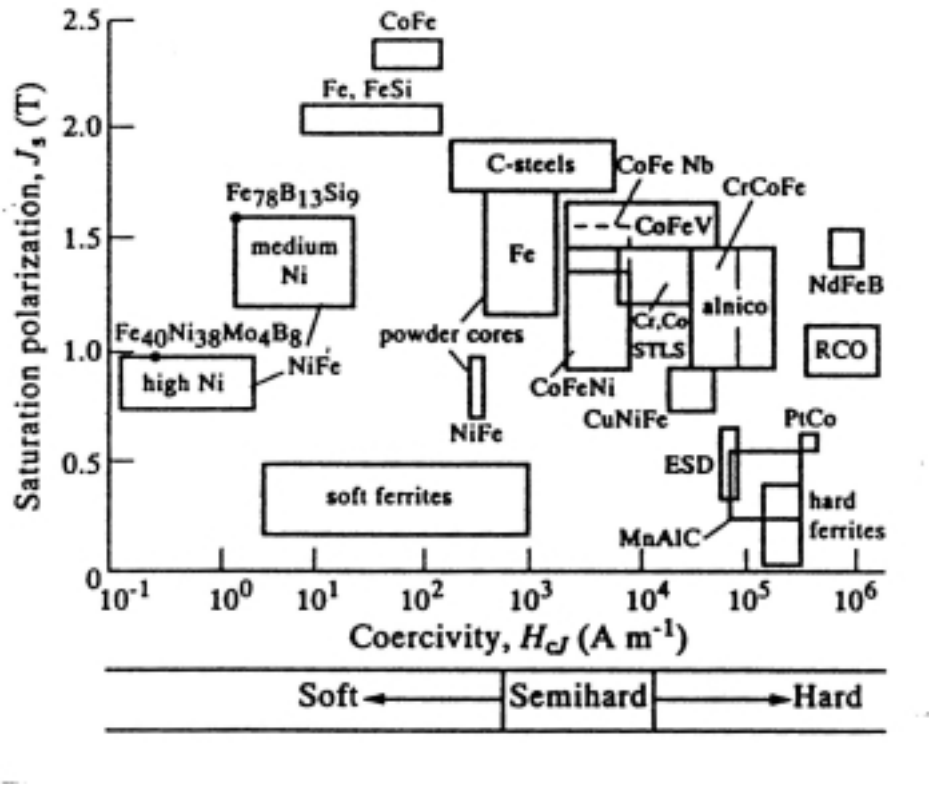

Figure 2. 3 Coercivity and saturation polarization of magnetic materials [33]

2.2.2 Magnetic Materials for MR fluids

In MR fluids, materials with lowest coercivity and highest saturation magnetization are preferred, because as soon as the field is taken off, the MR fluid should come to its demagnetized state in milliseconds. Due to its low coercivity and high saturation magnetization, high purity carbonyl iron powder appears to be the main magnetic phase of most practical MR fluid compositions. Iron powders made by the CVD decomposition of iron pentacarbonyl ($Fe(CO)_5$) [34, 35] are preferred as opposed to for example, those prepared using the electrolytic or spray atomization process. This is because carbonyl iron is chemically pure and the particles are meso-scale and spherical in nature in order to eliminate the shape anisotropy. The meso-scale particles are necessary since they have many magnetic domains. The high level of chemical purity (~ > 99.7%) means less domain pinning defects. The spherical shape helps minimize magnetic shape anisotropy. The impurities that cause magnetic hardness in metals also cause mechanical hardness, due to resistance to dislocation motion, and make the iron particles mechanically harder. In MR fluid based devices it is preferred to have particles that are non-abrasive. This is another reason why spherical, high purity iron powders are more appropriate for applications as a dispersed phase in MR fluids. Thus, carbonyl iron is chosen because of its high saturation magnetization (~2.1 Tesla, at room temperature) [36] and magnetic softness.

Among other soft magnetic materials Fe-Co alloys (composition 50 wt%Fe) have a saturation magnetization of ~2.43 T [36]. Although some researchers reported an enhanced yield stress for Fe-Co based fluid , the settling problem of the fluid will be aggravated due to the higher bulk density (8.1 gr/cc) than that of Fe (7.8 gr/cc). Also the cost of these alloys makes them undesirable for MR fluids. Carlson and Weiss reported that as well as iron-cobalt alloys,

iron-nickel alloys in ratio ranging from 90:10 to 99:1 showed a significant increase in the yield stress of MR fluids [37].

MR fluids have been prepared based ferrimagnetic materials such as manganese-zinc ferrite and nickel zinc ferrite of an average size of 2 μm. The saturation magnetization of ceramic ferrites is relatively low (~0.4-0.6 T) [30] and therefore the yield stresses also tend to be smaller. Phulé and co-workers reported a yield stress of ~15 kPa at a magnetic flux of 15 kPa [38].

2.2.3 Magnetic Properties of MR fluids

Besides the magnetic properties of isolated particles, the static magnetic properties of MR fluids characterized by B-H and M-H hysteresis are also important. Theoretical models for fluids and devices (that will be discussed in the next section) need magnetization as an input. These magnetic properties will also be helpful in predicting the dependence of the MR response on the applied current in the device. The induction in the fluid under different fields is measured by various methods, such as Vibrating Sample Magnetometer (VSM), Alternating Gradient Magnetometer and other induction techniques.

At very low magnetic fields, the magnetic dipole moment induced in particles within MR fluid is given by [13]

$$m = 4\pi\mu_0 R^3 \beta H \tag{2-9}$$

$$\beta = \frac{\mu_p - \mu_f}{\mu_p + 2\mu_f} \tag{2-10}$$

where R is the particle radius and μ_p and μ_f are the relative permeabilities of the particle and the fluid, respectively.

At higher fields where the magnetization of the particles reach saturation, the magnitude of the moments becomes independent of the field and it is given by [39]

$$m = \frac{4}{3}\pi\mu_0 R^3 M_s \tag{2-11}$$

where $\mu_0 M_s$ is the saturation magnetization.

The saturation magnetization of the fluid, $\mu_0 M_f$ is related to the saturation magnetization of the bulk magnetic solid, $\mu_0 M_s$, through the volume fraction ϕ of the solid present

$$\mu_0 M_f = \phi\mu_0 M_s \tag{2-12}$$

Phulé and Ginder reported static magnetic properties of 2 kinds of fluids using a custom-built magnetic hysteresis graph. For the fluid based on 36 volume fraction of Fe powder, $\mu_0 M_f$, was 0.75 T and for the 35 vol% ferrite based fluid it read ~0.14 T . The bulk saturation magnetization of Fe is 2.1 T and for ferrite it is 0.4 T [40].

2.3 Fundamentals of Rheology

2.3.1 Flow Properties of Concentrated Suspensions

Suspensions simply consist of solid particles randomly distributed in a fluid medium. The viscosity of dilute, monodisperse suspensions was first developed by Albert Einstein 1906. His simple equation for viscosity is [41]

$$\eta_l = \eta(1 + k_E\phi) \tag{2-13}$$

where η is the viscosity of the suspension and η_l is the viscosity of the carrier liquid and k_E is the coefficient for particles of various shapes and orientation and ϕ is the volume fraction of the dispersed phase [41]. For spherical particles, this coefficient is 2.5 [41]. The volume fraction of

the solid loading is given as ϕ which is ≤ 0.03. This equation indicates that the viscosity does not depend on the particle size but depends on the particle shape and solid concentration.

The addition of the solid particles to a liquid not only increases the viscosity but also alters the flow field and this can introduce deviations from the Newtonian behavior, which is usually observed at volume fraction of $\phi \geq 0.3$. The viscosity of a Newtonian fluid is independent of time and rate of shear (**Figure 2-4**). Deviation from this behavior reveals time dependence and shear rate dependence, in general known as non-Newtonian behavior. *Rheopexy* and *thixotropy* are time dependent properties where the apparent viscosity increases and decreases respectively with time when a stress is applied. The decrease in the viscosity of the thixotropic material occurs due to the break down of the microstructure. Rheopexy, on the other hand, can occur as a result of temporary aggregation due to inter-particle forces rather than breakdown due to collision of the attractive particles. As a result, the structure builds up and this increases the viscosity with time. These time-dependent properties are reversible, that is, when the stress is removed the structure that was disturbed by shearing builds up in the thixotropic material and breaks down in a rheopectic material. Thus, the material settles back into its original consistency. The rheopectic behavior is observed at high concentrations, in the range of 30-60vol-% of dispersed phase [42]. When steady state apparent viscosity decreases with increasing shear rate, the behavior is called *shear–thinning* or *pseudoplastic*; when steady state apparent viscosity increases with increasing shear rate, it is called *shear-thickening* or *dilatant*. Clay in water, starch in glycerol are given as examples of shear thickening suspensions. The particle-particle interactions, concentration of the phase volume, shear rate, particle shape and size, particle density and particle size distribution (PSD) are the factors that increase the apparent viscosity [42, 43]. In principle, shear thinning proceeds from thixotropy and shear thickening proceeds

from rheopexy. Some of the examples of thixotropic suspensions are paints, clay suspensions, greases, and electrorheological fluids. Types of flow curves are given in **Figure 2-4**. In non-Newtonian fluids, the relationship between stress and shear rate is often described by the power law model [44].

$$\sigma = K\dot{\gamma}^n \tag{2.14}$$

where K is a constant referred to as the consistency index and n is the flow index which indicates the degree of deviation from Newtonian behavior where n=1. The shear thickening is represented by n>1 and shear thinning by n<1.

A suspension can be shear thinning due to various reasons such as break down of the flocs, loss of junctions in polymer solution, rearrangement of microstructures in suspensions and alignment of rod-like particles in the flow directions [46]. Strong shear thinning behavior of magnetic iron oxide suspensions in mineral and silicone oils with volume fractions <15%was reported by Navarette *et. al* and Yang *et. al* [47, 48]. Kanai and Amari reported rheopectic behavior of the suspension consists of flocculated colloidal, single domain, needle like magnetic iron oxide in mineral oil above a shear rate of 50 s^{-1} due to strong tendency to flocculate of the magnetic particles [49]. These particles are mostly used in the magnetic recording. Below this range of shear rate, they reported a thixotropic behavior. They concluded that the reason for the rheopexy to occur at high shear rates was due to the loosening of the flocs by shearing which increases effective volume phase. They also compared the flow properties of magnetic and non-magnetic iron oxide particles with respect to the inter-particle forces acting between the particles.

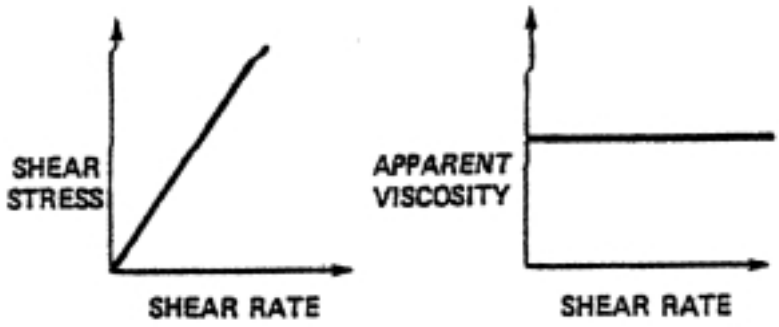

A

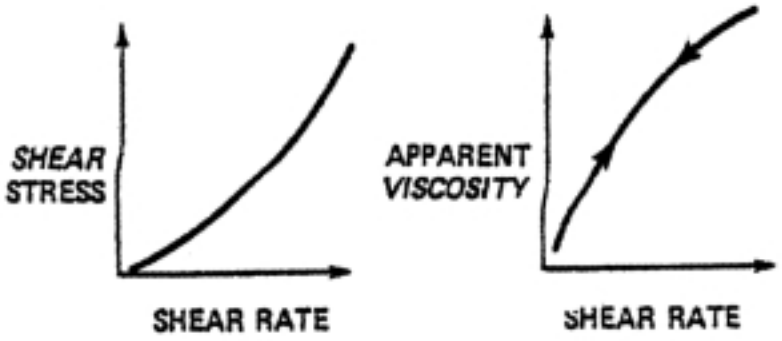

B

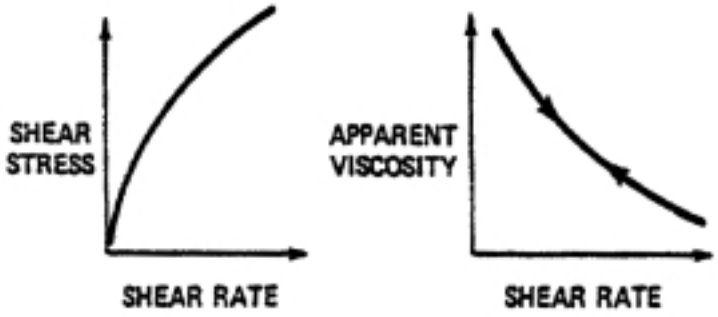

C

Figure 2. 4 Types of flow curves (A) Newtonian Flow (B) Shear Thickening (C) Shear Thinning [45]

2.3.1.1 The Volume Fraction and Particle Size Dependence of Viscosity. At high volume fractions, the particles are close enough to each other that the flow field of one particle is affected by the neighbors. Thus the particles are said to experience hydrodynamic interactions. At a concentration of about 50%, a rapid increase in the viscosity is noticeable [50] (**Figure 2-5**). The loose packing of uniform spheres assuming simple cubic packing, corresponds to 52% by volume. At this concentration, the friction due to particle interactions would become a significant factor and the resistance to shear seems to cause a rapid increase in viscosity. At high volume fractions, the maximum packing volume fraction, ϕ_m, becomes important and the relationship can be given by Krieger-Dougherty equation [51]. This is a general empirical expression for suspensions of particles of spherical and other shapes.

$$\eta = \eta_{ls}\left(1-\frac{\phi}{\phi_m}\right)^{-[\eta]\phi_m} \tag{2-15}$$

where $[\eta]$ is the intrinsic viscosity. **Figure 2-5** presents the viscosity changes with the increase of the dispersed phase.

For concentrated suspensions, Chong and co-workers also developed a relation for viscosity as a function of solid concentrations and maximum packing volume fraction [50]

$$\eta = \eta_l\left[1+0.75\left(\frac{\phi/\phi_m}{1-\phi/\phi_m}\right)\right]^2 \tag{2-16}$$

where ϕ_m is the maximum solid concentration and ϕ/ϕ_m is the reduced volume fraction. If ϕ_m for monodisperse systems is taken to be equal to 0.605, **Equation 2-16** reduces to the well-known Einstein's Equation for dilute concentrations. From geometrical considerations, ϕ_m ranges from

0.52 for simple cubic packing to 0.74 for rhombohedral packing. In practice, the maximum packing usually ranges from 0.601 to 0.637 for random packing spheres for monomodal systems [41].

For high concentration of particles, the particle size distribution (PSD) has a strong effect on viscosity as well as the particle shape and surface roughness. The packing of the particles can be affected by mixing two different size spheres or by using a broad continuous particle size distribution [50, 52-56]. The smaller particles act as ball bearings among the bigger particles which gives rise to a decrease in the viscosity. Chong and co-workers reported that at a fixed volume fraction of smaller particles, there is a particle size ratio below which the viscosity does not decrease in any significant amount [50]. The limiting particle size ratio of small to large spheres is about 1/10. If the ratio is smaller than 1/10, then the small spheres seem to behave essentially like a fluid toward the larger spheres. The minimum viscosity can be obtained at a volume fraction of 25 - 35% of small particles [50].

The magnetic particles in the MR fluids are usually coated with a surfactant in order to prevent the particles from getting close to each other that would cause agglomeration. These coatings take up a volume and limit the concentration of magnetic solids, and the volume fraction can be corrected as [32]

$$\frac{\phi_M}{\phi_t} = \frac{1}{(1+2\delta/d)^3} \tag{2-17}$$

where ϕ_m is the volume fraction of the solid and ϕ_t the volume fraction of the coated particles. The solid particle diameter and the length of the adsorbed polymer are given by d and δ respectively.

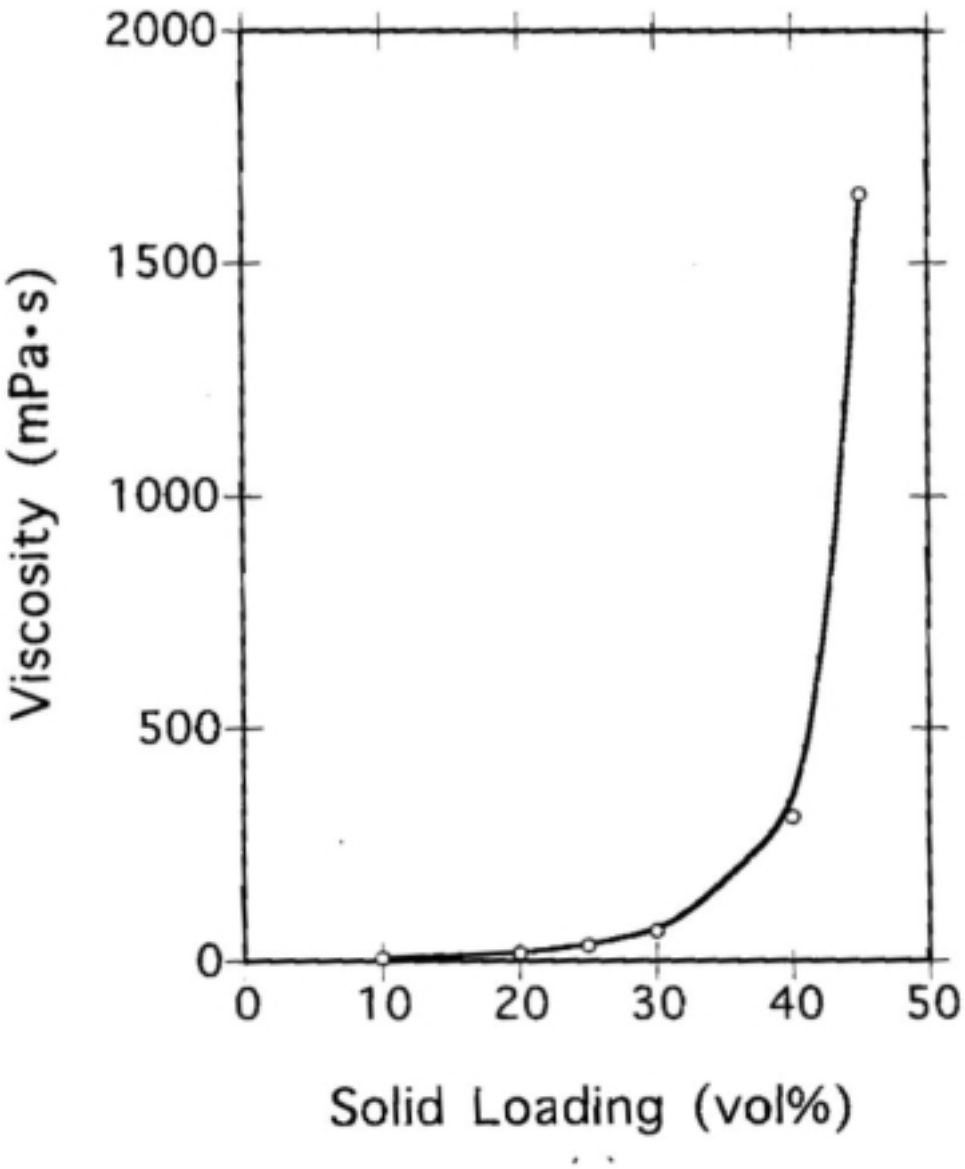

Figure 2. 5 Dependence of viscosity on the solid loading of alumina of 0.7 μm mean particle size [57].

2.3.2 Linear Viscoelasticity

2.3.2.1 Steady Shearing. Linear viscoelasticity is the time dependent mechanical response of a material to an applied stress. Under constant deformation, the viscoelastic solid stores part of the input energy and dissipates the rest of this energy whereas a viscoelastic liquid dissipates all of the energy eventually. An essential characteristic of the viscoelastic behavior can be shown in various transient experiments such as creep and stress relaxation. In creep experiments, the stress is suddenly created and maintained constant and the deformation is observed. In the stress relaxation experiments, a strain is suddenly imposed and maintained constant and the change in stress is observed. In a creep experiment, in order for the material to be considered linear viscoelastic one requirement is that the strain in the creep experiment must be proportional to the applied stress. The stress history of the linear viscoelastic material in simple shear has to correspond to the strain history. This most powerful law of polymer physics is known as the Boltzmann Superposition Principle. If the strain varies in a continuous function of time, then the strain at any instant of time t depends on the stress of the previous times. The strain is given in Equation 2.18 as an integral over all previous times [58].

$$\gamma(t) = \int_{-\infty}^{t} J(t-\theta)\frac{d\sigma(\theta)}{d\theta}d\theta \qquad (2\text{-}18)$$

where J is the shear creep compliance. The behavior of the linear viscoelastic solid and liquid when a stress is applied in a shear creep experiment are illustrated in **Figure 2-6**. The creep measurements are usually followed by recovery where the applied stress is suddenly removed and the viscoelastic solid, when given enough time, returns to its original state completely (**Figure 2-6**). The limiting creep strain is given by [58]

$$\gamma(t) = \sigma_0[J_e] \qquad (2\text{-}19)$$

where J_e is the equilibrium compliance. The recovery strain is given as

$$\gamma_r(t) = \sigma_0[J_e - J(t - t_2)] \tag{2.20}$$

where t_2 is a time after an equilibrium deformation has been attained. For viscoelastic fluids, however, after a creep run long enough to reach steady state flow, irrecoverable deformation is observed where the strain reaches a value given by

$$\gamma(\infty) = \sigma_0 t_1/\eta \tag{2.21}$$

where t_1 is the time at which the recovery starts. For a linear viscous fluid under a constant stress, the deformation is also given by Equation 2.21. The value of recoverable deformation approaches an asymptotic value $\tau_0 J_s$ where J_s is called **steady state shear compliance**. The Equations 2-22 and 2-23 give the relationship of the creep and recovery strains respectively [58],

$$\gamma(t) = \sigma_0[J_e + t/\eta] \tag{2-22}$$

where $\tau_0 t/\eta$, the permanent deformation, is the viscous flow contribution. The recovery is given by

$$\gamma_r(t) = \sigma_0[J_e + t/\eta - J(t - t_2)] \tag{2-23}$$

where γ_r is the recovery strain and t_2 is the time after recovery strain reaches a constant value of $\tau_0 t_2/\eta$.

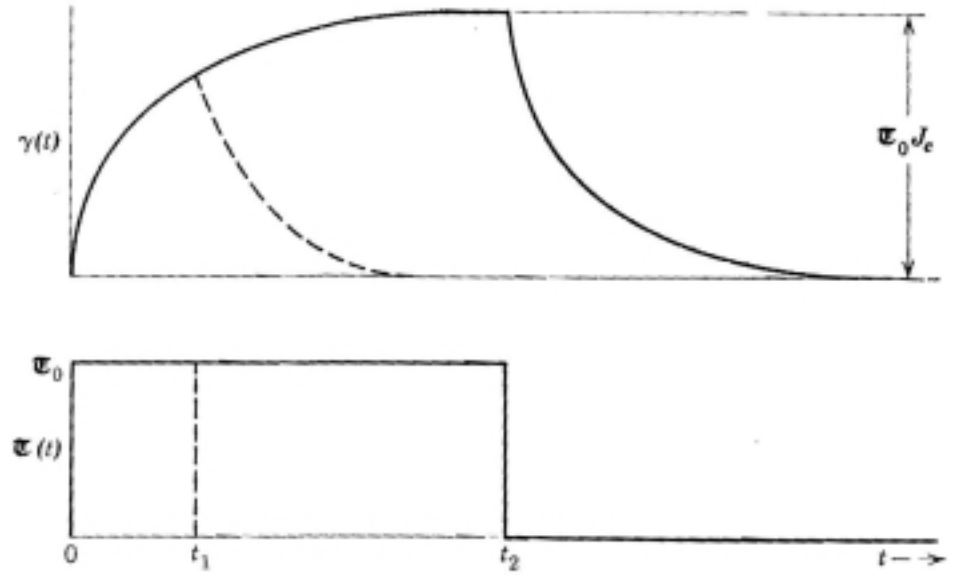

(a)

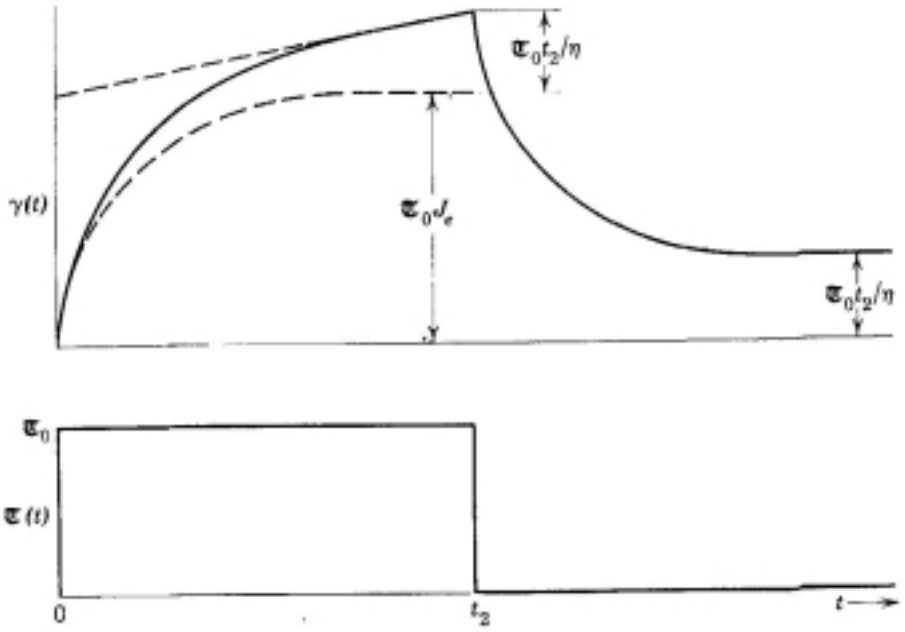

(b)

Figure 2. 6 Creep-recovery curves for (a) viscoelastic soild (b) viscoelastic liquid [58]

2.3.2.2 Dynamic Measurements. In a linear viscoelastic material, when the strain varies sinusoidally with time, such as $\gamma \ \gamma_0 \sin\omega t$, the stress, unlike the elastic solid which is in phase or the viscous fluid which is 90^0 out of phase with the strain, will oscillate sinusoidally with the strain at the same frequency but will be shifted by a phase angle, δ. The relationship between stress and strain under sinusoidal deformation for elastic, viscous and viscoelastic material is given in Figure2-7. In a linear viscoelastic material, the sinusoidal stress can be decomposed into two stress waves such as in phase and out of phase with the strain. These stress components suggests two dynamic moduli, G and are given as

$$\sigma_1 = \gamma_0 G'(\omega) \tag{2-24}$$

$$\sigma_2 = \gamma_0 G''(\omega) \tag{2-25}$$

where τ_1 is the component in phase with the strain and G′ is the measure of the energy stored and recovered per cycle, known as **storage modulus** (in phase), τ_2 is the out of phase component of stress and G″ which is called as **loss modulus** is the measure of the energy dissipated or lost as heat per cycle of sinusoidal deformation (out of phase). The ratio of energy lost to energy stored known as the **loss tangent** and is given by

$$\tan\delta(\omega) = \frac{G''(\omega)}{G'(\omega)} \tag{2-26}$$

where ω is the angular frequency of the oscillation. The dynamic viscosity can be calculated analogous to a fluid such as

$$\eta'(\omega) = \frac{G''(\omega)}{\omega} \tag{2-27}$$

at very low frequencies, the dynamic viscosity is equal to the zero shear rate viscosity η_0. Thus, viscoelastic behavior can be described with a complex modulus defined as

$$G^* = G' + iG'' \tag{2-28}$$

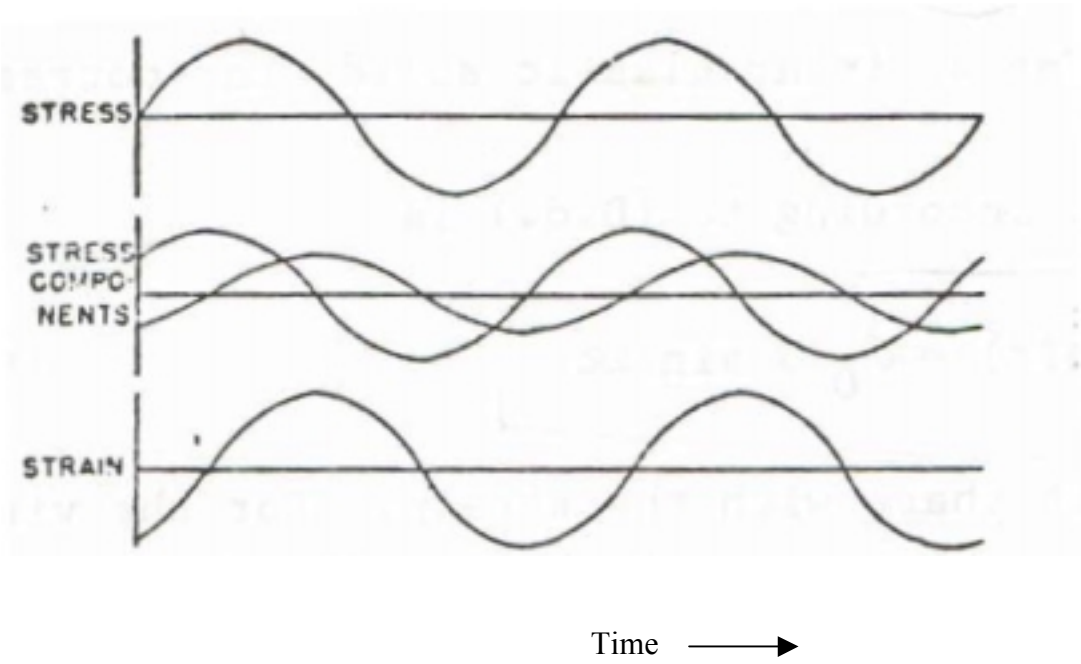

Figure 2. 7 Stress and strain relationship in an oscillatory measurement

2.4 Rheology of Ferrofluids

The rheological behavior of magnetic dispersions in the presence of a magnetic field is rather difficult to interpret both experimentally and theoretically. In this section some of the quasi-static models where hydrodynamic effects are ignored will be discussed.

Lemaire and Bossis [39] modeled static yield stress of magnetic fluids that are composed of monodisperse suspensions of equally spaced chains of spheres. The minimum yield stress required to cause the MR fluid or ferrofluid to flow from an initially static state is called static yield stress, τ_s. Dynamic and static yield stresses are not equivalent [59]. **Figure 2-8** illustrates these different stresses. They calculated the restoring force that tends to align 2 spheres on the axis of the field as follows

$$F_r = 3\mu_f a^2 H^2 \beta^2 f \tag{2-29}$$

Where **a** is the diameter of the particles, μ is the permeability of the suspension **H** is the effective field, $\beta = (\mu_p - \mu_f)/(\mu_p + 2\mu_f)$ and function f depends on the separation between 2 spheres and on the ratio of μ_p/μ_f. Once μ_f (H) and μ_p (H) are known, the restoring force can be calculated and its maximum value, F_r^m, force necessary to break a chain, will give the yield stress.

$$\tau_m = n_s F r^m \tag{2-30}$$

where n_s is the number of chains per unit surface. The experimental studies conducted by Lemaire and co-workers [39] did not show agreement with their theoretical predictions.

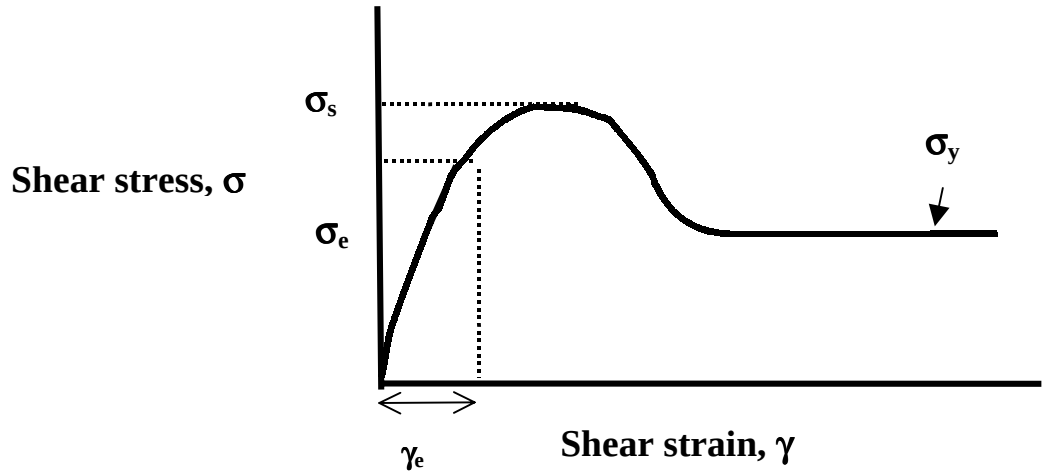

Figure 2. 8 The stress-strain curve for a quasistatic shear deformation illustrating the elastic-limit yield stress, τ_e, static yield stress, τ_s, and the dynamic yield stress, τ_y [60].

They used aqueous suspensions of polystyrene spheres containing iron oxide inclusions and ordinary polystyrene dispersed in a ferrofluid (inverse ferrofluid). They attributed the difference in measured and theoretically predicted yield stress to polydispersity of the dispersed phase and wall slip effects [39, 61, 62]. Their microscopic analysis on the structure of the fluids revealed that there were aggregates forming rather than chains of spheres that can be approximated by ellipsoids.

For microscopic models, finite element method and multipolar expansion were used. Macroscopic approaches that are only characterized by their shapes (stripes, cylinder and ellipsoids) and by their internal volume fraction were considered in modeling MR fluids. Shulman [63] and Bossis et al. [61] modeled the magnetic fluids by using macroscopic approaches that are only characterized by their shape. Their models are based on non-interacting ellipsoid aggregates that are valid only at low volume fractions. For higher volume fractions Bossis et al [61] proposed to consider mean field theory where each ellipsoid is immersed in the average medium of volume fraction ϕ and of permeability $\mu(\phi)$. The effective field is given by $H=H_0/\ \mu(\phi)$.

$$\frac{\tau}{\mu_f H^2} = \frac{1}{2}\frac{\phi}{\phi_a}\frac{\mu(\phi)}{\mu_f}\mu_m^* \frac{\partial}{\partial\gamma}\left(\frac{1}{(1+\gamma^2)(1+\mu_m^* n_{ll})} + \frac{\gamma^2}{(1+\gamma^2)(1+\mu_m^* n_{\perp})}\right) \tag{2.31}$$

where $\mu_m^*=[\mu_s(\phi)/\mu(\phi)]-1$ and $n_{||}$ and $n_{\perp}$ are the demagnetizing factors for the ellipsoid [64]. Volkova et. al [65] and Bossis et. al [64] expanded this model to the magnetic fluids composed of aggregates of cylinders and stripes of internal volume fraction of ϕ_a.

Another model was developed by Rosensweig considering the unsymmetric stress states [32, 66]. He adopted the continuum point of view of a substance that is homogeneous on a

macroscale. The magnitude of the mechanical stress is given by **Equation 2-32** based on the antisymmetric part of the elastic stress state [66].

$$\sigma = \frac{1}{2}\mu_0 M_x H_D \tag{2-32}$$

Rosensweig applied this theory to predict the yield stress to a model of parallel layers or laminae (**Figure2-9**). The layers have susceptibilities χ_1 and χ_2, providing that $\chi_1 \neq \chi_2$. Assuming that only one of the material is magnetizable ($\chi_1 = \chi$,, $\chi_2 = 0$), the susceptibility components were calculated as [66]

$$\chi_{xx} = \phi\chi/(1+\chi(1-\phi)) \tag{2.33}$$

$$\chi_{zz} = \phi\chi = \chi_{yy} \tag{2.34}$$

where ϕ is the volume fraction of the magnetic phase.

For a composite without demagnetization, the yield stress is given as

$$\frac{\sigma_x}{\left(\frac{1}{2}\mu_0 H_0^2\right)} = \frac{1}{2}\frac{\phi(1-\phi)\chi^2}{1+(1+\phi)\chi} \tag{2.35}$$

and with demagnetization

$$\frac{\sigma_x}{\left(\frac{1}{2}\mu_0 H_0^2\right)} = \frac{\frac{1}{2}\phi(1-\phi)\chi^2}{\sqrt{(1+\chi)(1+\phi\chi)[1+\chi(1-\phi]}} \tag{2.36}$$

The model that was developed revealed anisotropic susceptibility as a physical parameter of key importance.

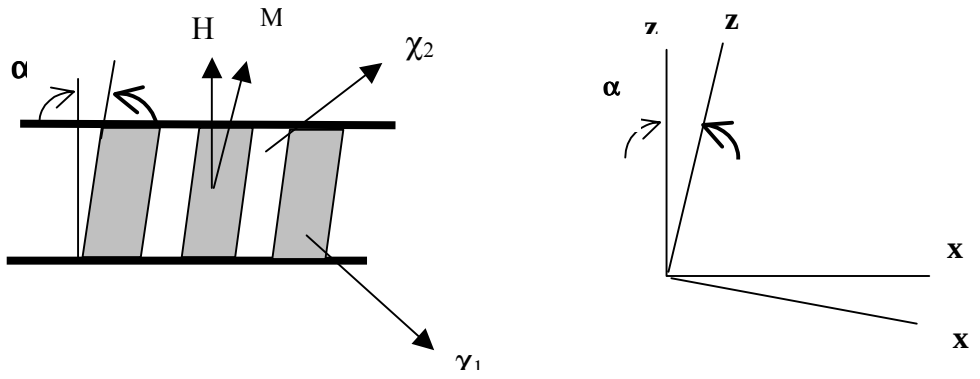

Figure 2.9 Strained state of the material. After the material is strained, the magnetization M of the layer deviates from collinearity with the applied field, H (66).

2.5 Rheology of Magnetorheological (MR) Fluids

It has been previously pointed out that, the magnetic properties such as saturation magnetization, permeability, susceptibility of the dispersed phase, as well as the applied magnetic field are important parameters in obtaining high magnetorheological (MR) effect which is defined as the shear stress increase $\Delta\tau$ (B) due to the magnetic field [67]. Many of the models, developed for ER fluids can be adopted for MR fluids in low magnetic fields. However, at high magnetic fields, due to the non-linearity and magnetic saturation of the particles, the linear models used to treat ER fluids are no longer valid for MR fluids. The models discussed above are linear approaches and they predict the shear stress, yield stress and the shear modulus are proportional to $\phi\ \mu_0\ H_0^2$. These models do not take the saturation of the magnetic particles into consideration. However, there has been studies to develop models where the non-linearity and the saturation of the magnetic phase are considered [20, 68].

In their Finite Element Analysis (FEA), Ginder and co-workers determined the static yield stress as the maximum shear stress which was modeled as tensile component in the shear direction of the linear infinite single chains of spherical particles [68, 69]. They found that at very low inductions, the on state yield stress varied as B_{ave}^2 and as the applied magnetic field increased the dependence was to be proportional to $B_{ave}^{3/2}$. According to the analytical approach developed by Ginder and co-workers, the yield stress of an MR fluid is found to be proportional with H_0^2. However, this prediction neglects the important role of magnetic saturation. The saturation, at very low fields, starts to occur at the poles and contact regions of the particles. At intermediate levels, when this local saturation of magnetization reaches its maximum, the yield stress is predicted as [68]

$$\sigma_y = \sqrt{6}\phi\mu_0 M_s^{1/2} H^{3/2} \tag{2-37}$$

When the field is high enough, the particles reaches complete saturation throughout and can be treated as dipoles. At this point the yield stress becomes independent of the applied magnetic field H. In the high field regime, the yield stress for non-interacting particle chains is given by [68]

$$\sigma_y^{sat} = \frac{4}{5^{5/2}} \xi(3) \phi \mu_0 M_s^2 \tag{2-38}$$

where ξ (3) =1.212 which is a constant.

Ginder and co-workers also predicted the shear modulus G, by analytical models at intermediate and high magnetic fields [68]. At intermediate magnetic fields, they reported G as:

$$G \propto \phi \mu_0 M_s H_0 \tag{2-39}$$

and at very high magnetic fields G is given as [68]

$$G^{sat} = \frac{\xi(3)}{4} \phi \mu_0 M_s^2 \tag{2.40}$$

where H_0 is the applied magnetic field, M_s is the saturation magnetization, μ_0 is the permeability and ϕ is the volume fraction of the magnetic phase and $\xi(3)$ is a constant which is equal to 1.02.

Another study was performed by Jolly and co-workers [70] to develop a model of MR effect as a function of particle magnetization based on the dipolar interaction. The shear stress induced by the application of the magnetic field can be calculated by

$$\tau = \partial U / \partial \gamma \tag{2.41}$$

where U is the interparticle energy density and γ is the shear strain. The yield stress of the particle chains occurs at the strain for which the stress is at maximum.

$$\partial\tau / \partial\gamma = 0 \tag{2.42}$$

and the yield stress is calculated by Jolly et al. [70] as

$$\sigma_y = \frac{0.1143\phi J_p^2}{\mu_1 \mu_0 h^3} \tag{2.43}$$

where ϕ is the volume fraction of magnetic particles, J_p is the particle polarization given in Tesla, μ_1 is the relative permeability of the medium and h is r_0 / d (r_0 is the center to center spacing when the particles are aligned in the direction of the field and d is the particle diameter).

The maximum possible field induced change in the stress occurs when the aligned particles become magnetically saturated i.e. when $J_p = J_s$. It can be seen easily that the maximum field induced stress increases quadratically with saturation magnetization Js of the particle material.

Rheology of magnetic particle dispersions are generally analyzed in 2 steps which are known as pre-yield and post-yield conditions, respectively **(Figure 2-10)** [4].

$$\text{Pre-yield :} \quad \sigma = G'\gamma \ , \ \dot{\gamma} = 0 \qquad \sigma < \sigma_y \tag{2.44}$$

$$\text{Post-yield :} \quad \sigma = \eta\dot{\gamma} + \sigma_y \qquad \sigma \geq \sigma_y \tag{2.45}$$

where η is the plastic viscosity and γ' is the shear rate and τ_y is the **dynamic yield stress**. The MR fluids within the pre-yield region exhibit viscoelastic properties and these are important in understanding MR suspensions, especially for vibration damping applications. For applied stresses $\tau > \tau_y$, the material is able to flow.

According to Barnes and co-workers, the Bingham Plastic model is only valid at high shear rates and given the right measuring techniques (i.e. stress controlled and very low shear rates), the yield stress doesn't exist [71, 72]. Plazek and co-workers are among the scientists who first reported that the deviation from linear behavior occurred at a critical strain rather than critical stress [73]. However, the post-yield behavior, also known as Bingham Plastic model is used to model the flow properties of MR fluids for practical and industrial purposes. The dynamic yield stress can be obtained according to **Equation 2-45** by extrapolating the shear stress vs. strain rate curve to zero shear rate. This model recognizes that the property of an MR fluid that changes upon application of the magnetic field is the yield stress defining the breaking of the chains of magnetic particles formed by dipolar interactions and thus the fluid starts to flow. Phulé and co workers reported a dynamic yield stress of 100 kPa for 40% iron based MR fluid at a magnetic induction of 0.8T measured by a custom-made double concentric cylinder rheometer.

The importance of the "off-state" viscosity of MR fluids comes from the figure of merit for MR fluids which is given by the "turn up" ratio defined as the ratio of "on-state" yield stress to the "off-state" viscosity. "On-state" refers to the state of the MR fluid under an applied magnetic field and the on-state yield stress behavior depends on the magnetic properties and the volume fraction of the magnetic phase [69]. The off-state viscosity, which is a function of carrier liquid, additives, surfactants [74], particle loading and particle size distribution (PSD) [75], is the value when no magnetic field is applied. Due to the addition of additives and surfactants and changes in magnetic particle microstructure during shear, most MR fluids exhibit thixotropic behavior and shear thinning [76]. The break up of weak agglomerates or bonds in the shear field is a major cause of a shear thinning behavior of MR fluids.

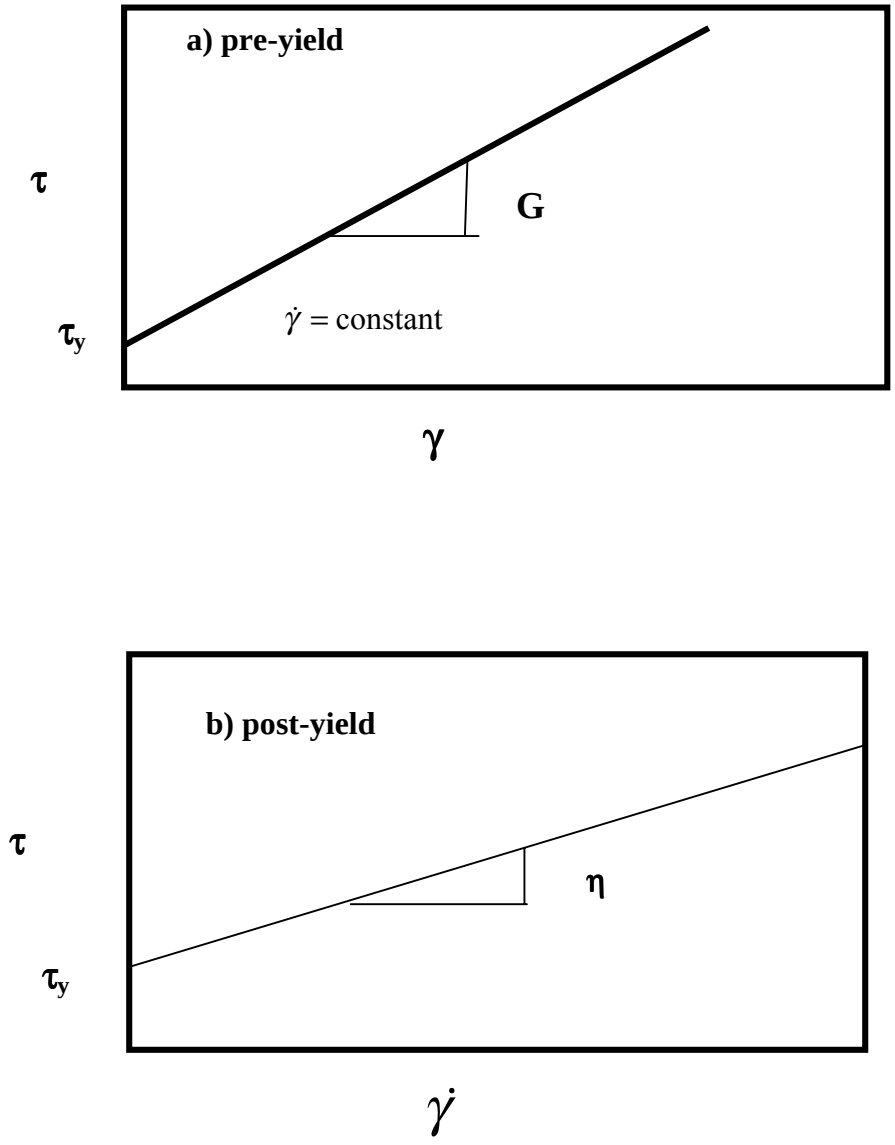

Figure 2. 10 Bingham Plastic Model

For MR fluids, the plastic viscosity which provides a more useful measurement for design purposes is typically in the range of 0.1 to 0.7 Pa-s [77]. The plastic viscosity is determined with the Bingham Plastic Model (Equation 2-45) where it is defined as the slope of the linear curve fit to the measured shear stress vs. strain rate data. In literature, there aren't many reports on the "off state" viscosity of the MR fluids, especially at higher volume fractions ($\phi > 0.3$). Kordonski and co-workers reported several data on the particle size and volume fraction dependence of initial viscosity for MR fluids based on 25vol% magnetic particles [78]. They reported no dependence of particle size on the initial viscosity of MR fluids.

The structure of MR fluids is anisotropic (**Figure 2-11**) due to the formation of the particles along the field lines of the applied magnetic field. Thus, the yield stress will depend on the orientation of the magnetic field and the direction of three fundamental orientations between magnetic field and shear direction where only shear in the x direction is considered, is given in **Figure 2-11**. Most MR fluid applications such as clutches, brakes and dampers use the situation in which the magnetic field is applied along the gradient direction (**Case B**). However, for optical polishing application, **Case C** is preferred [79]. Shorey and co-workers compared the anisotropy of MR fluids by measuring the shear stress for case B and C where both cases have a field orthogonal to the direction of the flow. They found that in general the yield stresses were similar in magnitude but slightly higher for Case C [79]. They concluded that the slight difference in the yield stress may be due to the internal structure formation which would need to be investigated further.

The yield stress of the MR fluids mainly depends on the saturation magnetization ($\mu_0 M_s$) and volume fraction of the magnetic particles. In the analytical models developed by Ginder and co-workers, the yield stress increases linearly with increasing volume fraction [68, 69]. However,

at high volume fractions, the exponential increase of yield stress with increasing volume fraction was reported by Volkova and Chin [65, 80]. This can be attributed to the higher packing of particles where the affine deformation can be restricted leading to higher stresses [80]. Lemaire *et al*. [81] reported a dependence of yield stress on the size of the particle when the ratio of magnetostatic energy to thermal energy is larger than unity. However for very large values of this ratio, they found no size dependence of yield stress [81]. This also confirms that the magnetic properties of the particles are independent of size. They proposed that a mono-disperse sample would optimize the MR effect. Foister [75] investigated the yield stress and viscosity dependence of bimodal distribution. He reported that MR fluid prepared with a mixture of 25 % of smaller particle and 75 % larger particle iron powder showed the minimum viscosity. He also proposed that the yield stress increases with mixing of two different sizes, however no explanation was given for the reason of increased yield stress [75].

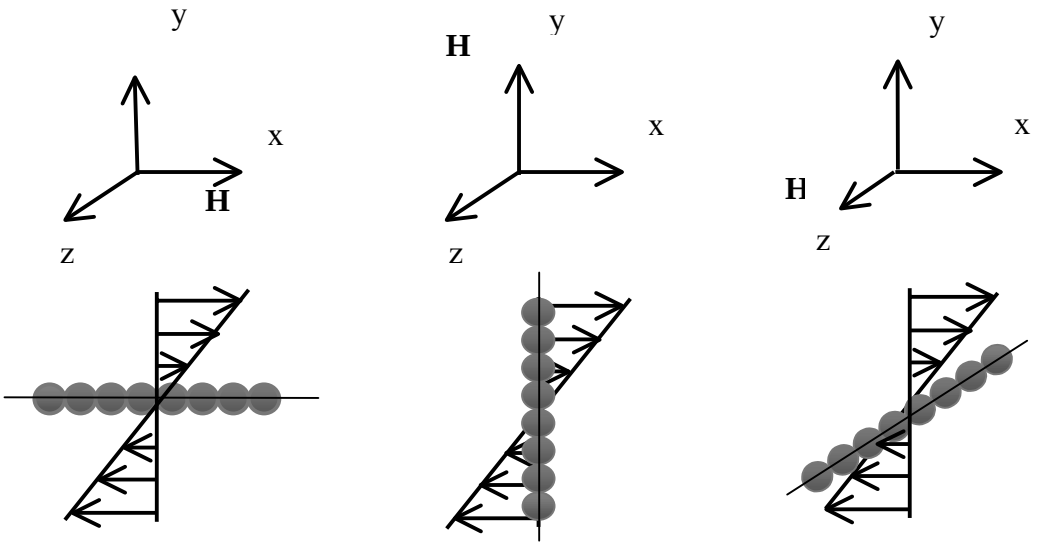

Figure 2. 11 Anisotropy of MR fluids: The value of the yield stress depends on the direction of the applied magnetic field and the shear direction.

Being multiphase materials consisting of magnetizable particles in a carrier liquid, MR fluids also exhibit viscoelastic properties. In order to measure linear viscoelastic properties of MR fluids, the applied maximum strain amplitude should be smaller than the yield strain which was reported as 0.5-0.8% by Weiss et al [82]. Li and co-workers reported yield strains varying from 0.2 to 0.6% for a 10vol% iron based MR fluid synthesized in silicone oil. The creep measurements conducted by Yang et al. on magnetic iron oxide suspensions in silicone oil showed that at low stress (2 Pa), complete recovery, indicating that the material was behaving like an elastic solid, and at higher stresses some irrecoverable strain were observed [48].

The creep and recovery behaviors of MR fluids provided from Lord Corporation were investigated by Li and co-worker under an applied magnetic field [83]. They determined the dynamic yield stress by Bingham Plastic Model under various magnetic fields. The dynamic yield stress at 340 mT was determined as 6750 Pa at 20 ^{0}C. According to their creep experiments, when a creep stress of 2000 Pa was applied the MR fluid behaved as a viscoelastic fluid. As the stress was increased in the creep experiment, plasticity came into play and at a stress slightly below the yield stress there is almost no elastic recovery. When the applied creep stress was equal to the yield stress, stepwise behavior in the strain-time plot was observed. This was attributed to the rupture, i.e. yielding, and reformation of the chain structure of the MR fluid. Their study revealed that instead of single chain of particles, thick columnar structures were responsible for the plastic response of the MR fluid. The same kind of transition from linear viscoelastic material to a plastic fluid was also observed by Otsubo and Edamura in their ER fluids [59]

According to Li et.al the storage modulus G' showed an increase in the frequency range of 10-100 Hz, however, loss modulus G″ did not exhibit increase as much as G' This result

indicated that 10 vol% MR fluids exhibited energy storage capability more than dissipation capability. The same scientists also determined the magnetic field dependence of both G' and G'' and these properties of MR fluids showed an increase with increasing magnetic field. The loss tangent decreased sharply at low magnetic fields in the same frequency range, on the other hand, at high magnetic fields the loss tangent showed almost no change. This was attributed to the internal structure formation of MR fluids; at high magnetic fields the particles formed solid like structures [84].

Weiss *et.al* reported storage modulus G' of $2.5*10^6$ Pa for MR fluids at 2000 Oe magnetic field and at a frequency of 1.5 Hz. The highest value of the storage modulus G' was $4.2*10^6$ Pa at the same magnetic field but at a higher frequency of 16 Hz [82].

The effect of the particle and resin interactions and the time of milling on rheology of the magnetic paints by dynamic measurements were studied by Potanin and co-workers. They studied the changes in G' and G'' with the concentration of the resin [74, 85]

2.6 Rheometry

In MR fluid applications, most devices operate using pressure driven flow mode, direct shear mode or squeeze mode. Examples of pressure drive flow mode devices include servo-valves, dampers and shock absorbers. In case of direct shear mode, clutches, brakes, chucking and locking devices can be given as examples. The squeeze mode has been used in low motion, high force applications [21, 86]

The design and realization of an actuator with MR fluid requires exact description of the rheological and magnetic properties of the MR fluids. Basic classes of rheometry are considered as stress driven and strain rate driven. Rotational rheometers such as concentric cylinder

rheometer, cone and plate rheometer, parallel plate rheometer and double Couette rheometer are basic types of rheometers used in rheological measurements [4, 67, 87] **Figure 2-12**. The shear stress, shear rate, strain and viscosity relations for different geometries are given in **Table 2-2**.

The concentric cylinder rheometers are best for lower viscosity systems and high shear rates. The gravitational settling of suspensions has less effect than cone and plate and parallel plate. The shear rate across the gap is not uniform whereas in cone and plate rheometers, the shear rate is constant. Cone and plate rheometers are good for high and low viscosity systems. However, this geometry is not good as high shear rates. Rotational parallel plate rheometer is very useful for obtaining viscosity and normal stresses at high shear rates. It allows changing the gap height very easily which can be very useful in terms of determining the wall slip at two different gaps [88] .

A rotational parallel-plate geometry inserted into a coil was used by Lemaire and Bossis [62] whereas Laun et al.[67] presented measurements performed with a concentric rheometer. A cone and plate type rheometer was utilized by Gans and co-workers in order to measure rheological behavior of the inverse ferrofluids. By choosing a small cone angle, they minimized the sample variations in the radial direction [89]. Shorey and co-workers developed a magnetometry for understanding properties of MR fluids for optical polishing [79].

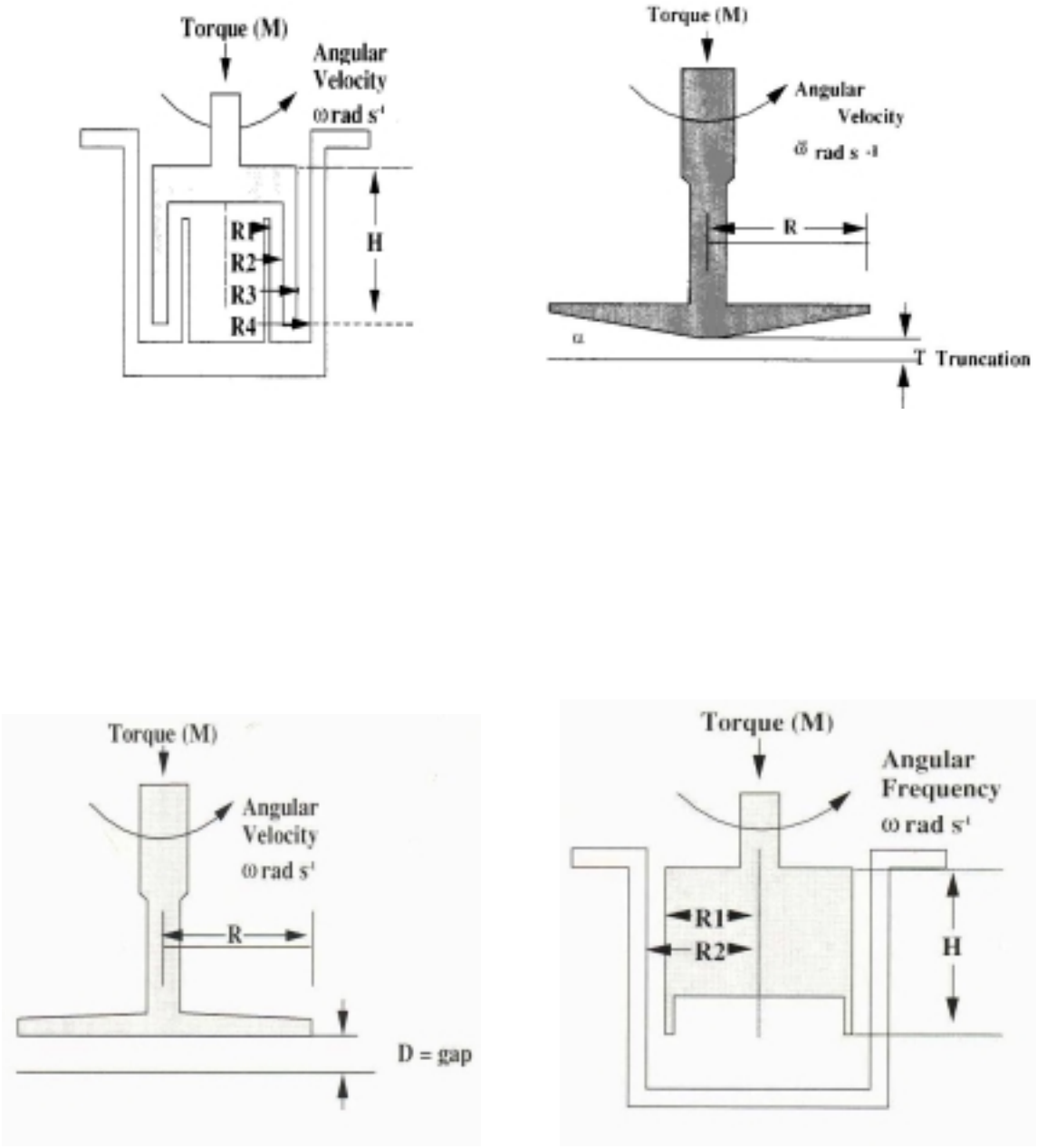

Figure 2. 12 Types of rheometer geometries : a) double concentric cylinder, b) cone and plate, c)parallel plate, and d) concentric cylinder

Table 2. 2 Equations of rheological properties for different geometries. In these equations M is the torque, h is the height, R, is the radius (Figure2-12, Ω is the angular velocity, θ is the angular displacement and α is the cone angle [4, 58].

	Shear stress	**Shear rate**	**Strain**	**Viscosity**
Concentric Cylinder	$\frac{M}{(2\pi R_{ave}^2 h)}$	$\frac{2\Omega R_1^2 R_2^2}{r^2(R_2^2 - R_1^2)}$	$\frac{\theta R_{ave}}{R_2 - R_1}$	$\frac{M(R_2^2 - R_1^2)}{4\pi h \Omega R_1^2 R_2^2}$
Parallel Plate	$\frac{M}{2\pi R^3}$	$\frac{\Omega R}{h}$	$\frac{R\theta}{h}$	$\frac{\pi\Omega M R^4}{2h}$
Cone and Plate	$\frac{3M}{2\pi R^3}$	Ω/α	$\frac{\theta}{\alpha}$	$\frac{3\alpha M}{2\pi R^3 \Omega}$
Double Concentric	$\frac{M}{2\pi h(R_1^2 + R_4^2)}$	$\frac{\Omega R_4^2}{(R_4^2 - R_3^2)} + \frac{\Omega R_1^2}{(R_2^2 - R_1^2}$	$\frac{\theta R_4^2}{(R_4^2 - R_3^2)} + \frac{\theta R_1^2}{(R_2^2 - R_1^2)}$	$\frac{M(R_4^2 - R_3^2)(R_2^2 - R_1^2}{2\pi h}$

Besides the rotational rheometers, there are also other methods to measure the dynamic yield stress of the MR fluids. Dang and co-workers used a pressure driven apparatus to determine the yield stress of MR fluids [90]. The yield stress which is given by **Equation 2-46,** is the pressure drop necessary to start the flow.

$$\sigma_y = \frac{rP_{flow}}{2L} \tag{2-46}$$

where L is the length, r is the radius of the cylindrical fluid element and P is the pressure drop.

2.7 Wall Slip Effects

Slip occurs in the flow of two or multi phase suspensions because of the displacement of the dispersed phases away from the walls of the geometries used in the rheometer leaving a layer of particles next to the wall more dilute than in the bulk dispersion. For suspensions, gravity can enhance the slip effect especially in parallel plate or cone and plate geometries. During flow, shear induced particle migration can occur due to the shear rate gradient [91] and this results in a low viscosity layer adjacent to the wall that leads to an "apparent wall slip". The conditions that lead to large and significant slip effects can be summarized as: large particles as the dispersed phase, smooth wall, small flow dimensions, low speeds and flow rates, walls and particles carrying electrostatic charges which would cause the walls of the platens to repel adjacent particles [92]. The slipping at the walls can be prevented by roughening the surface of the walls as to increase the friction between the walls and the suspension. Yoshimura and Prud'homme proposed a method of calculating the wall slip velocity. In their work, the authors performed measurements on geometries with different gaps but they kept the ratio of radii equal. For Couette geometry, the slip velocity is given by:

$$v_s = \left(\frac{\kappa}{\kappa+1}\right)\left[\frac{\Omega_1 - \Omega_2}{\frac{1}{R_1} - \frac{1}{R_2}}\right] \tag{2-47}$$

where κ is the ratio between the cup and the bob, R_1 and R_2 are the radii for 2 different cups and Ω_1 and Ω_2 are the angular velocities. For parallel plate geometry, the slip velocity is,

$$v_s = \frac{\dot{\gamma}_{aR1}(\tau_R) - \dot{\gamma}_{aR2}(\tau_R)}{2\left(\frac{1}{H_1} - \frac{1}{H_2}\right)} \tag{2-48}$$

where H_1 and H_2 are the two gap heights. These velocity corrections can be used to correct the shear rate readings to give the true material viscosity [88].

In rough surfaces, the particles become trapped whereas in the smooth surfaces, they can roll over small bumps more easily. The rough surfaces can be obtained by sand blasting [43]. Lemaire and Bossis measured magnetic colloidal suspensions in different fixtures made of stainless steel, iron and glass. The wall slip is minimum in the iron fixture and the most pronounced in the glass fixture [62].

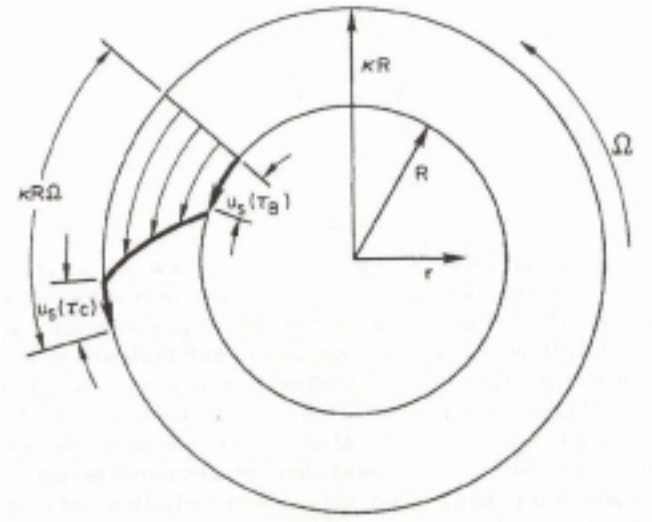

(a)

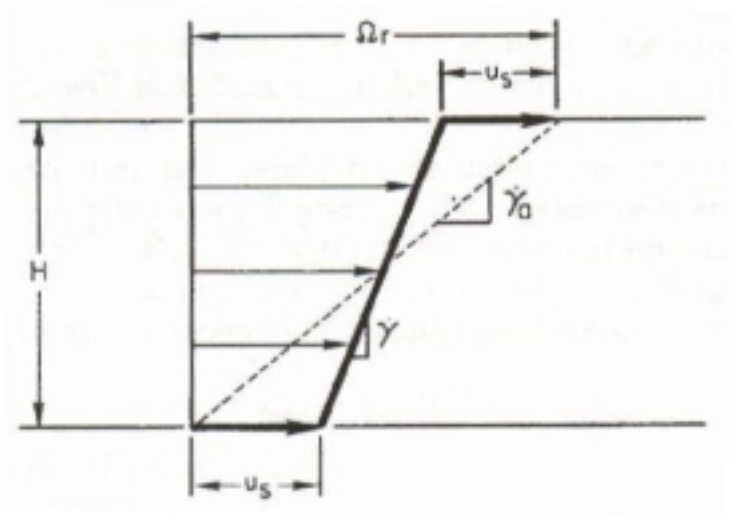

(b)

Figure 2. 13 Angular velocity profiles of (a) concentric cylinder and (b) parallel plate geometry [88]

2.8 Stability of MR fluids

The stability and redispersibility of MR fluids have been one of the most important issues of these materials. Stable MR fluids are considered to exhibit no or very little amount of particle settling. For dilute systems, the dependence of the sedimentation velocity of a spherical particle can be obtained from Stoke's law as follows [93]:

$$v = \frac{2}{9}\frac{R_s^2(\Delta\rho)g}{\eta} \tag{2-50}$$

R_s is the particle radius, $\Delta\rho$ is the difference in density of the magnetic phase and carrier liquid, η is the viscosity of the carrier liquid and g is the gravitational acceleration (9.8 m/s^2). Since, less viscous liquids will aggravate the settling of the particles in an MR fluid, Rankin and co-workers formulated a suspension with viscoplastic continuous phase (e.g., grease) to prevent sedimentation [94]. When the yield stress of the viscoplastic medium is bigger than the critical yield stress that was defined for each particulate material and particle radius, the particles are suspended. Although, for most of the applications the figure of merit for MR fluids is to keep the off state viscosity as small as possible, for applications such as control of seismic vibrations, paste-like MR fluids can be more appropriate since the gravitational settling over an extended period of time can be prevented.

If the settled magnetic particles in the MR fluid can be easily dispersed by applying very little mechanical energy, i.e. stirring or shaking, then the fluid is said to be *redispersible*. Some fluids exhibit poor redispersibility and therefore "cake-like" formation is observed at the bottom of the fluid which would degrade the MR response. Long range magnetic interaction of particles and short range van der Waals attraction energy are strongly related with the agglomeration and settling of particles in magnetic suspensions (**Figure 2-14**) [95-98].

According to Rosensweig, ferrofluids composed of particles smaller than 10 nm without any surfactants added, show stability against magnetic agglomeration and gravitational settling [32, 99]. Kormann and co-workers synthesized sedimentation stable MR fluids composed of polymer coated magnetic ferrites (diameter = 30 nm) for fast damping applications such as fast hydraulic dampers [67].

The agglomeration of the powders suspended in a liquid can be prevented by creating mutually repelling charged double layers or by physically preventing the close approach of particles due to steric hinderance of the molecule adsorbed onto the particle surface As the thickness of the adsorbed polymer increases and the size of the magnetic particles decreases, the stability of the magnetic particle dispersion increases [100]. The surfactants could be long chain molecules and a functional group at the end that could be cationic, anionic or nonionic. The functional group is attached to the outer layer of the magnetic particles by either chemical bonding or physical or combination. The adsorption of the long chain molecules onto the particle surface provides steric repulsion increasing the hydrodynamic radius (**Figure 2-15).**

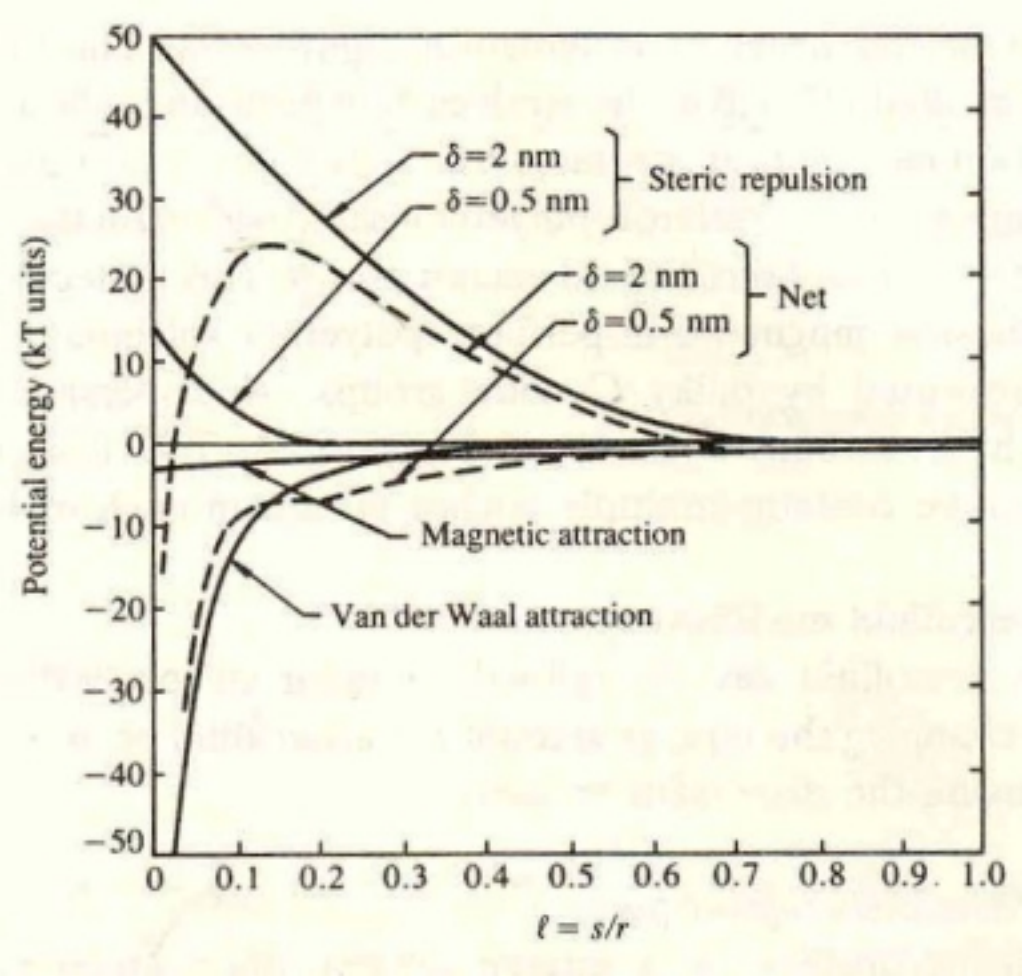

Figure 2. 14 Illustration of magnetic attractive energy, van der Waals attractive energy and steric repulsion energy and the net potential energy for different lengths of adsorbed molecule, δ. The ratio between the interparticle distance and the radius of the particle is denoted as "l".

The tail of the surfactant provides a permanent distance between the particles and compatibility with the liquid. A surfactant molecule reacts with an OH^- group on the Fe surface to produce an ether type linkage plus one molecule of free water:

$$M — OH + ROH \rightarrow M — OR + H_2O$$

where M –OH is the Fe surface and ROH is the surfactant [101]. One of the classic examples of an agent for dispersing magnetite particles into hydrocarbons is oleic acid. Although the particles are coated with polymeric binders or coated with adsorbed surfactants, the magnetic attractive forces cause reagglomeration of the particles with time. This reagglomeration process is more irreversible for the particles larger in size and larger in magnetic moment. The stability of MR fluids can also be improved by injection of protective colloid type substance (such as silica gel, or silicon dioxide, etc.). Homola and co-workers prepared a dispersions composed of silica coated particles [102]. The bonding between the magnetic particles and the silica occurred by the reaction of the hydroxyl (OH^-) groups forming on the surfaces of both magnetic and silica particles. The reaction leaves covalent oxygen bond to bond the particles together. Phulé also used nano-sized ceramic particles and a polymer that forms a multitude of nano-bridges in between silica particles and the network formed encapsulated the magnetic particles and therefore prevented their permanent aggregation [103]. Foister reported that the combination of carbonyl iron particles containing surface hydroxyl groups with a non-polar solvent selected from the group consisting aliphatic hydrocarbons and glycol esters provide MR fluids that resist particle separation [101] . The iron particles with hydroxyl groups at the surface can be dispersed into a proper hydrocarbon liquid without adding any surfactant. The carrier liquid should not react with the surface hydroxyls so that they provide electrostatic repulsion between iron particles preventing them getting close to each other and form agglomerates. On the other hand,

unlike classical nonmagnetic thickening agents, Kordonski and Demchuk [104] studied the stability of MR fluids by adding magnetically hard single domain powder into the carbonyl iron based (magnetically soft, multidomain) MR fluid . Since the additive is single domain particles, they represent tiny magnets that adhere themselves with one of their ends to coarse carbonyl iron particles and thus, they store the viscosity even after the field is cut off.

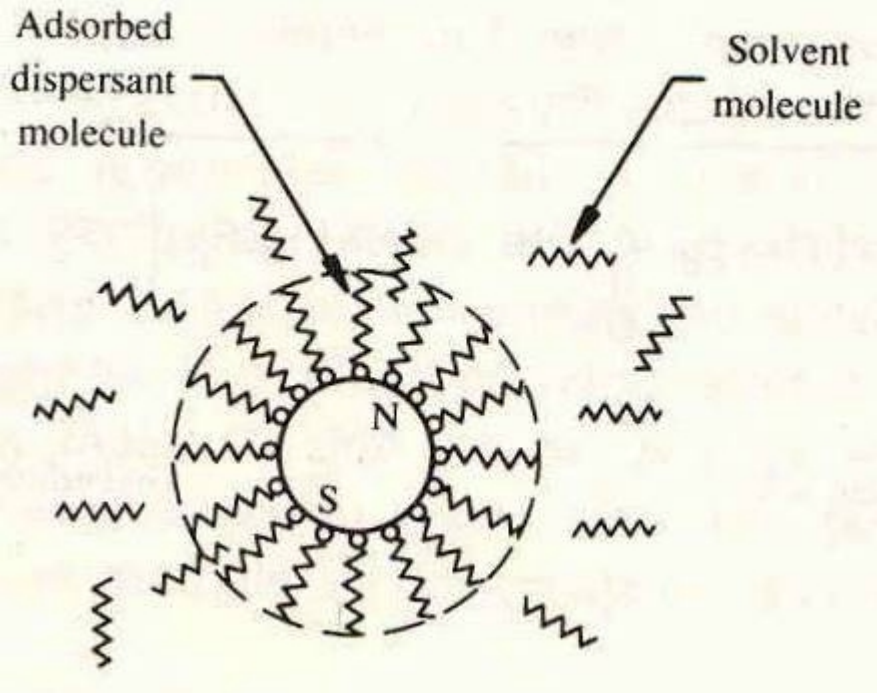

Figure 2. 15 Adsorption of the long chain molecules onto the particle surface provides steric repulsion increasing the hydrodynamic radius

3.0 EXPERIMENTAL PROCEDURES

3.1 Characterization of Magnetic Particles

A magnetically active dispersed phase is the main source for the strength of the MR fluids. In order to understand the MR effect and the stability of MR fluids better, particle characterization was performed on the as received carbonyl iron powders provided by ISP technologies. The selection of Fe powder was to optimize the MR effect since it is the element with the highest saturation magnetization [36].

In this research, two different grades of carbonyl iron powders, reduced and straight were used to synthesize the MR fluids. These reduced and straight grades are denoted as GRADE A and GRADE B in this thesis, respectively. Carbonyl Fe powder was manufactured by thermal decomposition of iron penta-carbonyl ($Fe(CO)_5$) producing spherical particles with the size ranging from 1-9 μm [34]. The difference between the straight (GRADE B) and reduced (GRADE A) powder is that the reduced one is further processed and reduced in nitrogen atmosphere after decomposition of iron penta-carbonyl, therefore the carbon, oxygen and nitrogen concentrations are lower than they are in GRADE B. The purity of GRADE A and GRADE B were 99 and 98%, respectively. GRADE A had an average particle size of 7μm and GRADE B had a particle size of 2μm. The oxygen content in GRADE B is ~0.4 wt% and which suggests that FeO, Fe_3O_4, and Fe_2O_3 may be formed. The iron powders were studied using x-ray diffraction ((XRD), Philips X'Pert systems), scanning electron microscopy (SEM, Philips XL30FEG), energy dispersive x-ray analysis (EDXA), vibrating sample magnetometer (VSM, Lakeshore), and particle size distribution analysis (Horiba Centrifugal Automatic Particle Analyzer).

3.1.1 X-Ray Diffraction

The iron powders were characterized by XRD. The standard Bragg-Brentano geometry (θ-2θ pattern) was used to analyze the phase distribution of the iron powders. A tube of voltage of 40 kV and a current of 30 mA and CuKα (λ=1.54) radiation was used. The detector slit was ½ ° and the source slit was 0.3 °.

3.1.2 Scanning Electron Microscopy (SEM) and EDS Characterization

The morphology and the shape of the particles of the iron powders as well as the qualitative particle size analysis were studied by SEM. The powder samples for SEM analysis were prepared by placing small amount of powder on a double-sided carbon tape and pressing with the tip of the spatula and ensuring the powder was not loose. The tape was then placed onto an aluminum stub. Elemental analysis for iron powder was performed by energy dispersive X-ray spectroscopy (EDS).

Secondary electron and backscattered electron studies were conducted by SEM (SEM, Philips XL30FEG) on MR fluids in order to image the coating of the particles. The MR fluid samples were prepared by placing 1-2 drops of MR fluid onto an aluminum stub and letting it dry in a vacuum chamber. The dried samples were then sputter coated with Pd to reduce charging of the sample. The SEM was operated at 10-15 kV.

3.1.3 Particle Size and Particle Size Distribution Analysis

Particle size distribution analysis of Fe powders was conducted using a particle size analyzer (Horiba Centrifugal Automatic Particle Analyzer). Iron powders were dispersed in deionized water with few drops polyelectrolyte stabilizer known as Darvan C (R. T. Vanderbilt) to prevent the agglomeration of particles. Propylene glycol was also used as the medium to disperse powders. Some of the dispersions were also ball-milled for 24 hours to break up the

agglomerates. The suspension was also sonicated (Heat Systems, Inc. Farmingdale, NY) for 3 minutes to disperse particles thoroughly. The analyses were performed under a centrifugal speed of 500 RPM as well as gravitational settling.

3.1.4 Vibration Sample Magnetometry Analysis

The magnetic hysteresis of as-received iron powders was measured using a vibrating sample magnetometer (VSM, Lakeshore). The maximum field applied was
15 kOe. The Fe powders were sandwiched in between epoxy (Epo-Kwick) in brass tubes with dimensions of ~3mm in diameter and ~5 mm in length. The iron powder was weighed with the accuracy of ± 0.0005 g. The VSM was calibrated with Ni sample of known saturation magnetization prior to the experiment. The VSM studies revealed magnetic properties data in cgs system for magnetic powders. In our calculations the cgs units of saturation magnetization was converted to SI units.

3.2 Synthesis and Processing of MR Fluids

Conoco LVT oil, kerosene, light paraffin oil, mineral oil, silicone oil with viscosities varying from 1.5 cP to 700 cP at 100 F and water are some examples of the carrier fluids that are used in the synthesis of MR fluids [75, 105]. In this research, polydimethylsiloxane fluid (PDMS), with a kinematic viscosity of 100 cSt which corresponds to 0.96 Pa-s dynamic viscosity and colloidal silica in glycol ethylene monoprophyl ether, known as NPC-ST (Nissan Chemicals) were used in synthesis of the MR fluids. The silica concentration in NPC-ST was 20wt%.

In PDMS based MR fluids, the surfactant called hydroxy terminated PDMS (surfactant A) with a viscosity ranging from 90-150 cSt was added in order to provide steric stabilization and prevent Fe particles to from forming aggregates and caking.

In glycol ether based MR fluids, polyvinylpyrollidone (SURFACTANT B, MW=29000) (Aldrich) dissolved in octanol (Aldrich) was added to the dispersion in order to form a network by adsorbing on the silica and iron particles. In preparation of the fluids, ceramic processing techniques were used [103]. A schematic flowchart of the synthesis of PDMS based fluids is presented **Figure 3-1** In the synthesis of PDMS based MR fluids, appropriate amounts of the carrier liquid and the surfactant were mixed for 1 min. in 250 ml Nalgene bottles. The magnetic powder was then added and mixed for 10 min. at 1000 RPM. The MR fluid was then ball milled for 24 hours. For ball milling 5 mm yittria stabilized zirconia balls (YSZ: Union Process Inc., Akron, OH) were used. The grinding media was separated after ball milling. For glycol ether based fluids, a similar route was used.

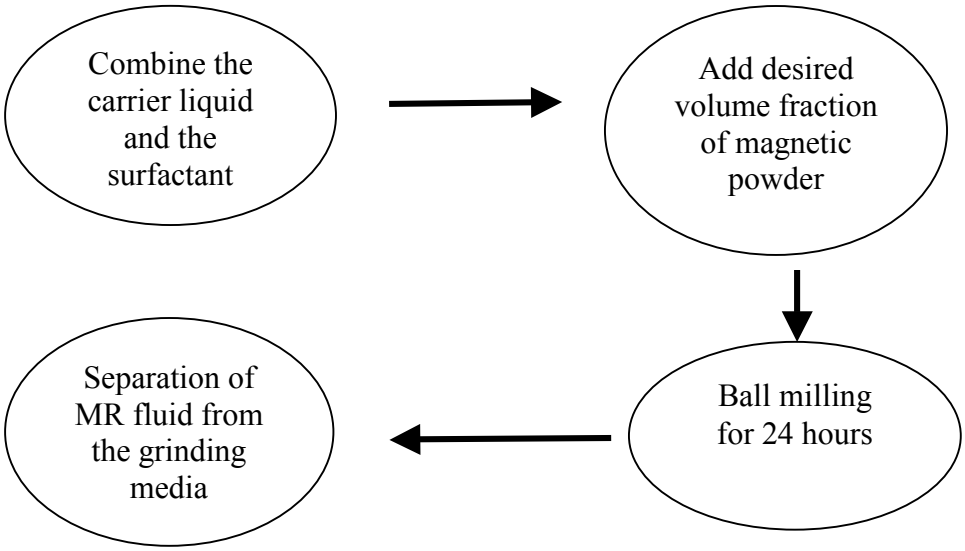

Figure 3. 1 Flow chart of synthesis of PDMS based MR fluid

3.3 Density Measurements

The density of MR fluids was measured by U.S. Standard Weight per Gallon Cup (Stainless Steel Series 300-Paul N. Gardner Co., Inc.). The cup was first calibrated with deonized water and the cup factor was determined. The volume fraction of the fluids can then be calculated from density measurements. These measurements and calculations could also confirm the volume fraction of iron powder in the MR fluid.

3.4 "On" State Rheological Measurements

Despite the expanding interest and research in MR fluids, there is no currently commercially available rheometer for MR fluids. In many research laboratories, scientists modify standard rotational viscometers with special magnetic field inductors and low carbon steel fixtures [39, 67, 79, 89]. Besides the rotational rheometers, there are also other methods to measure the dynamic yield stress of the MR fluids. Dang and co-workers used a pressure driven apparatus to determine the yield stress of MR fluids [90].

Fundamental laws of magnetostatics can be applied to understand the approximate behavior of simple magnetic circuit. **Figure 3-2** shows the schematic of the magnetic circuitry for MR fluids. The relationship between the magnetic field and the applied current is given by Ampere's Law [106]:

$$\oint H \bullet dl = NI \tag{3-1}$$

where I is the current in the coil and N is the number of turns/meter. And this relation can be expressed as follows,

$$NI = H_f L_g + H_s L_s \tag{3-2}$$

Referring to **Figure 3-2**, H_f is the field in the fluid and L_g is the width of the fluid gap. H_s is the field in the steel and L_s is the length of the steel path. Assuming no magnetic leakage, i.e. B is constant the relation between the magnetic induction B in the fluid and the magnetic field in the fluid can be calculated as

$$B_f = \mu_0 \mu_r H_f \tag{3-3}$$

where μ_r is the relative permeability of MR fluid which is 5-9 [76].

In this research the on state rheological measurements were conducted by specially built strain rate controlled double Couette MRF rheometer. This particular design, which was similar to that of a rheometer in Dr. Ginder's Ford Research Laboratory was chosen for the ability to complete the magnetic circuit more efficiently within the cup. The schematic of cup and bob fixture is shown in **Figure 3-3**. The MRF rheometer is shown in **Figure 3-4.** The cup and bob fixtures were built out of low carbon steel (**Figure 3-4**). For generating magnetic field, a wire coil was placed around the bob. The experiments were conducted at flux densities between 0.2 and ~0.8 T and at strain rates from 25 to 200 s^{-1}.

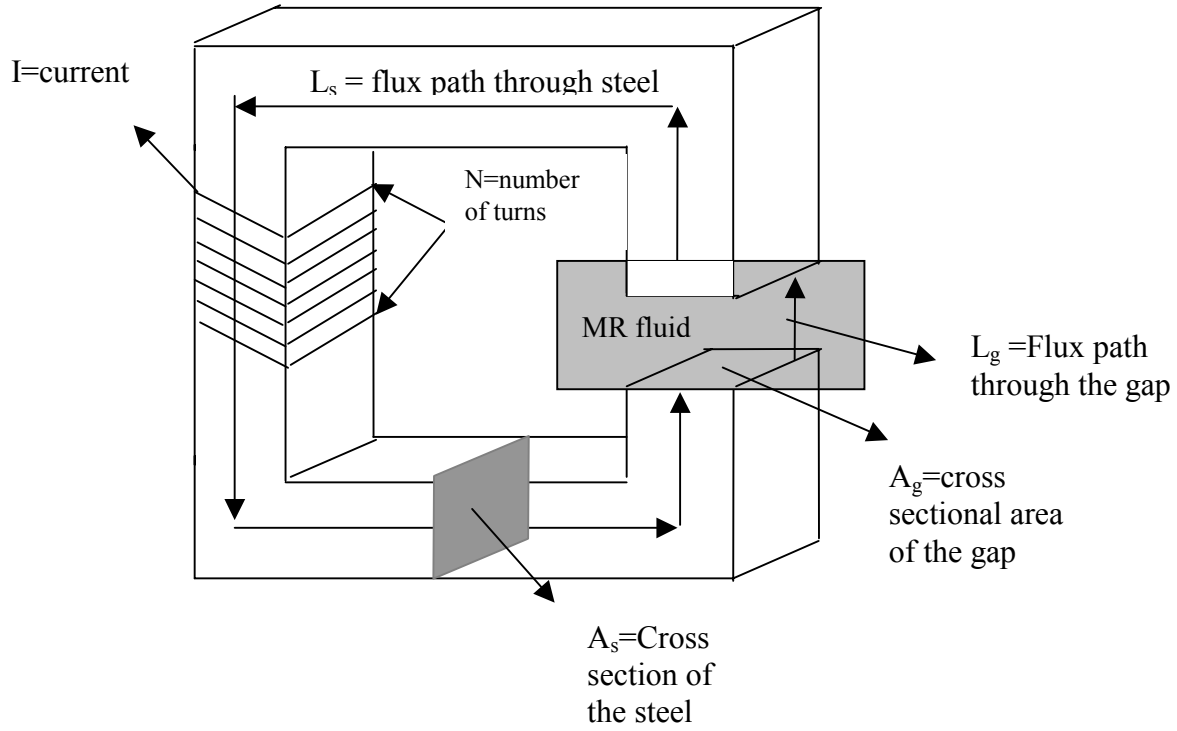

Figure 3. 2 Schematic of magnetic circuit for MR fluids.

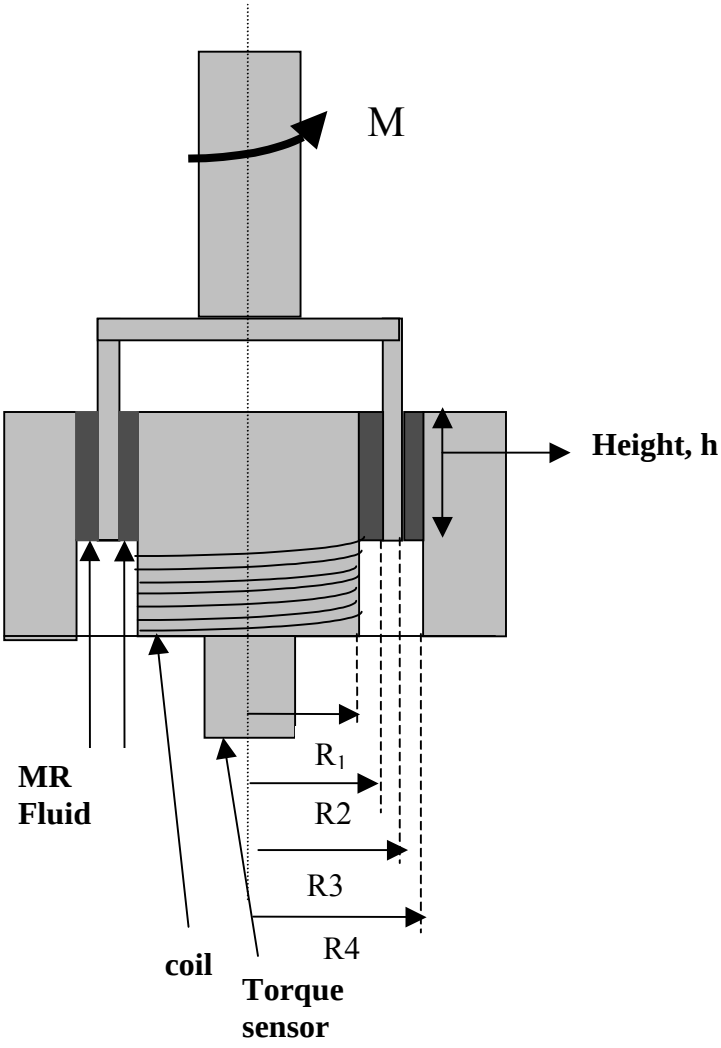

Figure 3. 3 Schematic diagram of cup and bob arrangement for the strain rate controlled double Couette MRF rheometer (R_1=20mm, R_2=21mm, R_3=24mm, R_4=25mm and h=10mm)

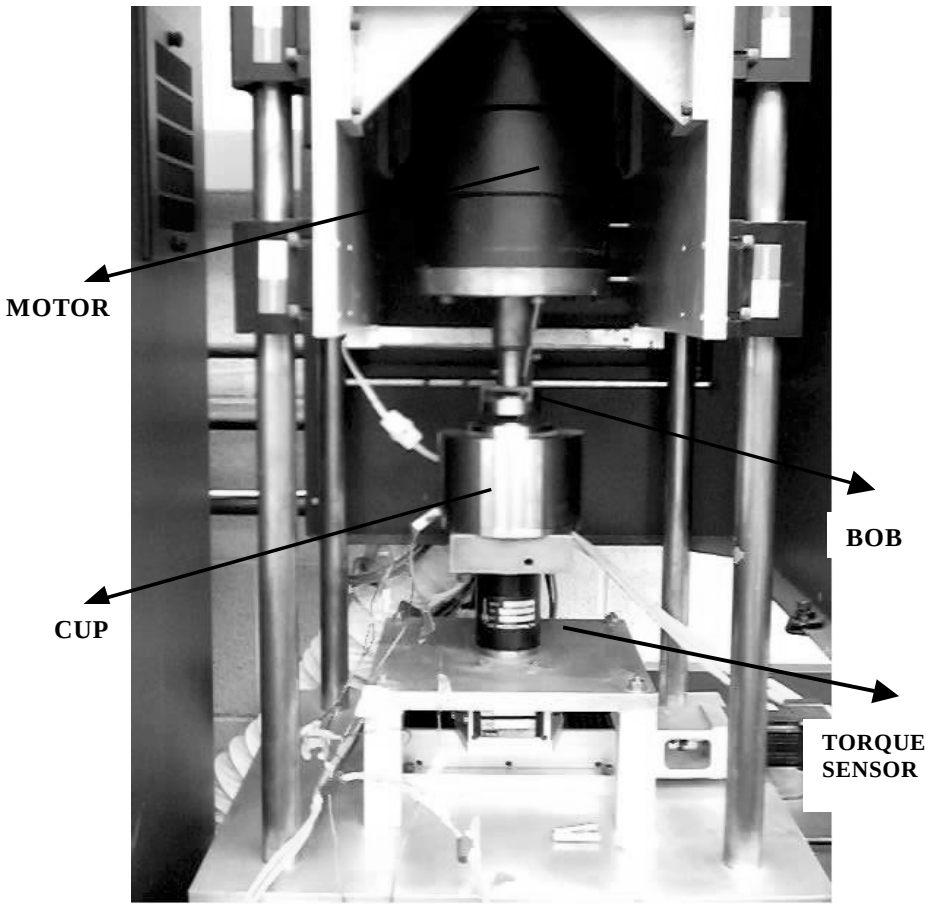

Figure 3. 4 The picture of custom-built strain rate controlled double Couette MRF rheometer

3.4.1 Calibration of the Fluxmeter

Prior to the measurements, the sense coil and the fluxmeter (Walker MF-3D) combination was calibrated specific to the fluid tested using a small sense coil, which was calibrated to 0.5 T with a pre-calibrated magnet (Lakeshore MRT-062-5K). The sense coil was wound from a 36 gauge insulated magnet wire for 10-20 times. The diameter of the small sense coil is ~1cm. The fluid was placed in the cup and then the bob was lowered. The sense coil was then inserted into the outer and inner gaps at each side of the double concentric cylinder. The current was increased from 0 to 2 A at a voltage of 10 V. The flux density was recorded at each applied current. After all the measurements were done, the small sense coil was detached from the fluxmeter and the flux induced by the coil was measured by a sense coil wrapped around the bob. The turns ratio calibration of the MR fluids was then conducted for iron based MR fluids at a constant shear rate of $10s^{-1}$. The cm^2 turns/turns dial on the fluxmeter was tuned to the same magnetic induction measured with the small sense coil. After averaging 2 small sense coil readings, the fluxmeter calibration was recorded as 9600 turns.cm^2/turns. The turn ratio for MnZn ferrite based MR fluids were reported as 8600 turns- cm^2/turns by Smart Materials group.

3.4.2 Measuring Technique for "On State" Rheological Properties

The "on state" experiments were conducted at flux densities between 0.2 and ~0.8 T and at strain rates from 25 to 200 s^{-1}. The bob was rotated by a micro-stepping motor (Parker 1008B), permitting the generation of the shear strain rates, while the torque transferred to the cup was measured by a strain-gauge torque sensor (Key Transducers 2508-5) excited by a strain gauge signal conditioner (Key Transducers 8120). The torque sensor is within 0.01% accuracy at a torque of 500 lb-in. In the "off state", when there is no magnetic field, and also at very low magnetic flux densities ($B<0.2T$), the torque sensor is not sensitive enough to give accurate

torque values. Therefore it is not used for "off-state" and very small levels of shear stresses encountered in low field "on-state" measurements The shear stress was calculated from the measured torque at different strain rates and flux densities by using the **Equation 3-4** [4, 67]

$$\tau = \frac{M}{2\pi H(R_1^2 + R_4^2)} \tag{3-4}$$

where R_1 and R_4 are the inner and outer radii of the cup (**Figure 3-3**). The dynamic yield stress of the MR fluids was calculated using the Bingham Plastic Model, **Equation 2-45.** The dynamic yield stress was then determined by extrapolating the shear stress versus strain rate curve to zero strain rate at which the intercept showed the dynamic yield stress of the MR fluids. The temperature near the cup was not controlled but measured.

3.5 Heat Treatment of MR Fluids

Silicone oil and synthetic oil based MR fluids were heated at 175 °C for 24 hours. MR fluids were stored in tin containers during heat treatment. The samples were weighed before and after heat treatment in order to control whether there was any evaporation. Some of the samples were vacuumed under -30 mm-Hg in order to vacuum the air trapped in the fluid. NPC-ST samples could not be heat treated due to low flash point of the liquid.

3.6 “Off State” Rheological Measurements of MR Fluids

The off state rheological measurements were conducted by dual mode (stress/strain rate controlled) rheometer (TA Instruments, Model R1000). Another stress controlled rheometer developed by Plazek called “Magnetic Bearing Torsional Creep Apparatus” (MBTCA-IVb) was also used in the off-state viscosity measurements [107].

a) TA Rheometer:

The TA rheometer consists of an air bearing for friction free application of the torque. The shear stress depending on the geometry ranges from $8*10^{-4}$ to $508*10^{3}$ Pa and angular velocity ranges from 10^{-8} to 100 rad/s for controlled stress and ranges from 10^{-2} to 100 rad/s for controlled strain rate. The temperature can be controlled between -40 and 99±0.1 ^{0}C with a Peltier Plate. When the double concentric geometry was attached, the temperature control was maintained by a compact refrigerated circulator (Julabo, Model F30-C). The working temperature range is from -26 ^{0}C to 200 ^{0}C with a temperature stability of ±0.01^{0}C. All the measurements were performed at 25 ^{0}C. Prior to the experiments, the instrument was calibrated. After the calibration of the rheometer, mapping step, a correction on the air bearings, was performed to ensure the steadiness of the air bearing. Prior to the experiments standards such as polybutene and light mineral oil with viscosities predetermined by the falling ball method were measured in both of the rheometers (TA rheometer and MBTCA-IVb) in order to compare the measured and calculated viscosities.

The MR fluid sample was stirred before it was installed in the cell in order to create a uniform distribution of particles. The sample was installed with a spatula or hypodermic needle.

Cone and plate and double concentric cylinder platens were used in the measurements. The cone and plate platen was made of stainless steel and had a diameter and cone angle of 40 cm and 2^{0}, respectively and the truncation was 51 μm. The amount of fluid in the gap was 0.5 ml. After the fluid was placed on the Peltier Plate the cone was lowered and the fluid that extruded from the gap was removed with a spatula in order to prevent edge effects.

The cup and the bob of double concentric cylinder was made of steel and aluminum respectively and had dimensions of 21.96 mm rotor outer radius, 20.38 mm rotor inner radius,

20.0 mm stator inner radius, 59.50 mm cylinder immersed height and 0.5mm gap. The volume of the gap between the double concentric cylinders was 6.5 ml. The fluis was injected with hypodermic needle.

b) Magnetic Bearing Torsional Creep Apparatus (MBTCA-IVb)

The rotor was the only moving element and should not touch anything but the specimen being studied and this was accomplished by magnetic levitation of the rotor. The optimum magnetic levitation current was maintained at 600 mA and at a height of DC voltage of 7.9 V at the top, 6.9 V in the middle and 5.3 V at the bottom. The magnetic field induced the required torque with a drag cup motor. A detailed description of the rheometer can be found elsewhere [107]. Two different types of platens, parallel plate with knife edges and concentric cylinder, were used in the measurements. The diameter of the parallel plate platen was 12.7mm (0.5in) and the gap between parallel plates was adjusted between 1-1.5mm. The knife edges of the parallel plates could prevent the flowing of the fluid out of the gap. The Couette device which consisted of rotating bob and stationary cup with diameters of 10.2mm (0.4 in) and 10.5 mm respectively, as used in the measurements. Bobs with different diameters (5.08mm (0.2in), and 2.54 mm (0.1in)) were also used. The height of the fluid in the cup was 1.048 cm (0.413 in).

3.6.1 Steady State Flow Measurements

The steady state flow measurements were performed in order to determine the "off state" apparent viscosity and flow properties such as shear thinning or shear thickening of MR fluids. The measurements were conducted at controlled strain rate mode with TA Rheometer (Model 1000). The strain rate was varied between 0.1-100 s^{-1}. The double concentric cylinder cell was preferred in order to prevent the fluid flowing out of the cell at high strain rates. The settling of

the magnetic particles in the cone and plate platen could be more pronounced and therefore there would be a very thin layer of clear liquid at the top which would affect the results of our experiments.

The same kind of experiment was also performed using MBTCA-IVb. The period of rotation of the spindle was recorded by a stopwatch and the viscosity was calculated by **Equation 3-5** and it is given as

$$\eta = \frac{\tau P h}{\pi^2 R^4} \tag{3-5}$$

where η is the viscosity, τ is the shear stress, h is the gap, R is the radius, and P is the period. The shear stress was calculated from AC voltage readings of the drag cup motor by

$$\text{logV} < 1.5 \qquad \log\tau = 2.111 * \log V - 0.223 \tag{3-6}$$

$$\text{logV} > 1.5 \qquad \log\tau = 1.852 * \log V + 0.169 \tag{3-7}$$

The shear rates were calculated from the steady state viscosity values as

$$\dot{\gamma} = \frac{\tau}{\eta} \tag{3-8}$$

and plotted against the apparent steady state viscosity values.

3.6.2 Creep-Recovery Measurements

The creep-recovery measurements were conducted at stress controlled mode by TA rheometer at a controlled temperature of 25 ^{0}C. Cone and plate and double concentric cylinder cells were used in these measurements. A constant stress was applied and this stress was attained for a certain period of time. The MR fluid was crept at different stresses and then a resting period was applied. The creep stress and resting time were varied in a controlled manner in order to determine the behavior of the MR fluid under different conditions in order to determine

1. The yield strain of the MR fluids at different stresses
2. The effect of pre-shearing on the creep behavior of the MR fluids

The yield strain was determined from strain versus time plots of compliance (J) versus time plots. The creep –recovery experiments were also performed on MR fluids that were heat treated at 175 ^{0}C for 24 hours.

4.0 RESULTS AND DISCUSSIONS

4.1 Magnetic Particulate Characterization

The carbonyl iron powder was obtained from ISP Technologies. Two kinds of Fe powder were used which are referred as GRADE AS and 3700. GRADE A grade is the reduced iron grade with an average particle size of 7 μm. This grade was "reduced" in hydrogen atmosphere, therefore carbon, oxygen, and the nitrogen concentrations are lower than that of the GRADE B grade, known as "straight" grade, which wasn't exposed to a reduction process. The average particle size for GRADE B is ~ 2 μm. The impurity contents of the powders are given in **Table 4-1**. The oxygen concentration in GRADE B is ~0.4 wt% which suggests that FeO, Fe_3O_4, Fe_2O_3 may be formed.

Scanning electron micrographs which show the morphology of as-received iron grades that were used in this research are given in **Figures 4-1** and **4-2** for GRADE A and GRADE B grades, respectively. Although SEM analysis is not an adequate technique for particle size analysis, the SEM studies revealed that the powders used had a relatively broad size distribution of particles ranging from sub-micrometer to 2-3 μm for GRADE B and particle sizes ranging from 1 to 9 μm for GRADE A.

4.1.1 Particle size distribution (PSD) Analysis

The particle size analysis revealed that as-received Fe powder is highly agglomerated. The ball milling of the powders for 4 hrs and for 24 hours in propylene glycol showed a decrease in the average particle size distribution (**Figure4-3**). Sonication of the dispersion also decreased the PDS. The mean diameter of the particles after 1.5 hour ball milling was measured as 2.39 μm and after 4 and 24 hours of ball milling the mean particle was 1.5 μm. The particle size

distribution of 4 hr and 24 hr ball milled samples did not show a significant difference which can suggest that the ball milling may not have an effect on the further breaking of the agglomerates after 4 hours. Due to the bigger particle size for GRADE A, they tend to settle down faster even though a dispersant was added (Darvan C) and thus the particle size distribution analysis was much harder to perform on these particles.

4.1.2 X-Ray Diffraction Analysis

As has been discussed in the powder diffraction file data (JCPDS), the results of XRD analysis that are presented in **Figures 4-4 and 4-5** for GRADE A and GRADE B grades of iron powder showed 44.84 and 65.21 $^{0}2\theta$ reflections that correspond to BCC (α) Fe. In our analysis we did not observe any peaks related to the impurities and oxide layer. This was expected since the concentration of impurities is relatively small and they may be dissolved in α-Fe and the thickness of the oxide layer may not be enough for X-ray analysis.

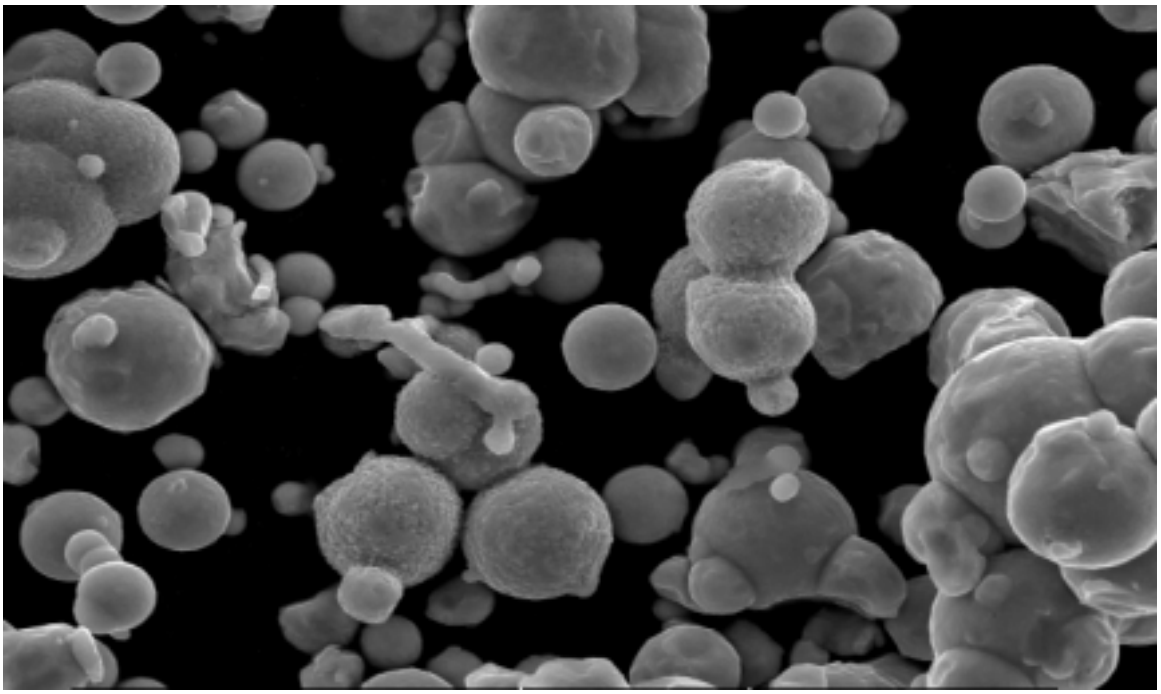

Figure 4. 1Scanning electron micrograph of GRADE A iron powder

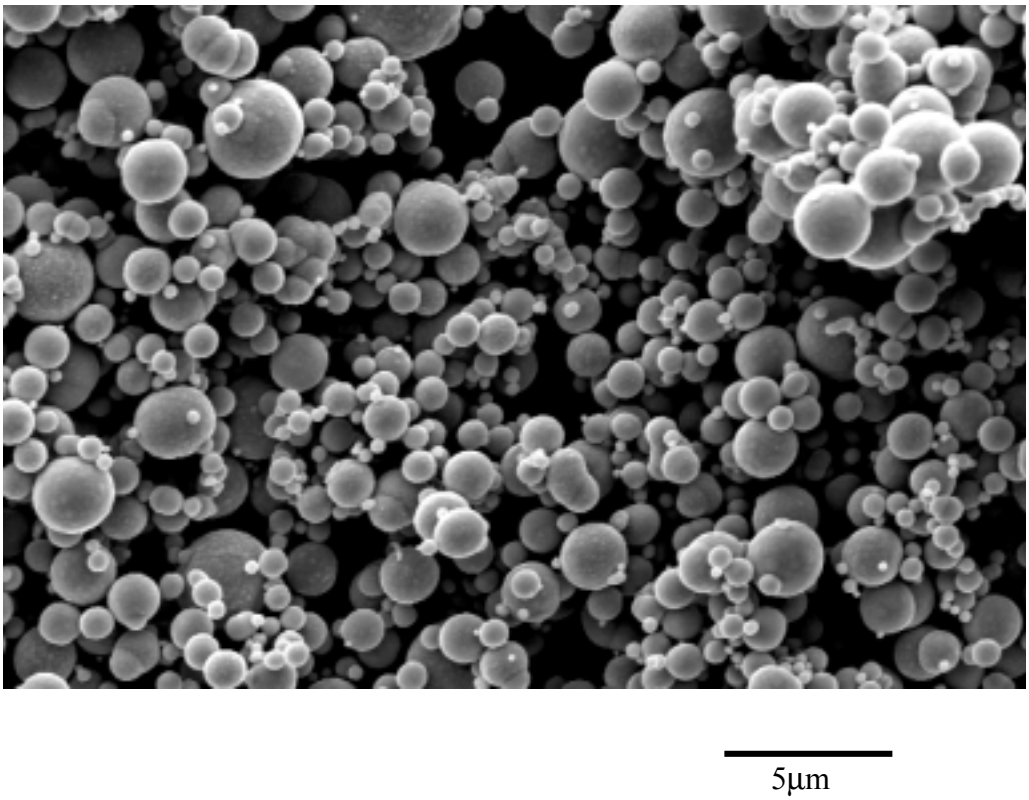

Figure 4. 2 Scanning electron micrograph of GRADE B iron powder

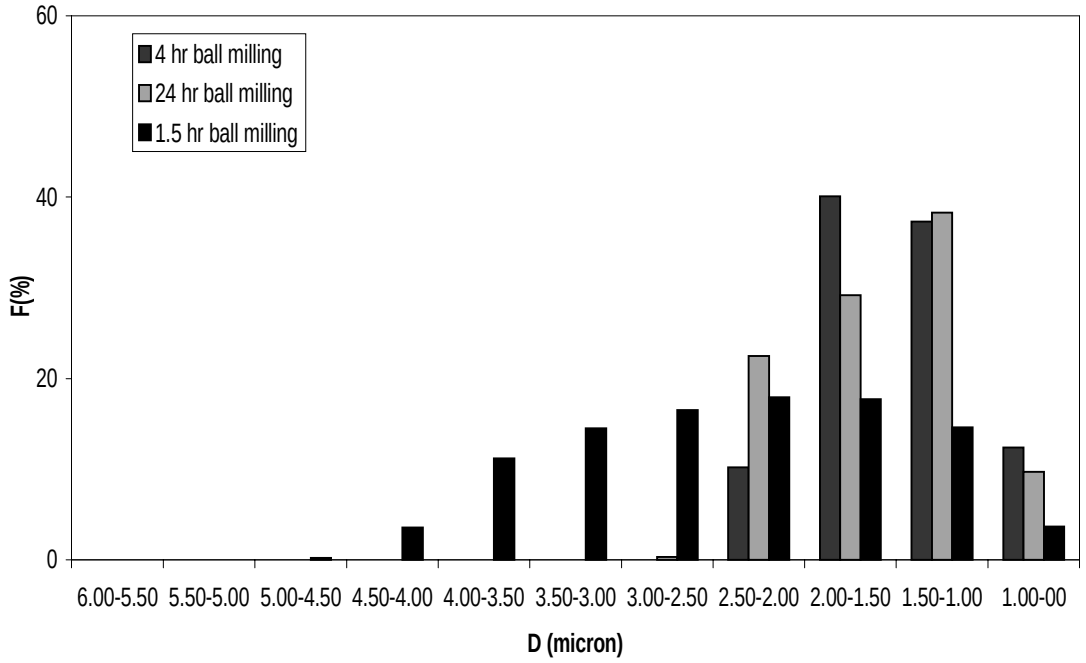

Figure 4. 3 Particle size analysis of GRADE B iron powder after various ball milling periods.

Table 4. 1 The certificate of analysis provided from iron provider, ISP Technologies.

Fe Grades	Average Size (μm)	%Iron	%Carbon	%Oxygen	%Nitrogen
GRADE A	7 - 9	>99.5	<0.3	<0.4	<0.1
GRADE B	2.31	98.2	0.67	0.43	0.69

counts/s

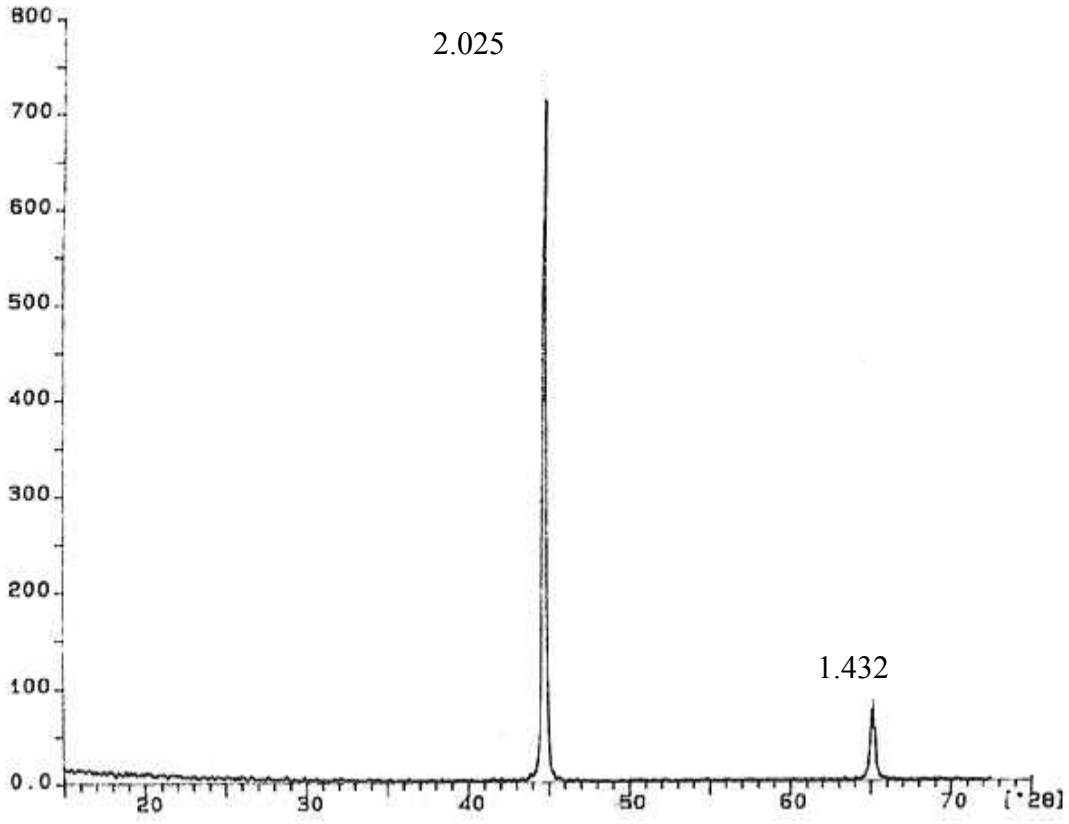

Figure 4. 4 XRD pattern for GRADE A iron powder

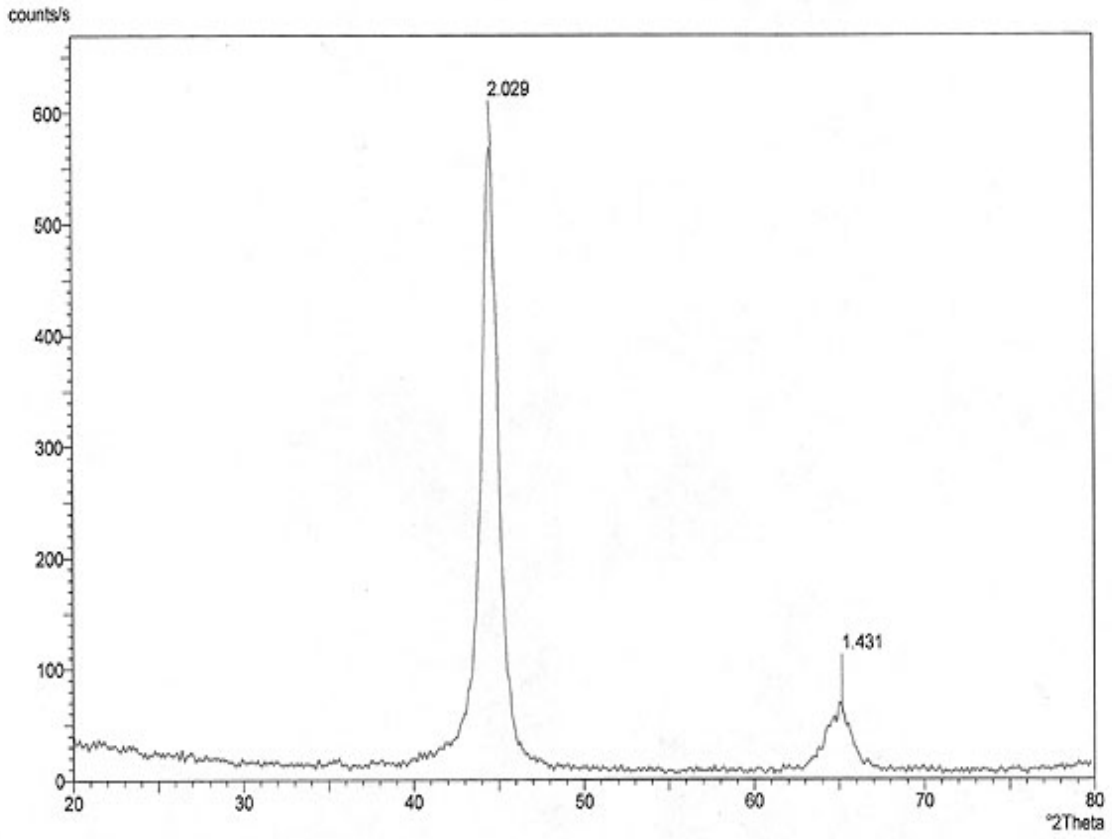

Figure 4. 5 XRD pattern for GRADE B iron powder.

4.1.3 Magnetic Properties

The hysteresis loops of the GRADE A and GRADE B grades of iron powder are presented in **Figures 4-6 and 4-7** respectively. The measured saturation magnetization GRADE A is 207emu/g (2.03T) and that of GRADE B is 193 emu/g (1.89T). These values are smaller than the values for bulk pure Fe reported given in the literature as 2.1 Tesla [36]. The coercivities for the powders were also measured. The remanent magnetization for GRADE A and GRADE B are 2.12 and 0.597emu/gr respectively. The coercivities for GRADE A and GRADE B were measured as 30.51, 14.22 Oe, respectively. These values are higher than those for the values for bulk material coercivity (1.01 Oe). A possible reason for the higher coercivities for iron particles is the presence of impurities, defects and oxide layer on the iron particles. It is known that such defects can cause domain pinning thereby increasing the coercivity. The lower coercivity of the GRADE B was somewhat surprising. It is possible that GRADE B with a broader particle size distribution can provide a denser packing which in turn lead to lower values of measured coercivity. The packing dependence of coercivity was can be fitted closely by [28]

$$H_c = H_{c,0}(1 - p) \tag{4-1}$$

where H_c and $H_{c,0}$ are the coercive force and the coercivity respectively and p is the packing factor. Further investigation is necessary to explain this observation.

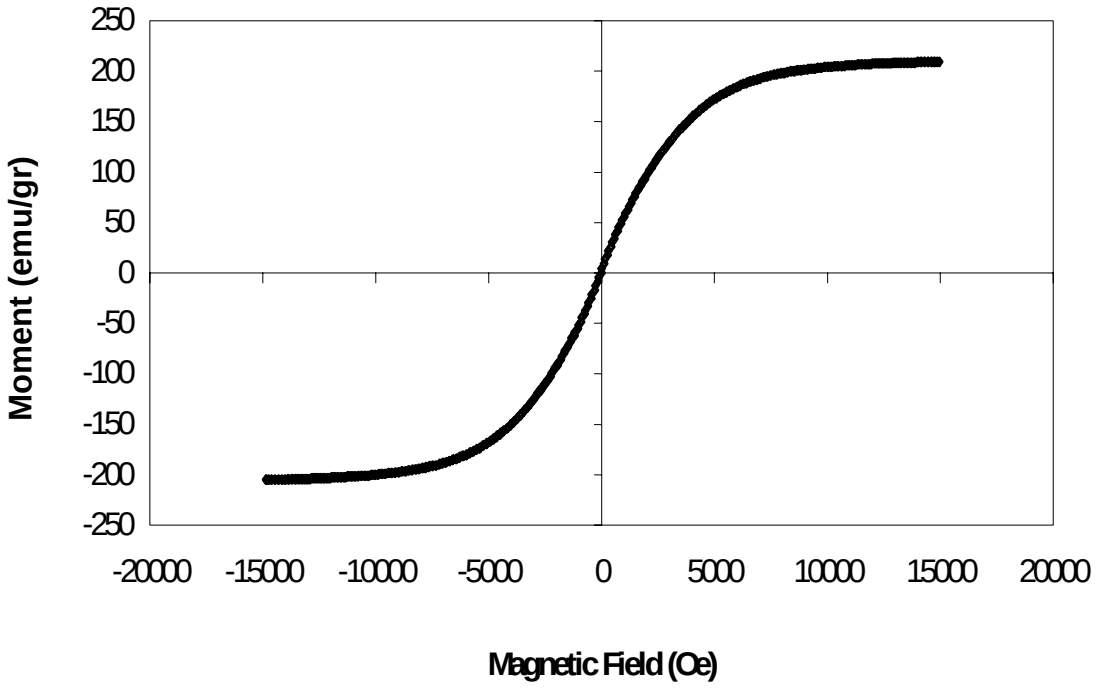

Figure 4. 6 Hysteresis loop (magnetic moment versus applied magnetic field) for GRADE A iron powder

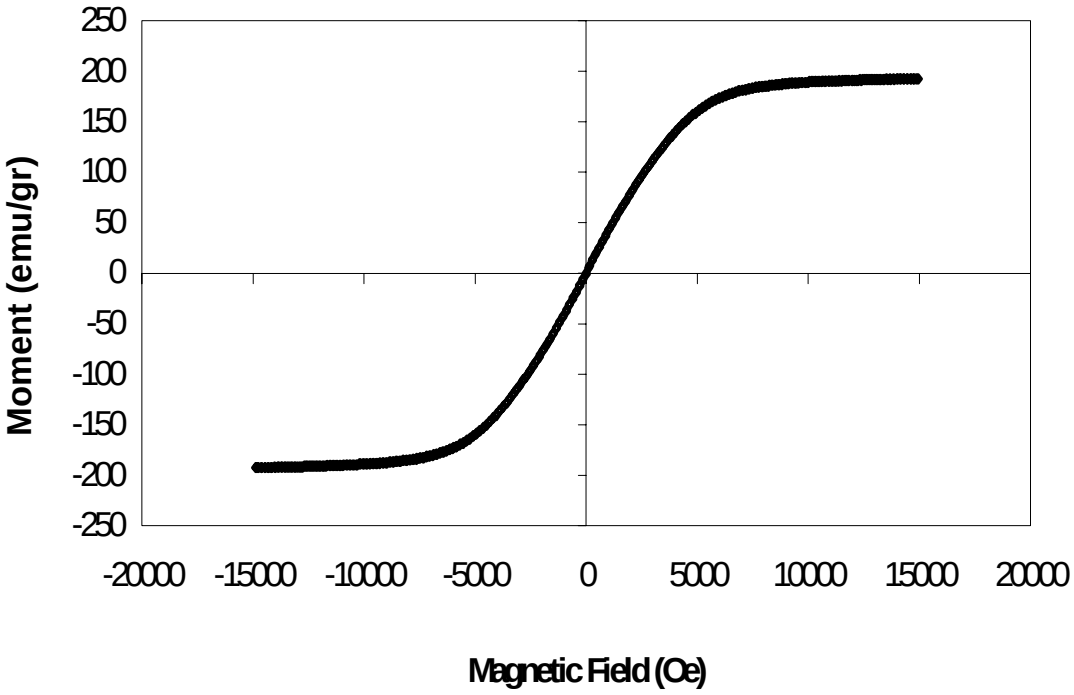

Figure 4. 7 Hysteresis loop (magnetic moment versus applied magnetic field) for GRADE B iron powder

4.2 Synthesis and Characterization of MR Fluids

Throughout this research, we tried to synthesize MR fluids in various carrier liquids using different surfactants and different grades of iron (Fe) powder. Polydimethylsiloxane (PDMS – 5 and 100 cSt) and colloidal silica in ethylene glycol monopropyl ether (NPC-ST) were used as based liquids and hydroxyl terminated PDMS (SURFACTANT A, 90-150 cSt) and polyvinylpyrrolidone (SURFACTANT B) were used as surfactants respectively. NPC-ST based MR fluid was patented by Phule [103].

PDMS with kinematic viscosity of 5 and 100 cSt at room temperature which correspond to 0.0045 and 0.096 Pa-s dynamic viscosity respectively, were used in the synthesis of the MR fluids. The conversion of viscosities is given in Appendix B. The disadvantage of using lower viscosity PDMS (5 cSt) was the high volatility of these products whereas fluids with viscosities of 50 cSt or greater have negligible vapor pressure.

The viscosity of the SURFACTANT A used was 90-150 cSt at room temperature. PMDS and SURFACTANT A were provided from Aldrich. The viscosities of PDMS (100 cSt, 5 cSt) and the mixture of PDMS+SURFACTANT A were measured with TA instruments. Prior to these measurements, viscosity of polybutene which was predetermined by falling ball method was measured for calibration purposes. The equation for the falling ball calculation is given as:

$$\log\eta = \frac{3420.7}{T(K)} - 7.732 \qquad (4\text{-}2)$$

The viscosity of polybutene according to **Equation 4-2** at 25 ^{0}C was calculated as 558.2 Pa-s. The measured value of viscosity was ~596 Pa-s. The apparent viscosity versus shear rate for polybutene is given in **Figure 4-8**. The higher value of the measured viscosity can be due to "drowned" edge or "sea" of liquid around the cone. The flow will extend out into the sea of liquid, increasing the torque. The viscosities of 5 and 100 cSt PDMS were then measured with

TA rheometer using cone and plate geometry and they are presented in **Figure 4-9 (a)** and **(b)** respectively. In the same figures the viscosity of these fluids with the addition of SURFACTANT A are also presented. The fluids show Newtonian behavior with or without the surfactant. The addition of SURFACTANT A did not make a difference in the viscosity of the mixture. However, the viscosity of the PDMS (5 cSt) and SURFACTANT A mixture show an increase in the viscosity from $4.7x10^{-3}$ to $6.7x10^{-3}$ Pa-s.

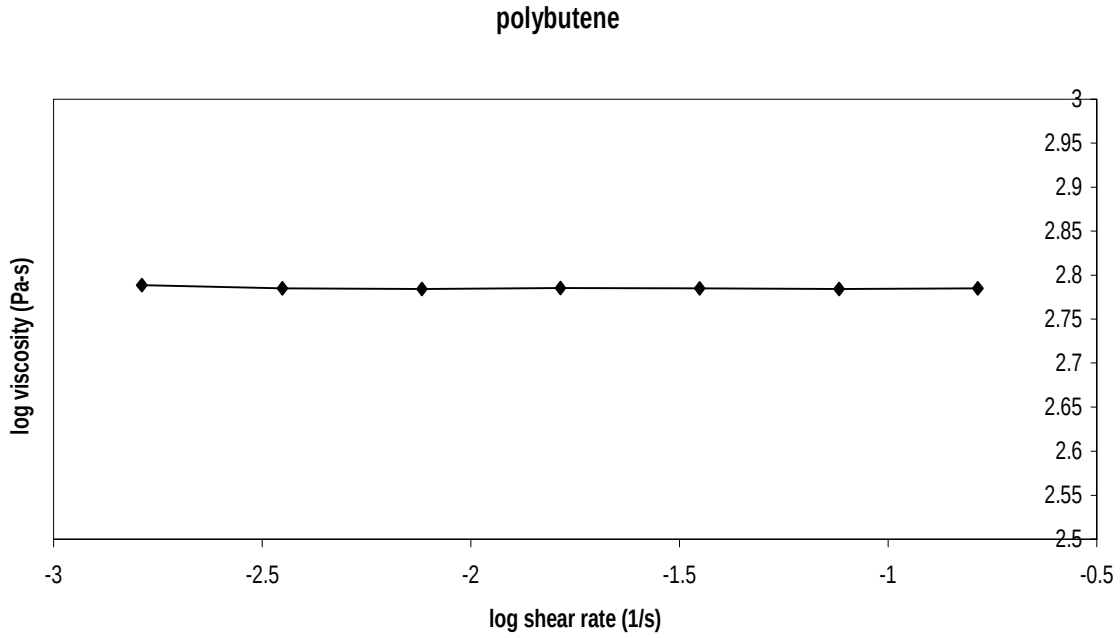

Figure 4. 8 Double logarithmic plot of viscosity versus shear for Polybutene

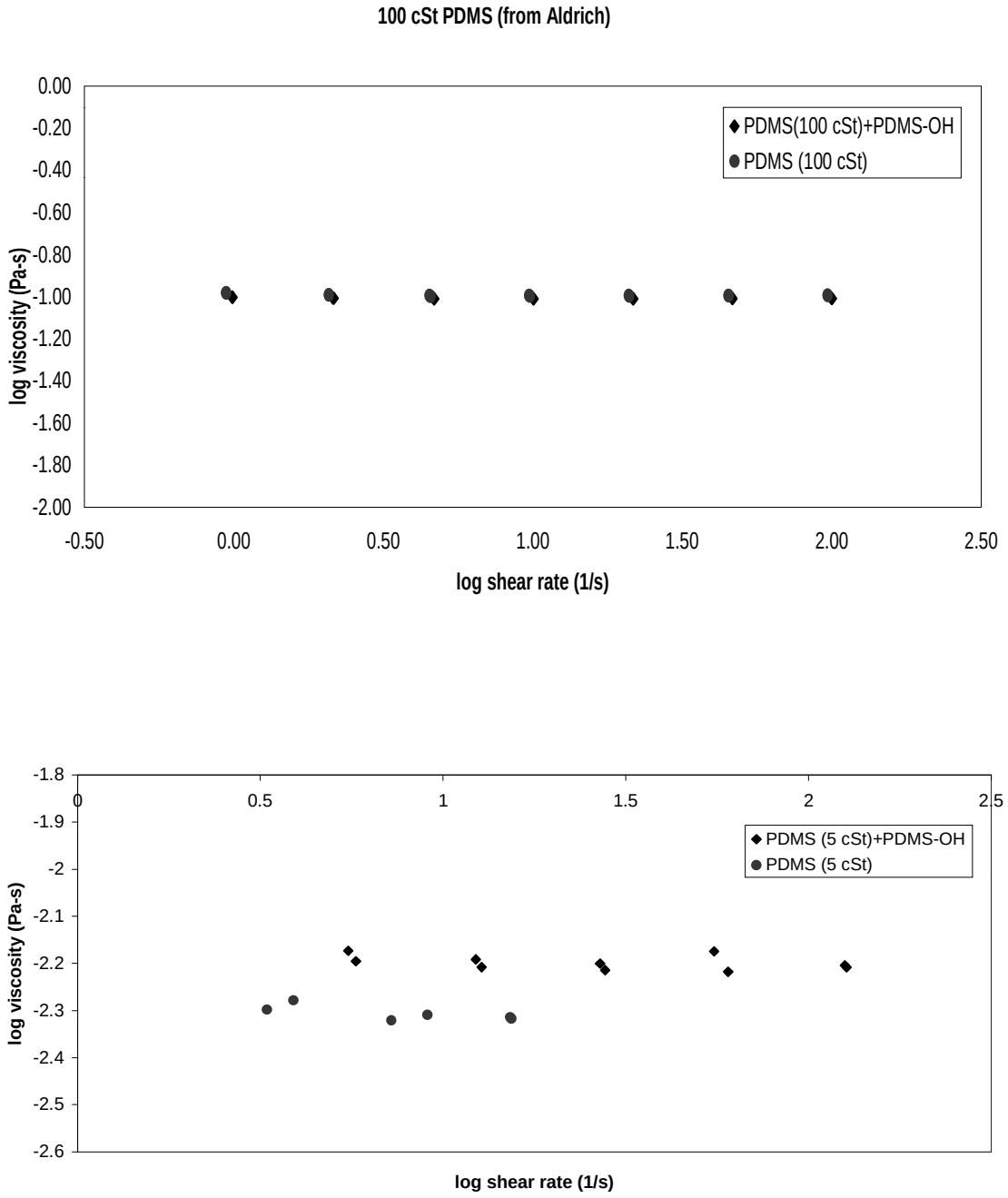

Figure 4. 9 Double logarithmic plot of viscosity versus shear rate for (a) 100 cSt PDMS and (b) 100 cSt PDMS+SURFACTANT A

The flow chart of synthesis of MR fluids is given in Section 3.1. Typical starting batch size was 100 ml and 128 ml for PDMS and NPC-ST based fluids, respectively. However during the synthesis process some fluid was stuck on the mixer and spatula, so ~30 gr of fluid was lost. The actual amount of each starting materials weighed for one batch are listed in **Table 4-2.** The density of 40 vol% iron powder and 100cSt PDMS based MR fluid was measured to be 3.69 ± 0.02 gr/cm^3.

The SEM micrographs, secondary electron and backscattered images, of the PDMS and NPC-ST based fluids are presented in **Figures 4-10, 4-11, 4-12, and 4-13** respectively. The coating around the iron particles in PDMS based MR fluid is less visible than the coating around iron particles in NPC-ST. In the NPC-ST based MR fluid the coating around the iron particle is clearly seen. The contrast between the coating which is made from silica and SURFACTANT B polymer in NPC-ST based MR fluids is seen better in the backscattered SEM image **(Figure 4-13)** due to the differences in the average atomic number. The elemental analysis of the PDMS based MR fluid was performed by EDS. Iron (Fe) and silicon (Si) were detected in the MR fluid.

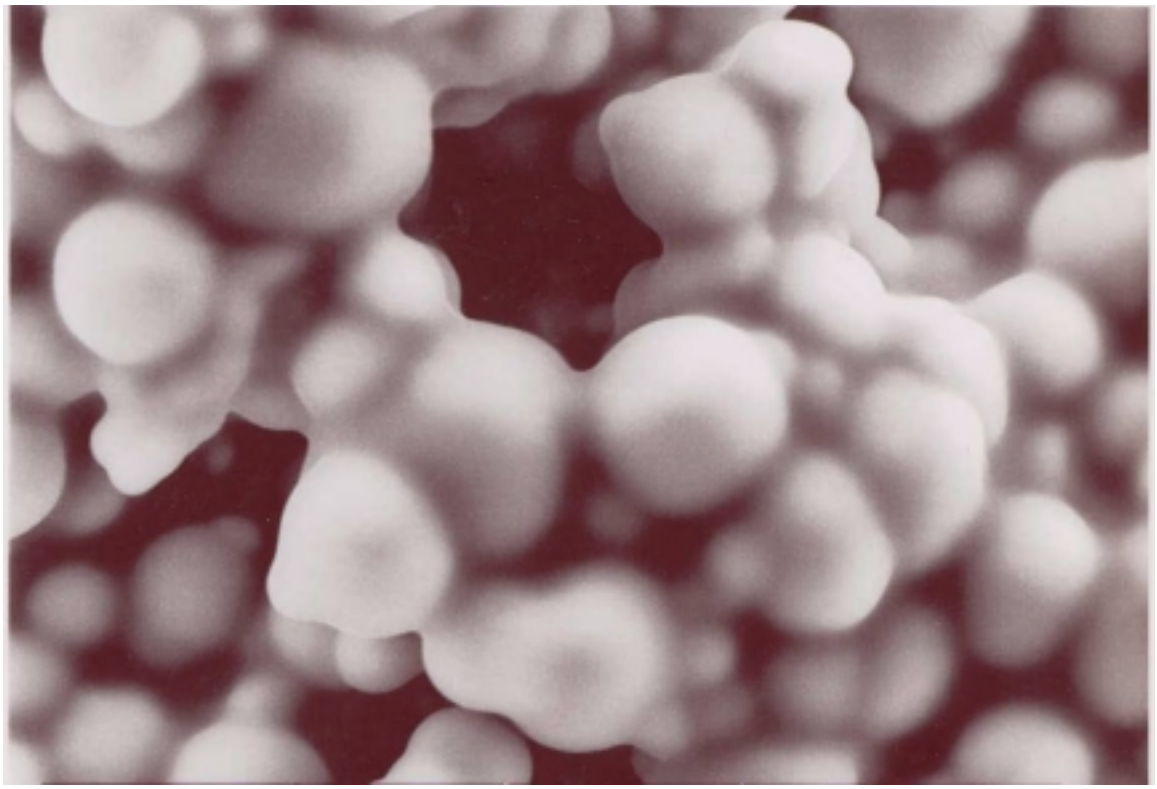

Figure 4. 10 Secondary electron image of PDMS based MR fluid

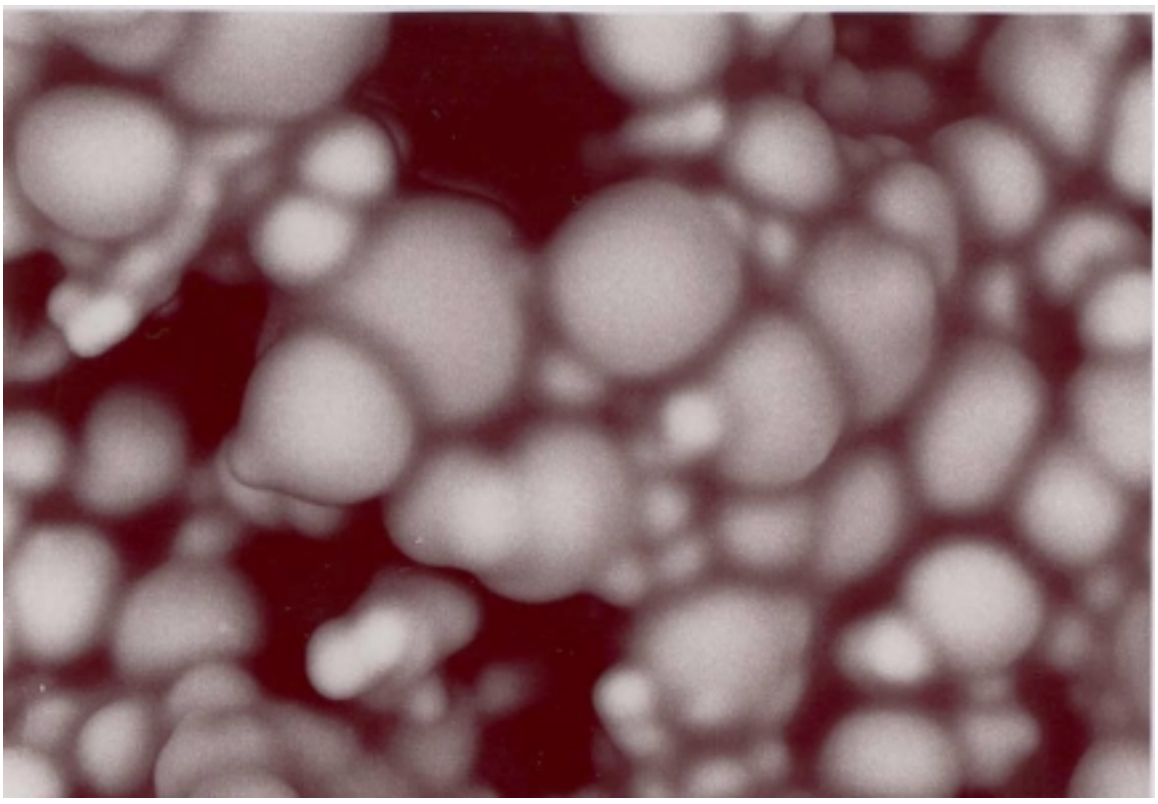

Figure 4. 11 Backscattered electron image of PDMS based MR fluid

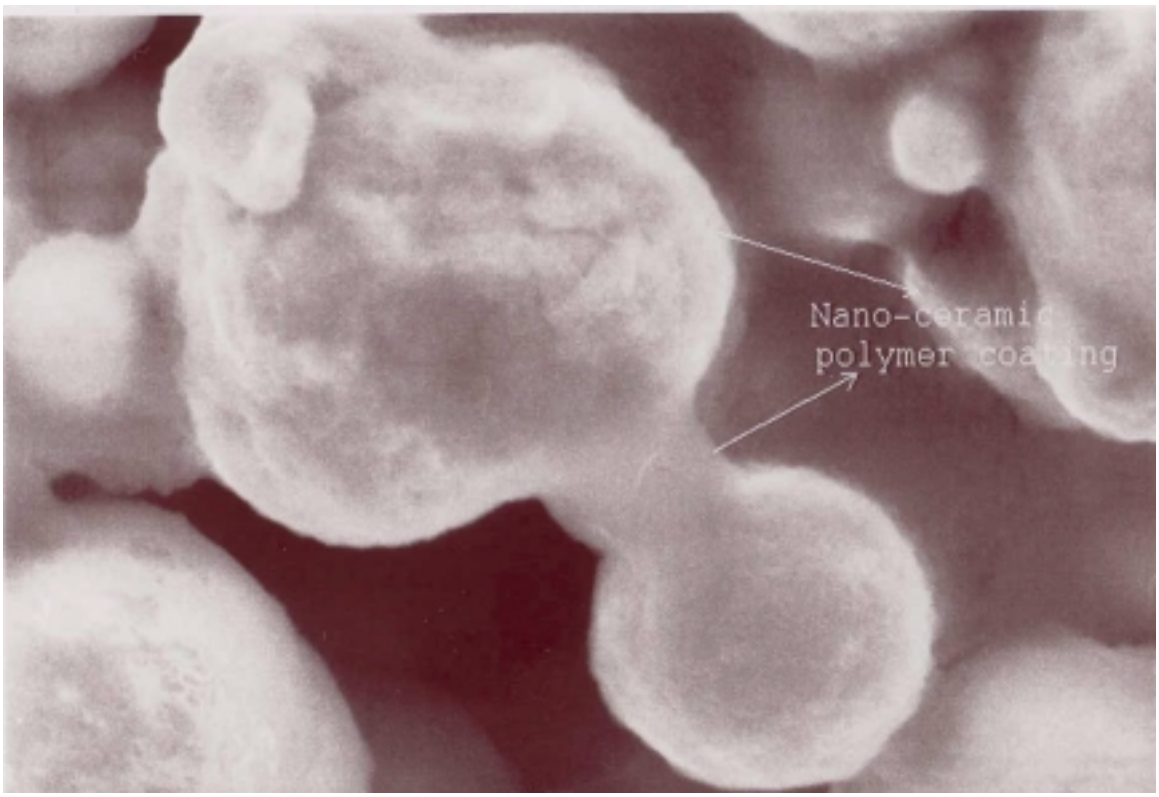

Figure 4. 12 Secondary electron image of NPC-ST based MR fluid.

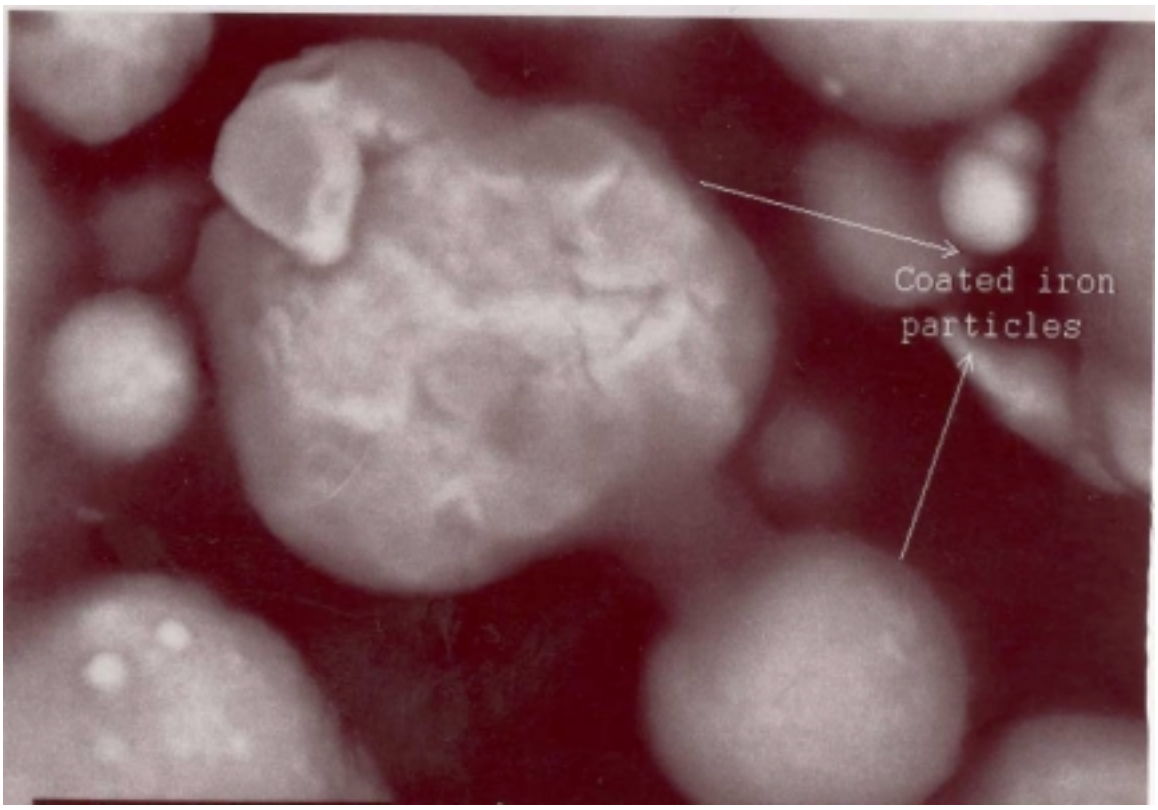

Figure 4. 13 Backscattered image of NPS-CT based MR fluid

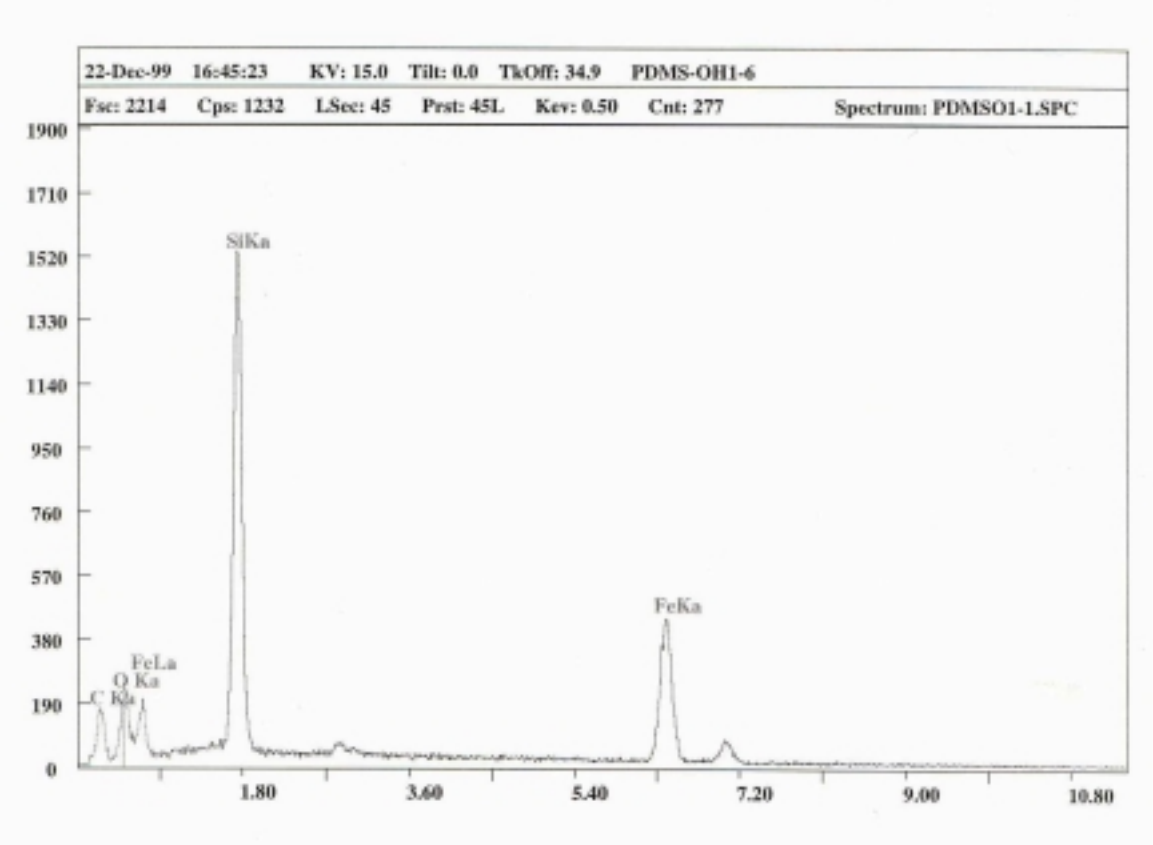

Figure 4. 14 EDS pattern for PDMS based MR Fluid.

Table 4. 2 : Actuals amounts used in PDMS based MR fluids

	Volume%	Density (g/cc)	Volume (mL)	Weightt%	Mass (g)
PDMS (100cSt)	55.0	0.960	55.0	14.3	52.80
PDMS (5 cSt)	55.0	0.913	55.0	13.7	50.22
SURFACTANT A (90-150 cSt)	5.0	0.970	5.0	1.3	4.85
GRADE A iron powder	40 33	7.8	40 33	84.4 81.7	312.00 257.40
GRADE B iron powder	40 33	7.8	40 33	84.4 81.7	312.00 257.40

Table 4. 3: Actuals amounts used in NPC-ST based MR fluids

	Volume %	Density (g/cc)	Volume (mL)	Weight %	Mass(g)
NPC-ST -20	43.0	1.05	55.05	12	57.80
Octanol	17.0	0.83	21.78	4.0	18.01
GRADE A iron powder	40 33	7.8	51.22 33	84.0 81.7	399.0 286.0
GRADE B iron powder	40 33	7.8	40 33	84.40 81.7	399.0 286.0
SURFACTANT B (MW 29000)		-	-		1.04

4.3 Redispersibility and Stability of MR Fluids

Throughout this research, one of our goals was to synthesize the most stable and redispersible MR fluid. The stability and redispersibility of MR fluids depend on the particle size, viscosity of the carrier liquid, density difference between the dispersed magnetic phase and the carrier liquid, and the interaction energies of the magnetic particles as discussed above.

Mostly qualitative observations, such as stirring with spatula or observing the settling of the particles have been conducted in order to evaluate the stability and redispersibility of MR fluids. Chin and co-workers [80] measured the dispersion stability of MR fluids containing carbonyl iron particles in silicone oil with Co-γ-Fe_2O_3 or Cr_2O_2 as additives to provide steric repulsion between Fe particles. They calculated the ratio of sedimentation by using Equation

$$\text{Ratio of Sedimentation}=1-\frac{\text{Volume of Supernatant}}{\text{Volume of entire suspension}} \tag{4-3}$$

Their measurements revealed that as the volume fraction of the stabilizing additive increases, the ratio of sedimentation gets smaller. Other than observing and recording the volume of the settled particles in gravitational field, Gorodkin and co-workers [108] developed a device to measure the sedimentation velocity of magnetic particles based on the principle of measuring the ac inductance of solenoid surrounding the MR fluid. As the particles settled out, the relative permeability μ will decrease in proportion to the number of particles leaving from within the solenoid region.

The MR fluids synthesized in PDMS and NPC-ST was put in graduated cylinder and the clear liquid at the top was recorded over a period of time. Our observations showed that GRADE B in 100 cSt PDMS and GRADE A in NPC-ST showed promising results. The MR fluids synthesized by using GRADE A and NPC-ST showed gel like behavior where there was no settling of particles. However, when GRADE B was used in NPC-ST, there was settling of

particles and caking was also observed. The use of nano-scale silica spheres and a polymer forms a multitude of nano-bridges in between the silica particles and this nano-ceramic-polymer network surrounds the magnetic particles. The bridging polymer has the ability to adsorb on the surface of magnetically soft particles. This network is strong enough to resist gravitational settling of the particles and therefore prevent them approaching a distance where particle interactions will lead to permanent aggregation. However, when the same kind of MR fluid was synthesized with GRADE B type iron powder, settling of the magnetic particles and a little cake like formation were observed. The cake-like formation could be broken by the application of mechanical energy, such as rigorous stirring. The difference between these two MR fluids may be attributed to the surface oxidation of the Fe particles. GRADE B may have more surface hydroxyl groups [101] and the polymer, SURFACTANT B, might be adsorbed on the magnetic particles as well leaving a weaker network. Thus this may cause the particles to settle out.

Among the MR fluids, 100 cSt PDMS, GRADE B Fe powder and SURFACTANT A gave a better result in terms of redispersibility of stability. The hydroxy terminated PDMS was adsorbed on the Fe particles through the surface hydroxyls of the iron particles, providing steric repulsion. The settling of GRADE A and GRADE B was observed in 5 cSt PDMS, however as can be seen in **Figure 4-15,** this settling was minimized by using a higher viscosity carrier liquid, such as 100 cSt PDMS. The reason for GRADE A and PDMS based MR fluids showing more settling than GRADE B based MR fluids can be due to the bigger particle size of GRADE A. In this research, although GRADE A particles in NPC-ST give best results in terms stability and redispersibility, the NPC-ST has very low boiling temperature. Evaporation could be a problem in our experiments. Rapid evaporation and settling of particles in 5cSt PDMS also focused us on 100cST based MR fluids especially in off state rheological measurements.

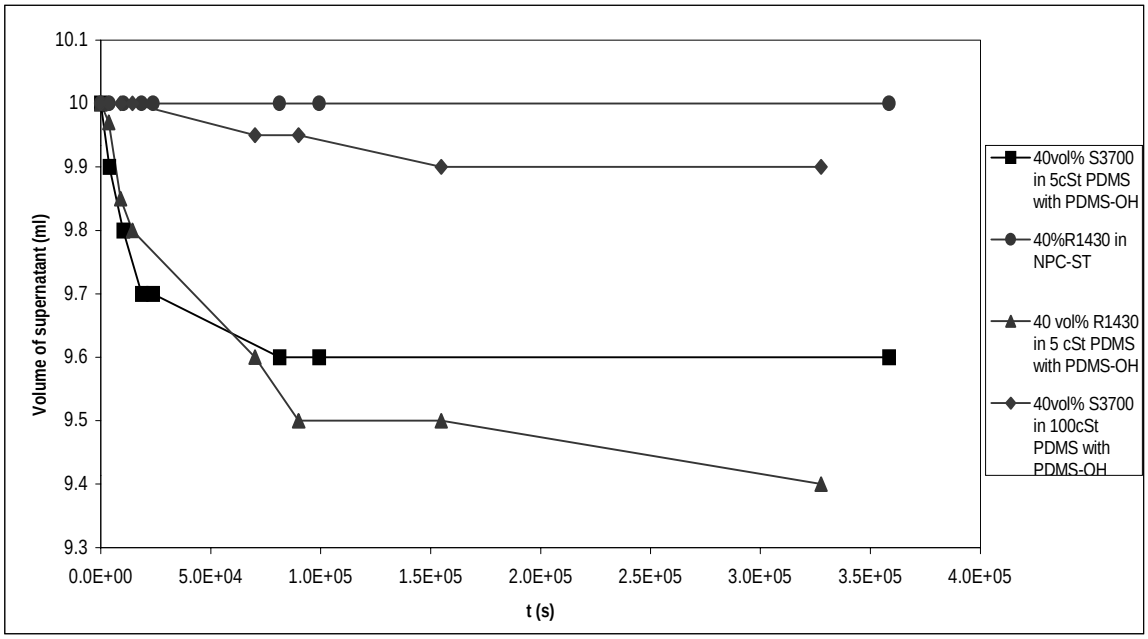

Figure 4. 15 Amount sedimentation over time for various kinds of MR fluids

4.4 Calculation of the Magnetic Dipole-dipole Interaction Energy

The lack of redispersibility of most MR fluids can be linked to the small but non-zero remanent magnetization of the magnetic particles. In order to gain more quantitative understanding of the influence of remnant magnetization, the magnetic contribution of the inter-particle potential energy was calculated based on the assumption of the simple cubic arrangement of the magnetic particles. In our calculations, we assumed that each soft magnetic particle, in the absence of a magnetic field, can be treated as a magnetic dipole moment with a dipole moment (M) such that:

$$M = \mu_0 M_r \frac{4}{3}\pi\left(\frac{a}{2}\right)^3 \tag{4-4}$$

where $\mu_0 M_r$ is the remnant magnetization of the material, μ_0 is the magnetic permeability of vacuum equal to $4\pi*10^7$ Weber/Ampere-m, and a is the average diameter of the particles used. The interaction energy between two magnetic particles can be calculated using the following equation.

$$V_m = \frac{-pM^2}{4\pi\mu_0 R^3} \tag{4-5}$$

where R is the distance between the center of two spherical particles and p is the alignment of the two particles ranges from –2 to 2 and given as

$$p = 3\cos^2\phi - 1 \tag{4-6}$$

where ϕ is the angle between the magnetic moment of the particle and the central radius vector R between the particles. The magnetic particles are aligned when ϕ =0 and p=2.

In order to obtain the interparticle distance in an MR fluid, we assumed that the particles in 0.33 volume fraction in an MR fluid to be packed in simple cubic (SC) arrangement.

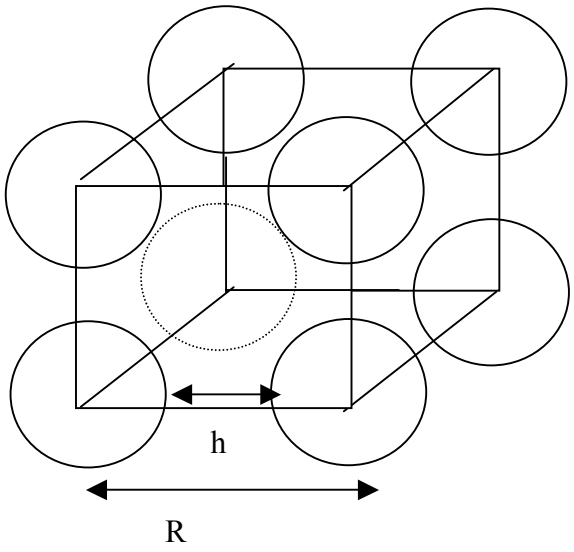

Figure 4. 16 Schematic presentation of magnetic particles in simple cubic (SC) arrangement

For SC arrangement the interfacial distance, h, between the particles became 0.16245a and center to center distance, R, will be ~1.1624a. The **Equation 4-5** becomes

$$V_m = \frac{-p(\mu_0 M_r)^2 a^3}{72\mu_0} \tag{4-7}$$

.

The magnetic interaction energy was then normalized to $k_BT=4.115*10^{-21}$J at 25 ^{0}C. The scaled interaction energies as a function of interfacial distances of a 0.33 volume fraction Fe, MnZn, and NiZn ferrite based MR fluids were presented in **Figure 4-17**. The particle size was varied from 6μm to 100 nm and the magnetic properties of different size particles are assumed to be the same.

In MR fluids, in addition to the magnetic interactions discussed above, van der Waals interactions are also present. In order to compare the van der Waals and magnetic interactions we also calculated the van der Waals energy between the magnetic particles using the following equation [32].

$$V_{VDW} = -(\frac{A_{212}}{6})\left\{\left[\frac{2}{(l^2+4l)}\right]+\left[\frac{2}{(l+2)^2}\right]+\left[\ln\frac{(l^2+4l)}{(l+2)^2}\right]\right\} \tag{4-8}$$

where l = 2h/a and h is the interfacial distance and a is the particle diameter. For simplicity we have assumed that the effective Hamaker constant for all MR fluids (A_{212}) is 10^{-16} J.

From **Figure 4-17**, it can be seen that the magnetic interactions originating from remnant magnetization are strong with respect to the distance and their influence on the formation of a cake-like formation or agglomeration of magnetic particles used is MR fluids is expected to be quite significant. **Figure 4-17** also indicates that for smaller particles (e.g. 2 μm Fe), with similar magnetic properties, the magnitude of the interactions is significantly smaller. This suggests that MR fluids prepared using finer particles may exhibit better redispersibility, especially if surfactants can be adsorbed on the particles. Kormann and co-workers [109] synthesized an MR

fluid based on ultrafine (~100nm) ferrite particles. However, the disadvantages of using ultrafine particles are that the dipole-dipole interactions are also small even in the presence of magnetic field and thus the yield stress achieved is also smaller and the yield stress lacks temperature stability. Since the same valeu of Hamaker constant was assumed for different materials (e.g. Fe, MnZn , NiZn), the effective van der Waals energy values for 2 μm iron and ferrite particles do not show a significant change.

The short range van der Waals interactions and long range magnetic interactions that could result from the remnant magnetization can play an important role on the stability and redispersibility of the MR fluids. The calculations of these interaction energies which are additive in nature suggest that MR fluids with enhanced redispersibilty can be prepared by increasing the average interparticle distance. Diluting the MR fluid would increase the interparticle distance, however it would also decrease the strength of the MR fluid. Using additives that would coat the surfaces of the magnetic particles by providing steric or electrosteric repulsion may be a more practical way to enhance the stability and redispersibility and maintaining the high strength of MR fluids.

Table 4. 4: Comparison of magnetic dipole-dipole energies for magnetic particles in 33% MR fluids.

	M_r [emu/gr]	a [μm]	Average h [μm]	V_m [Joules]	V_m/k_BT (298K)
MnZn Ferrite	1.68	2.30	0.374	-2.65×10^{-17}	-6400
NiZn Ferrite	1.31	2.12	0.344	-1.6×10^{-14}	-3900
Fe	1.20	8.0	0.975	-6.61×10^{-16}	-161000

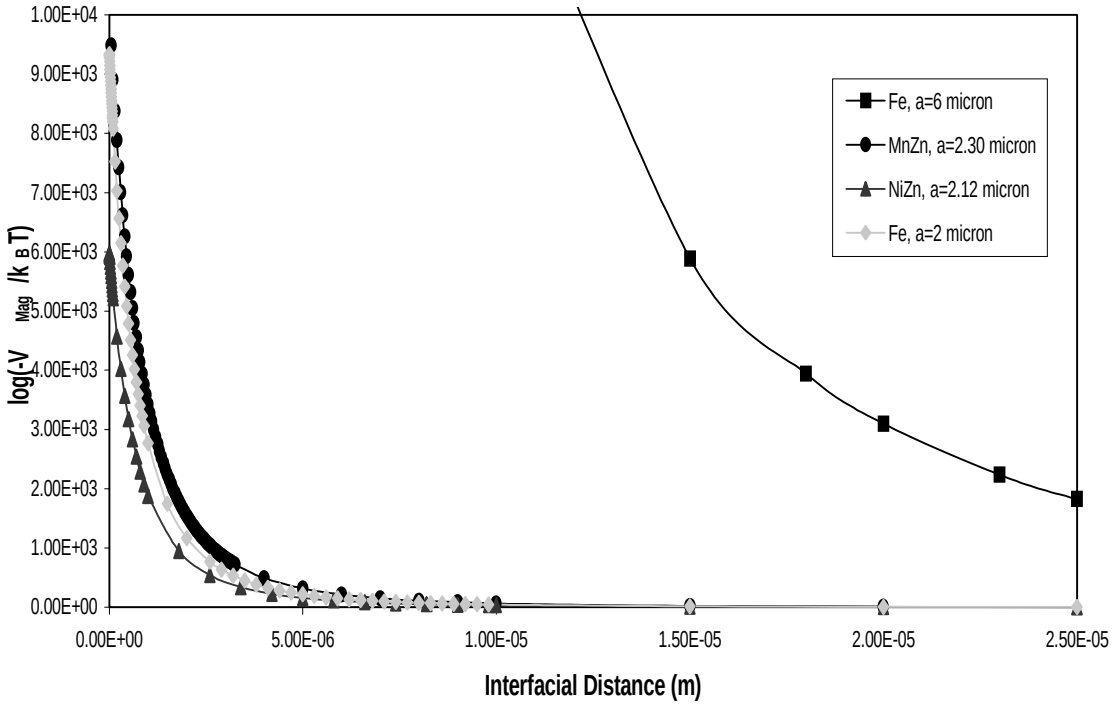

Figure 4. 17 Scaled magnetic energy as a function of interfacial distance (h) for particles in 6 and 2 μm iron, MnZn, and NiZn ferrite based MR fluids

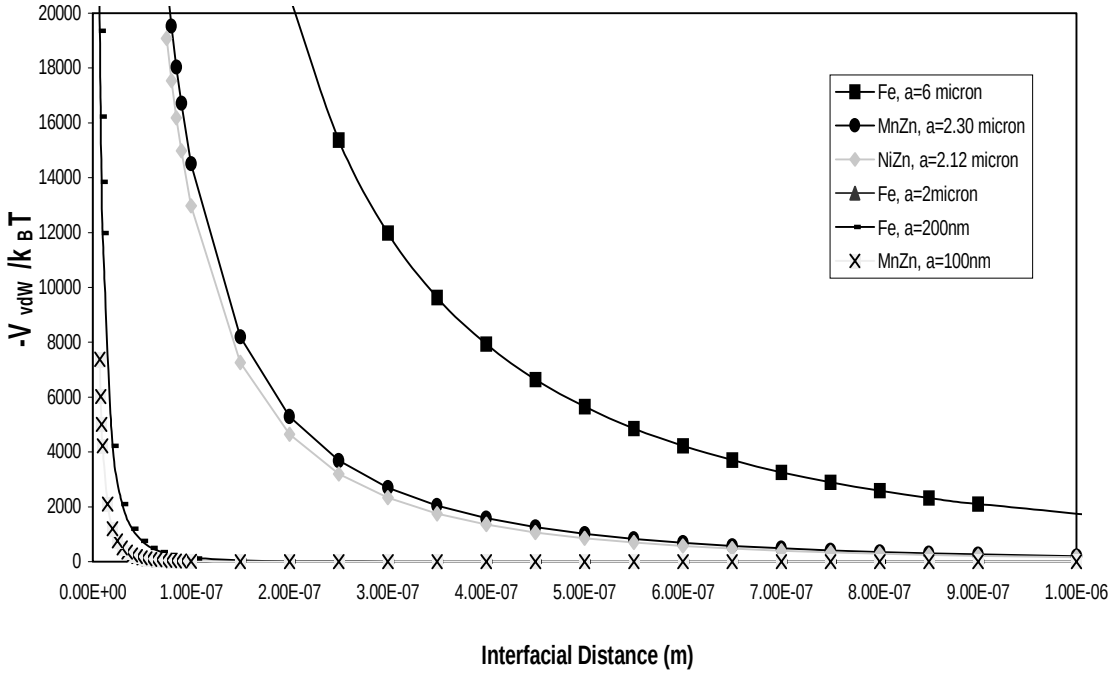

Figure 4. 18 Scaled van der Waals energy for irom particles (diameter=6, 2 μm and 200nm), MnZn (diameter=2.30 μm and 100 nm) and NiZn ferrite (2.12 μm) particles

4.5 Rheological Properties

4.5.1 On State Rheological Measurements

The "on-state" rheological measurements were performed on MR fluids prepared using GRADE A and GRADE B iron powders. The dependence of dynamic yield stresses on applied magnetic flux density, for GRADE A and GRADE B based MR fluids with particle volume fraction of 0.33 and 0.40 are presented. **Figures 4-19 and 4-20** present the shear stress versus strain rate plots for 33 and 40% GRADE A based MR fluids, respectively. The shear stress versus strain rate plot for 33 and 40 vol% GRADE B based MR fluids are shown in **Figures 4-21 and 4-22,** respectively.

The dynamic yield stress of MR fluid was calculated according to Bingham Plastic model [4]:

$$\tau = \tau_{ys} + \eta\dot{\gamma} \tag{4-9}$$

where τ is the shear stress, η is the viscosity, τ_{ys} is the dynamic yield stress and $\dot{\gamma}$ is the strain rate. The shear stresses for the double -Couette rheometer were calculated by using the torque values measurements by the torque transducer. The dynamic yield stress was then determined by extrapolating the shear stress vs strain rate curve to zero strain rate at which the intercept showed the dynamic yield stress of the MR fluids.

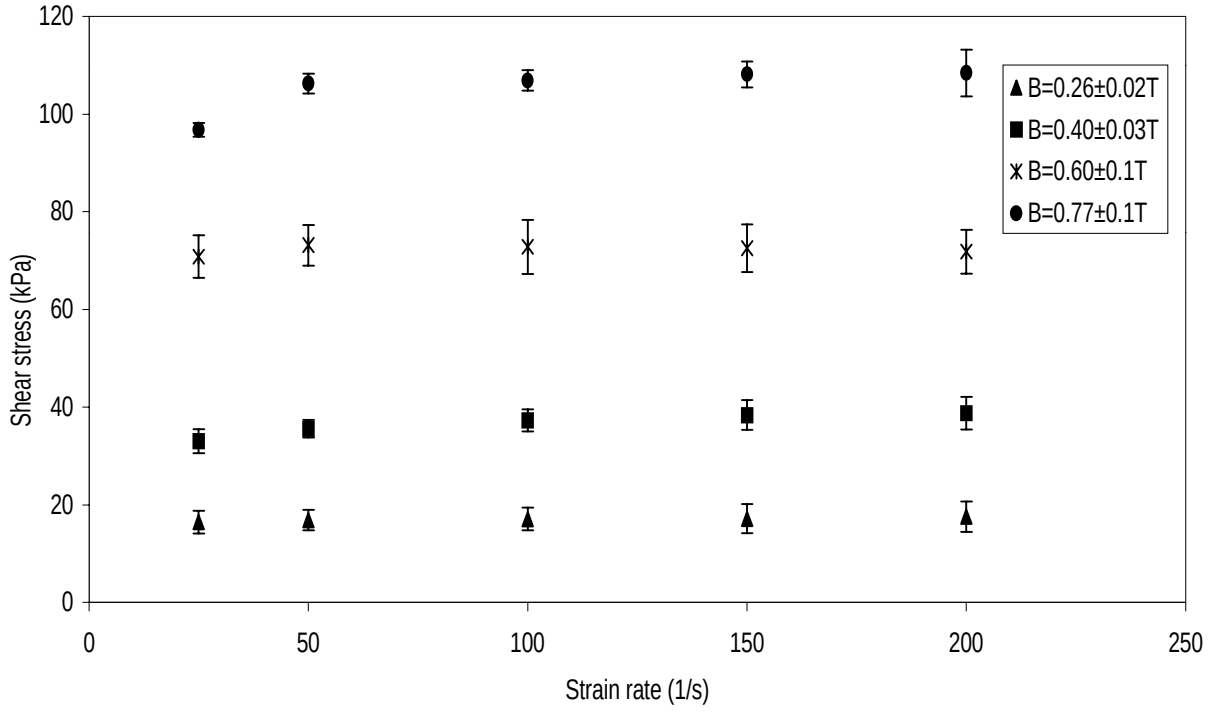

Figure 4. 19 Shear stress vs. strain rate for 33 vol% GRADE A grade iron powder based MR fluid

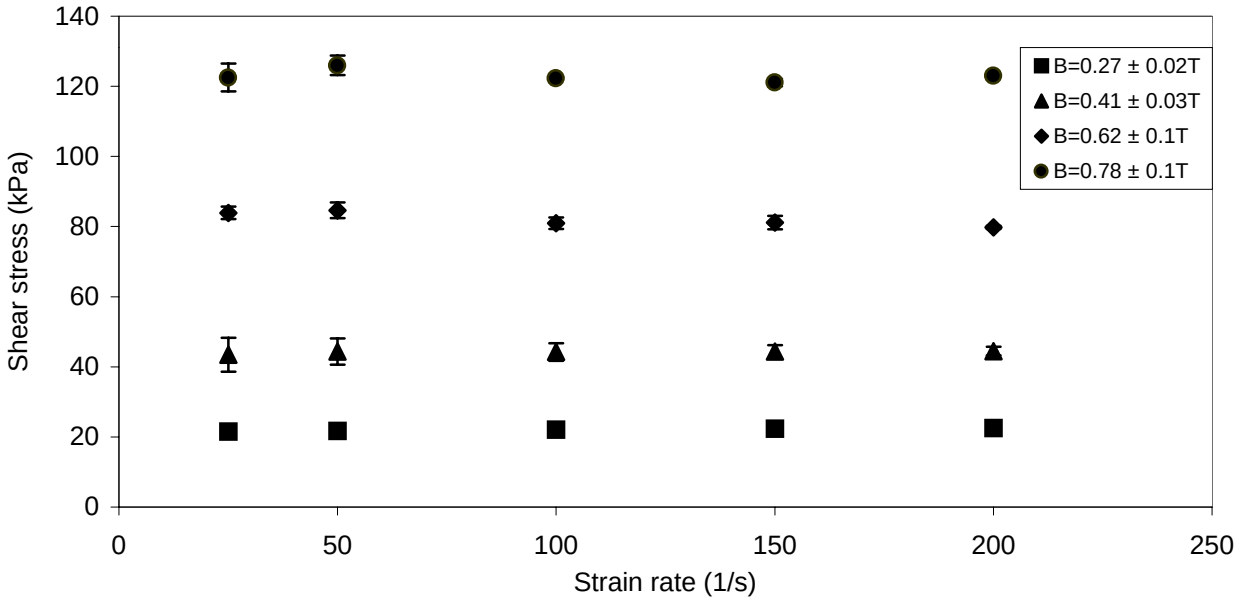

Figure 4. 20 Shear stress vs. strain rate for 40 vol% GRADE A iron powder base MR fluid

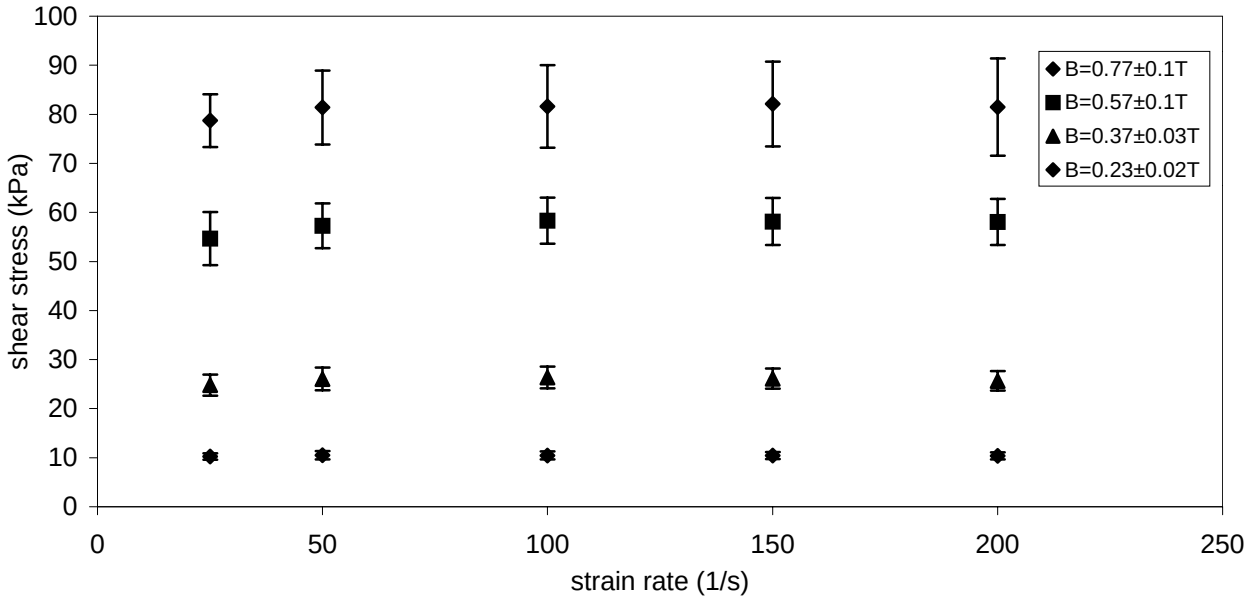

Figure 4. 21 Shear stress vs. strain rate for 33 vol% GRADE B iron powder based MR fluid

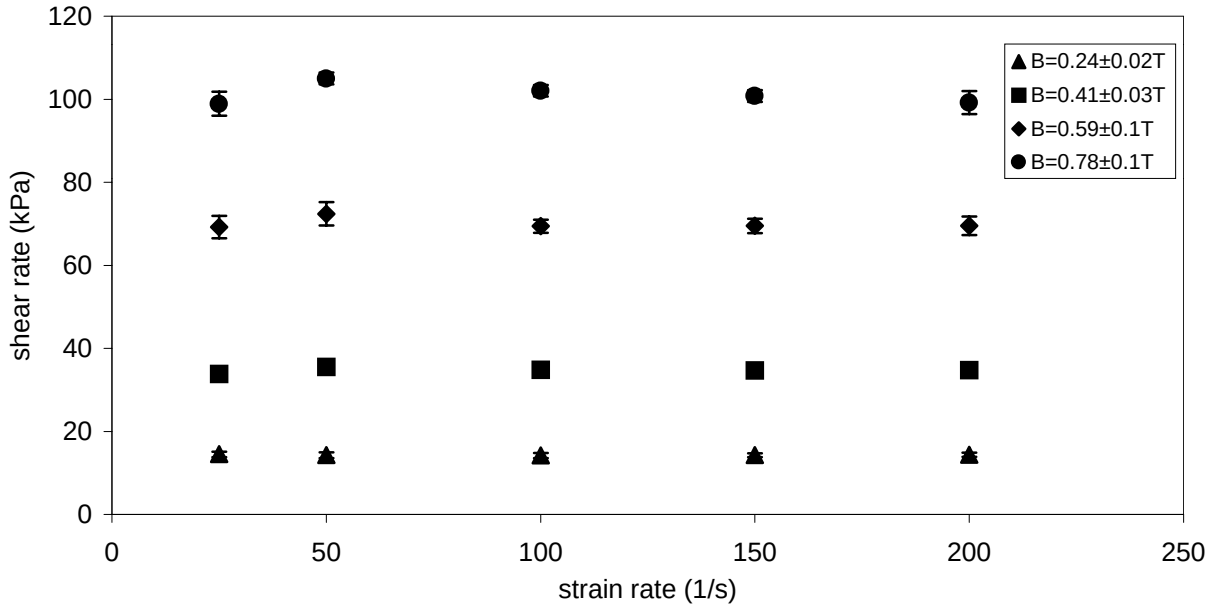

Figure 4. 22 Shear stress vs. strain rate for 40 vol% GRADE B iron powder based MR fluid

In **Table 4-5 and 4-6**, we compare these experimentally measured values of dynamic yield stresses with those predicted by mathematical models at high magnetic fields presented by Ginder and co-workers [68]. A word of caution may be in order here. The measured dynamic yield stresses may be artificially higher than the real values especially at higher magnetic fields, due to heating and evaporation of some of the carrier liquid thereby causing an increase in the volume fraction of the iron powder. Another cause for apparently higher yield stress values is the solid-liquid separation again giving rise to an increased volume fraction of iron.

At higher flux densities (B~0.8T) the values predicted by mathematical model match well with the experimental values. For MR fluid based on smaller particles Fe powder (GRADE B) show an apparently higher deviation from the value predicted by the model. However, when we account for the observed smaller value of $\mu_0 M_S$, then the predicted and measured values match rather well.

The models that Ginder and co-workers developed [68] predict the flux density-yield stress relationship for different field intensities. At very low levels of applied magnetic field (H), where M is expected to be linearly related to H, the relation between the yield stress and the applied field is given by

$$\tau_{ys} \alpha \phi \mu_0 H^2 \qquad (4\text{-}10)$$

where ϕ is the particle volume fraction, H is the applied field and μ_0 is the permeability of the free space ($4\pi \times 10^{-7}$ H/m).

At flux densities that are clearly above the linear region, but lower than those needed to cause complete saturation, the yield stress of MR fluids is predicted by the following equation [68]

$$\tau_{ys} = (6^{1/2})\, \phi\, \mu_0\, (M_S)^{1/2}\, H^{3/2} \qquad (4\text{-}11)$$

where $\mu_0 M_s$ is the saturation magnetization. At magnetic fields sufficient to cause complete magnetic saturation of particles, the yield stress depends only on the $\mu_0 M_S$ of the magnetically dispersed phase. The yield stress is predicted by the model due to Ginder et al. [69] and is given by **Equation 4-12**

$$\tau_{ys}^{sat} = (4/5^{5/2})\ \xi(3)\ \phi\ \mu_0 (M_S)^2 \qquad (4\text{-}12)$$

where $\xi(3) = 1.202$ which is a constant.

We compared the experimental values of observed yield stresses at flux densities of 0.2, 0.4 and 0.6 Tesla to the yield stresses predicted by **Equation 4-11**. We found that these values do not match well. This suggests that the fields necessary to induce flux densities ranging from 0.2 to 0.6 Tesla are above those that correspond to the $H^{3/2}$ dependence. And as pointed out before, the torque sensor is not sensitive enough to measure the torques at flux densities < 0.2T. There are no analytical equations that predict the H dependence of yield stress in the intermediate regime where the dependence is not predicted by $H^{3/2}$ or $\mu_0 M_S^2$. Therefore, we fitted the experimental data measured at flux densities between 0.2 and 0.6 T to a polynomial and the plots are given in **Figure 4-23**. The polynomial relations are given and the calculated yield stresses using these polynomials are given at **Tables 4-5 and 4-6.**

According to **Equation 4-12**, the dynamic yield stress at saturation, τ_{ys}^{sat}, for MR fluids should be independent of the particle size. This is true in general as long as the magnetic dipole-dipole energy is quite large compared to the thermal energy [81]. The models that predict that τ_{ys}^{sat} is independent of the particle size also assume that the magnetic properties of particulates of different size are identical. Our experimental measurements reported here clearly show that this is not always the case. In our study, the dynamic yield stress for 33 vol% MR fluid synthesized by GRADE A (coarser particles) was about 100 ± 3 kPa at about a flux density of 0.78 ± 0.1 T

(**Figure 4-19**). The measured dynamic yield stress for a 40 vol% MR fluids prepared using GRADE A was found to be 124 ± 3 kPa for a flux density of about 0.78 ± 0.1 T (**Figure 4-20**). For MR fluids synthesized with 33 and 40 vol% GRADE B iron, the yield stresses observed were 80 ± 8 kPa (**Figure 4-21**) and 102 ± 2 kPa (**Figure 4-22**), respectively at a flux density of ~0.78 ± 0.1T. At these high magnetic fields, the mathematically predicted yield stresses (**Equation 4-12**) were 80 and 98 kPa for 33 and 40 vol% GRADE B based fluids ($\mu_0 M_s$=1.89T), respectively and 93 and 114 kPa for 33 and 40vol% for GRADE A ($\mu_0 M_s$=2.03T) based fluids, respectively. It can be seen that MR fluids based on fine particles always exhibited a lower dynamic yield stress compared to yield stress of MR fluids based on coarser particles. As pointed out earlier, the lower yield stresses for GRADE B fluids are attributed to lower $\mu_0 M_s$. However, another factor that could lower the yield stress could be the relatively weaker chains due to thermal fluctuations formed by smaller particles. In this case, the particle size and PSD can play a role in influencing the yield stress of the MR fluids. The dynamic yield stress values at low and high magnetic fields are summarized in **Table 4-5 and 4-6**.

Table 4. 5: Comparison of experimental dynamic yield stress and theoretical yield stress values obtained by analytical methods for 33 vol% iron based MR fluids.

	33 vol% GRADE A		33 vol% GRADE B	
	calculated Y.S (kPa)	measured dynamic Y.S (kPa)	calculated Y.S (kPa)	measured dynamic Y.S (kPa)
B=0.2T	7*	16± 3	7©	10± 1
B=0.4T	21*	33± 3	20©	26± 2
B=0.6T	38*	72± 5	37©	56± 5
B=0.8T	93 #	100 ± 3	80 #	80± 8

$\tau_y^{sat} = (4/5^{5/2})\ \xi(3)\ \phi\ \mu_0 (M_S)^2$

* $\tau_{ys} = (6^{1/2})\ \phi\ \mu_0 (M_S)^{1/2} H^{3/2}$

Table 4. 6: Comparison of experimental dynamic yield stress and theoretical yield stress values obtained by analytical methods for 40 vol% iron based MR fluids.

	40 vol% GRADE A		40 vol% GRADE B	
	calculated Y.S (kPa)	Measured dynamic Y.S (kPa)	calculated Y.S (kPa)	measured dynamic Y.S (kPa)
B=0.2T	$9^{@}$	22±1	$7^{@}$	14± 0.6
B=0.4T	$25^{@}$	45±3	$20^{@}$	35±1
B=0.6T	$46^{@}$	84.3±2	$37^{@}$	71±2
B=0.8T	$114^{\#}$	124 ± 3	$98^{\#}$	102 ± 2

$\# \ \tau_y^{sat} = (4/5^{5/2}) \ \xi(3) \ \phi \ \mu_0 (M_S)^2$

$@ \ \tau_{ys} = (6^{1/2}) \ \phi \ \mu_0 (M_S)^{1/2} H^{3/2}$

The yield stresses are generally found to increase as $B^{3/2}$, as shown by the straight lines **in Figure 4-24, 4-25, 4-26, and 4-27**, consistent with the role of magnetic saturation [68]. The volume fraction (ϕ) dependence of the dynamic yield stress for either type of iron powder (finer or coarser) was similar to that predicted by models presented previously by Ginder and co-workers [69]. The ratio between the volume fractions of 0.40 and 0.33 was in good agreement with the ratio of the yield stresses. For 33 and 40 vol% GRADE A based fluids the ratio between the yield stresses are 1.2 ± 0.01, 1.2 ± 0.01, 1.3 ± 0.1, and 1.4 ± 0.1 for flux densities 0.2, 0.4, 0.6, and 0.8 T, respectively. The yield stresses of 40 and 33 vol% based samples linearly increased in the ratio of 1.3 ± 0.1 for GRADE B based MR fluids at flux densities 0.2 and 0.4 T, respectively and in the ratio of 1.4 ± 0.1 at flux densities 0.6 and 0.8 T. In the prior experimental studies by Kordonski and co-workers, the dynamic yield stress was shown to grow linearly only at $\phi > 40\%$ [78]. In a recent study by Dang et al. reveals an increase in yield stress of 10 - 30 vol% Fe based fluids with increasing volume fraction [90].

Another factor we did not investigate as part of this work is the effect of particle size distribution. As has been noted before, our SEM analysis showed that both powders, although not uni-modal or bimodal, had a range of particle sizes. A size distribution of particles may affect the "off-state" viscosity and also "on-state" yield stress, since particles of different sizes may have different magnetic properties [55, 75, 81]. The "off-state" viscosity has not been investigated and as mentioned before the torque sensor is not sensitive enough to measure very low torques.

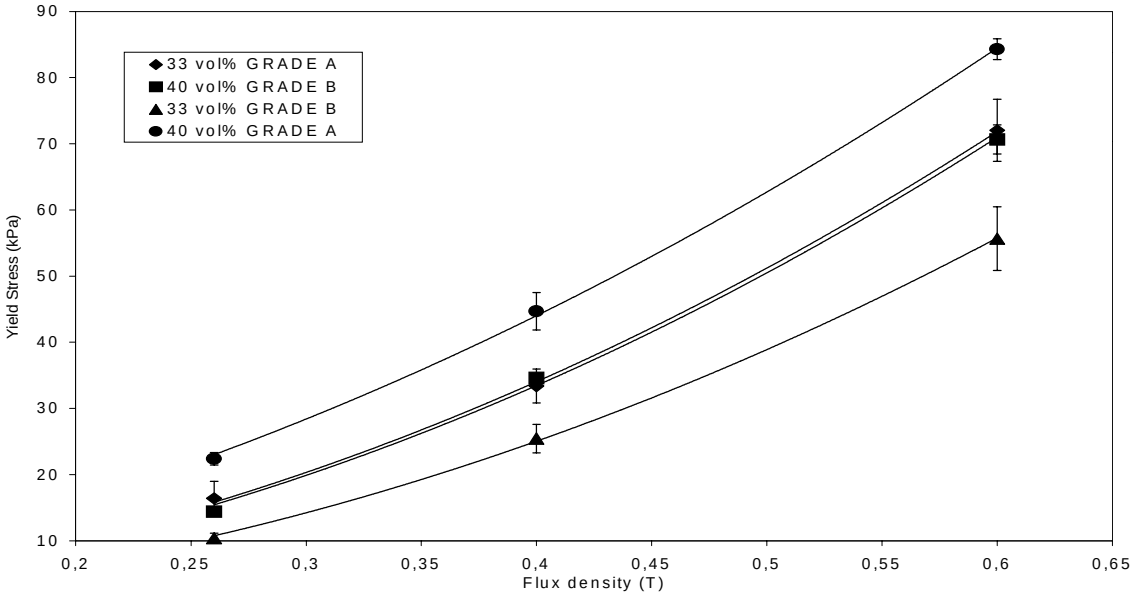

33 vol% GRADE A, τ_y =173.27 B^2 + 15.795 B
33 vol% GRADE B, τ_y =151.77 B^2 + 1.9086 B
40vol% GRADE A, τ_y =153.8 B^2 + 48.531 B
40vol% GRADE B, τ_y =173.35 B^2 + 14.299 B

Figure 4. 23 Dynamic yield stress versus flux density at intermediate flux densities and the polynomial fit giving the relationship between the yield stress and the flux density, B

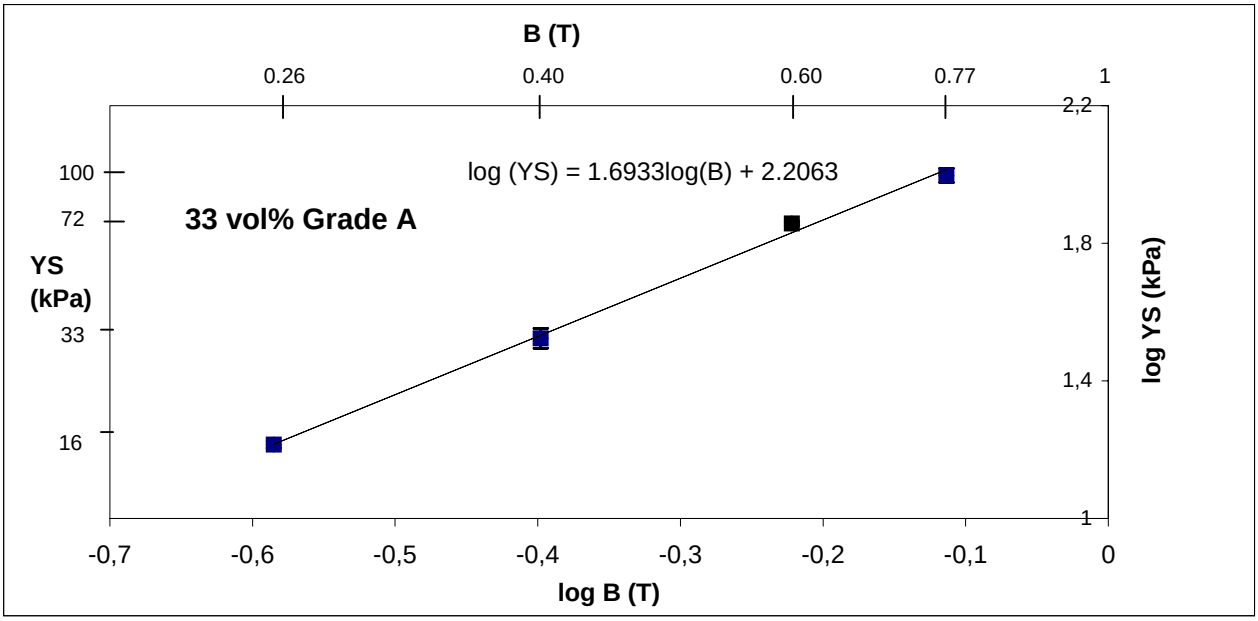

Figure 4. 24 Dependence of measured dynamic yield stress on the applied flux density for 33 vol% GRADE A iron powder based MR fluid.

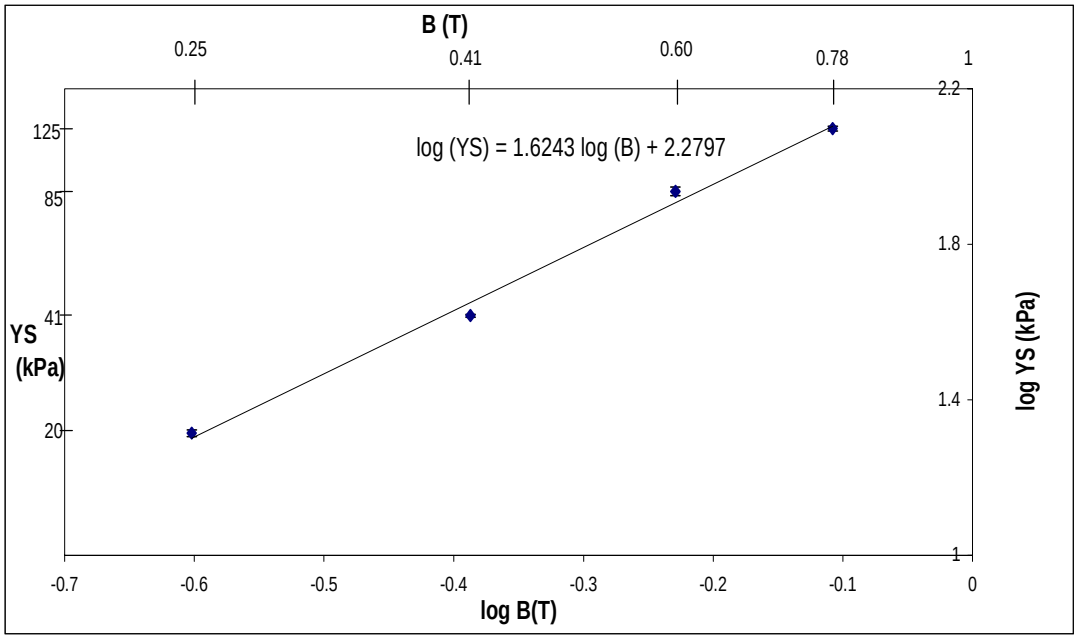

Figure 4. 25 Dependence of measured dynamic yield stress on the applied flux density for 40vol% GRADE A iron powder based MR fluid.

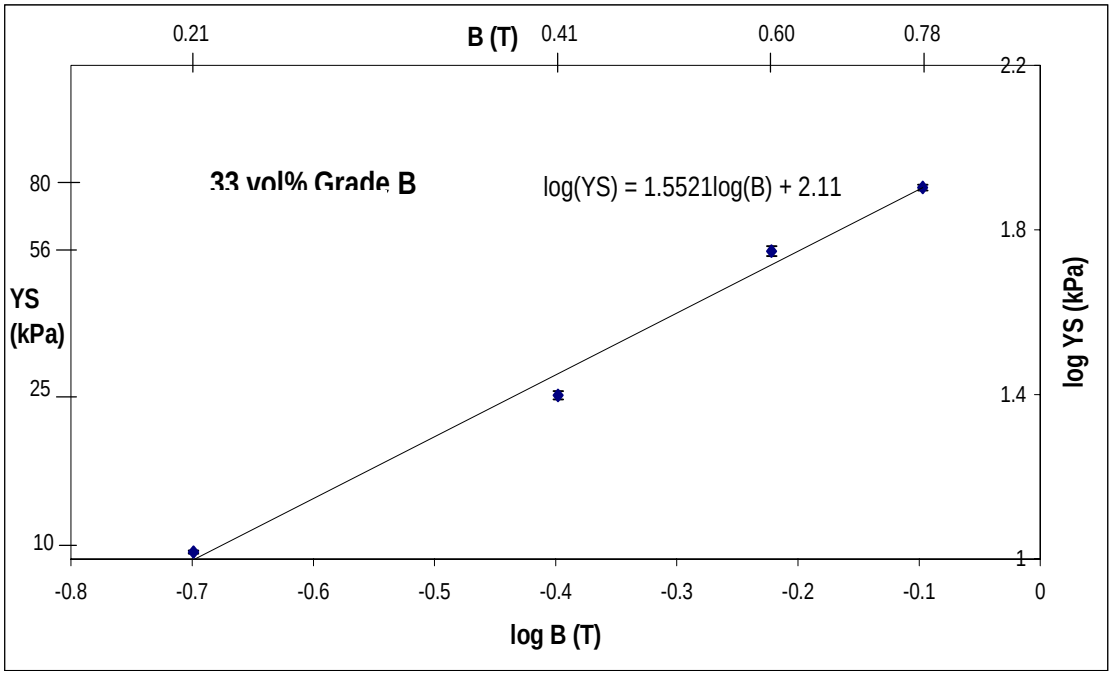

Figure 4. 26 Dependence of measured dynamic yield stress on the applied flux density for 33vol% GRADE B iron powder based MR fluid.

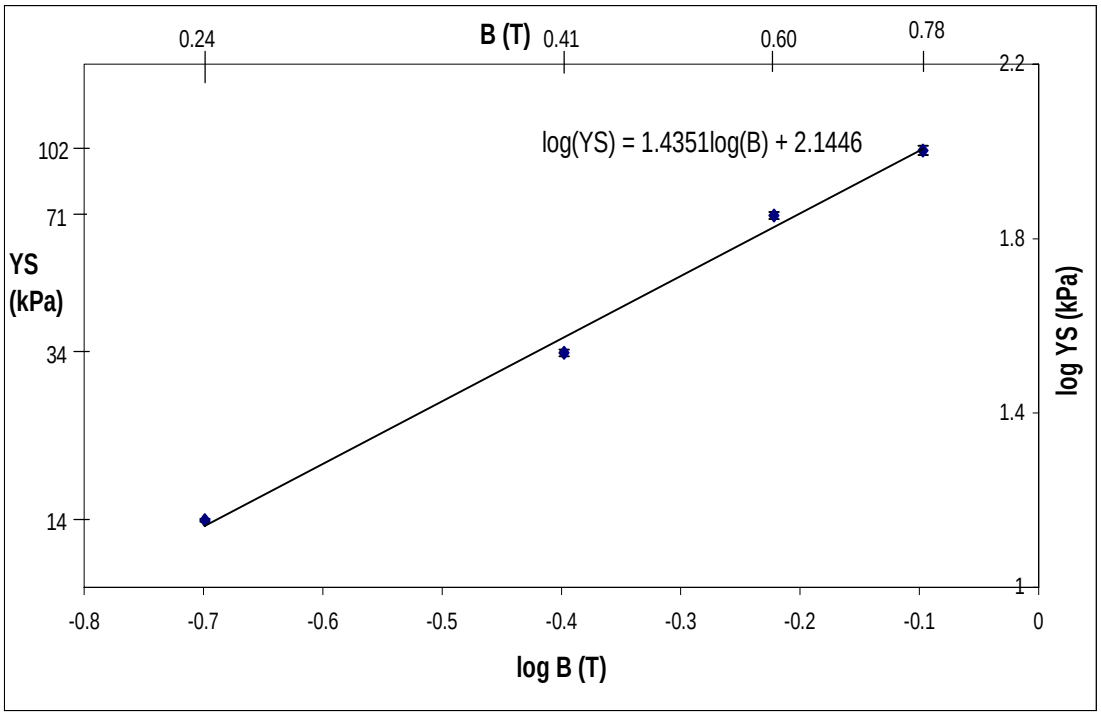

Figure 4. 27 Dependence of measured dynamic yield stress on the applied flux density for 40vol% GRADE B iron powder based MR fluid.

4.5.2 Off State Rheological Properties of MR Fluids

Off state rheological measurements of MR fluids were conducted by stress controlled (MBTAC-IVb) and dual mode, stress/strain rate controlled, rheometer (TA instruments - MODEL 1000). Cone and plate, concentric cylinder with different diameters and double concentric cylinder geometries were used in these measurements.

4.5.2.1 Off-State Viscosity Measurements. In our preliminary experiments we used parallel plate arrangement because in principle this arrangement is preferable to Couette geometry since the gap height could be changed easily. However, although we used knife edged platens to keep the fluid in the gap, it was very hard to maintain the MR fluid in between the platens. Therefore, the flow measurements were performed with MBTAC-IVb at constant stress mode with concentric cylinder geometry. The diameter of the cup was kept constant while the bobs with diameters 1.02, 0.51, and 0.25 cm (0.4, 0.2, 0.1") were used. Due to the rapid evaporation and settling problems of 5 cST PDMS, we focused on 100 cST PDMS and GRADE B based MR fluids. In order to analyze the flow properties, such as shear thinning, of the MR fluids, they were sheared at the constant stress until they reached a steady state.

Visual observations revealed that when small diameter bobs (0.1 and 0.2") were used, the bulk of the fluid was not sheared but instead only the fluid next to the bob wall was sheared. The lowering of the viscosity and our visual observations can be attributed to the slip on the walls of the concentric cylinder. The fluctuations seen in the viscosity versus time plot presented in **Figure 4-28** can also be an indication of the stick-slip behavior which is also enhanced by larger gaps. The stick-slip flow was also observed in the measurements performed using the bigger diameter bobs. In this stick and slip flow, large blocks of suspension stopped moving decreasing the shear rate. This kind of nonhomogeneties in Couette flow was also observed in magnetic

suspensions by Toy and co-workers [110]. Gadala-Maria and Acrivos reported shear induced anisotropic structures in the suspensions [111]. They reported that the viscosity of the fluids at steady state increased when sheared at shear rates above 100 s^{-1}. They concluded that the fluid at the bottom which was hardly sheared at low shear rates, entered the gap at high shear rates and thus replacing some of the suspension which had been undergoing shear for a long time [111]. **Figure 4-29** shows the differences in the flow curves measured with different diameter bobs. The flow curves obtained with the smallest diameter bob showed lower viscosities as well as inconsistency in the flow curves.

Measurements performed with MBTAC-IVb using the largest diameter (0.4" bob) on the 40 vol% GRADE B and PDMS based MR fluid covered the range of shear stresses from 18 ± 2 to 175 ± 1Pa and the corresponding shear rates were from 0.1 to 86 ± 3 s^{-1} (**Figure 4-30**). The viscosity at the lowest stress was 196 ± 8 Pa-s and at the highest stress it was 2.4 ± 0.1 Pa-s. The measurements were done for 3 independent batches. The shear thinning behavior of magnetic fluids and MR fluids, were reported by other scientists [3, 112].

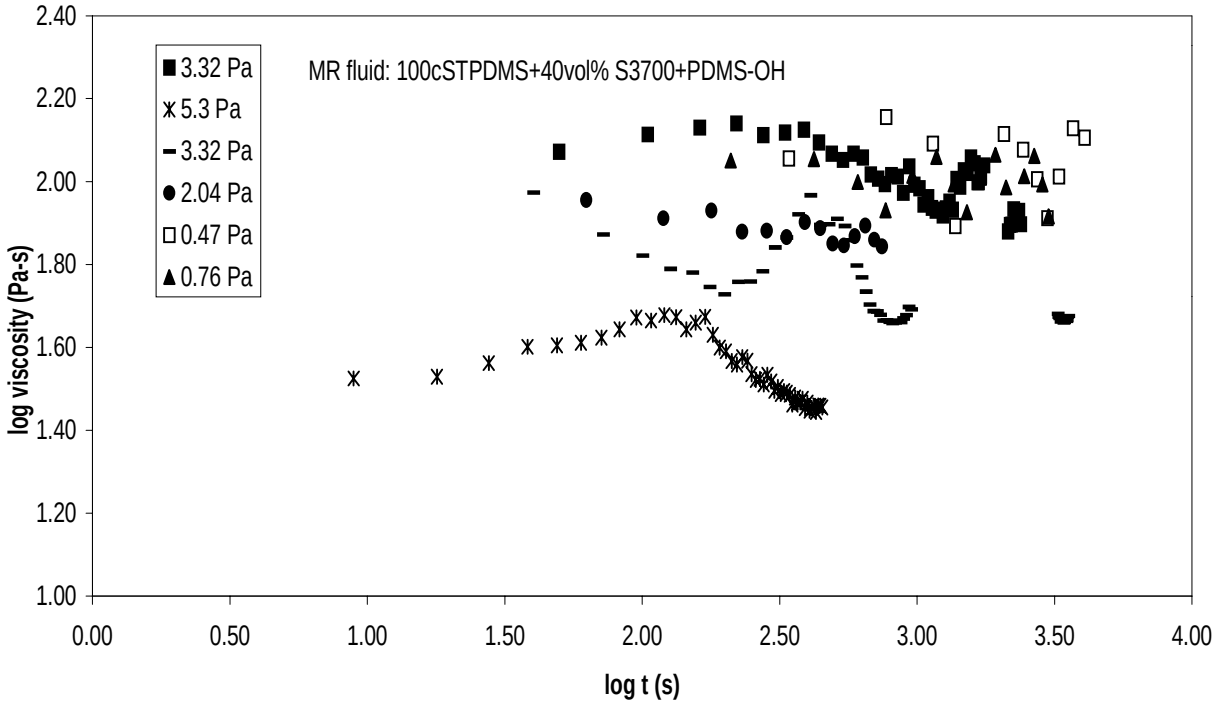

Figure 4. 28 Log apparent viscosity vs. Log time for 40 vol% GRADE B and 100 cSt PDMS based MR fluid measured with 0.1" diameter bob in concentric cylinder geometry (MBTAC-IVb). The fluctuations can be an indication of the stick-slip on the surface of the concentric cylinder geometry.

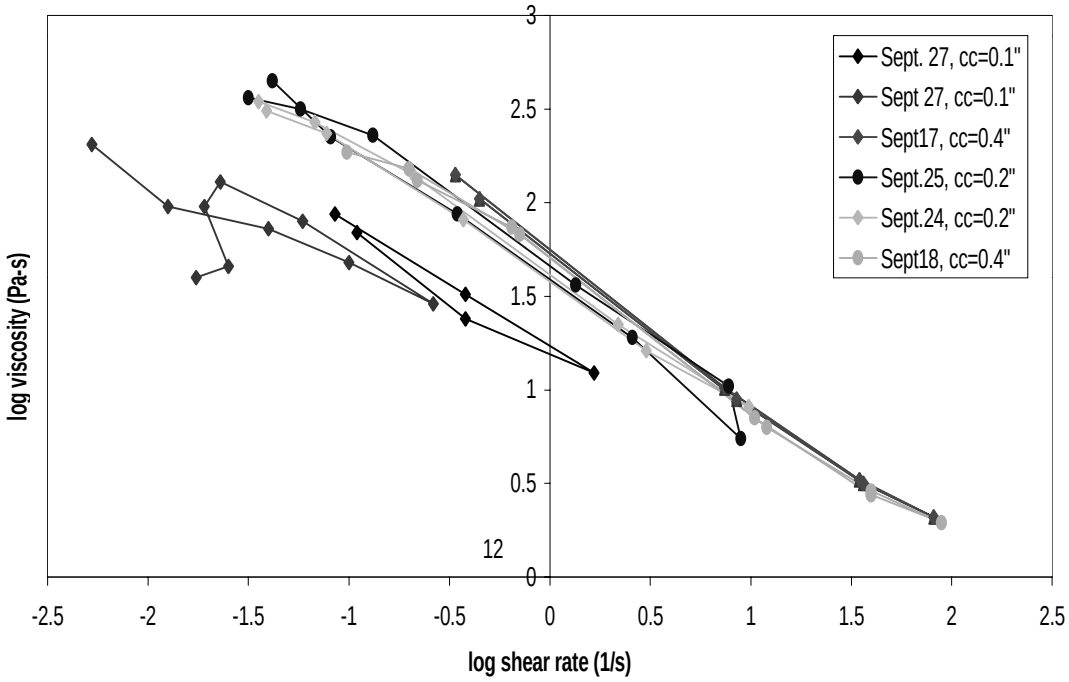

Figure 4. 29 Log viscosity vs. log shear rate for 40 vol% GRADE B and PDMS based MR fluid measured with MBTAC-IVb. Different diameter bobs were used.

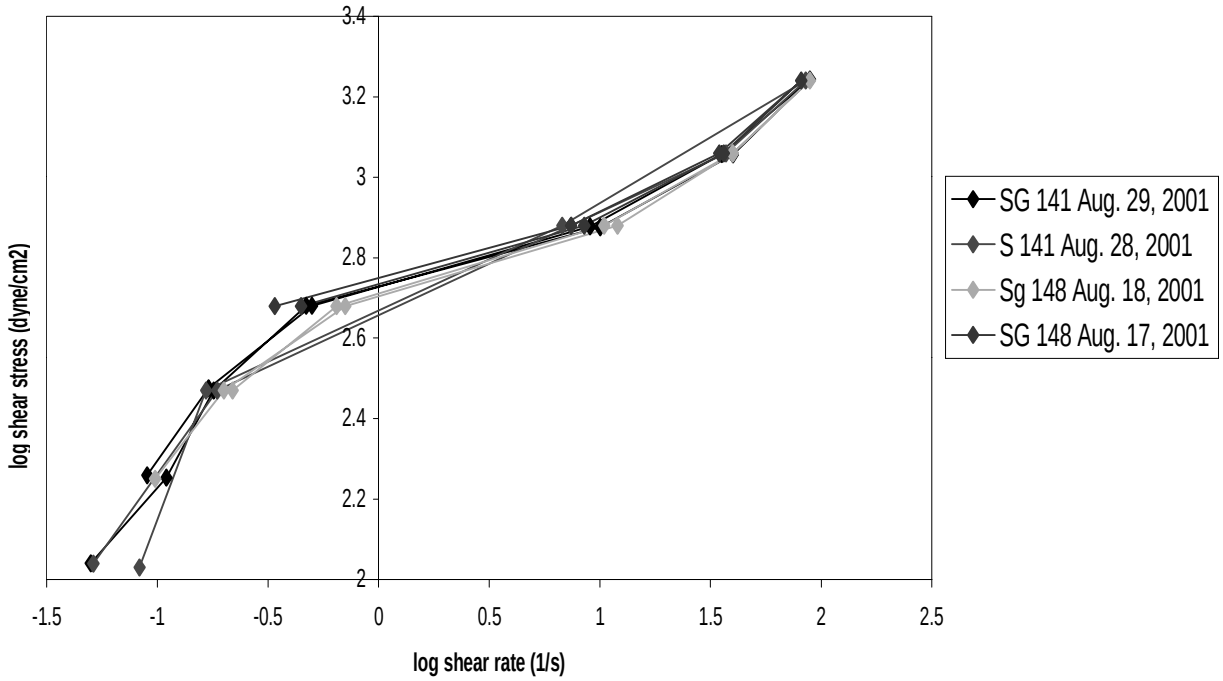

Figure 4. 30 Log shear stress vs. log shear rate for 40 vol% GRADE B and 100 cSt PDMS based MR fluid measured with 0.4" bob in MBTAC-IVb.

The steady state flow measurements were performed in constant stress and constant strain rate mode by TA instruments rheometer. These measurements were done with double concentric cylinder geometry where the strain rate was varied between 0.1 and 100 s^{-1}. At shear rates between 0.1-1 s^{-1}, the MR fluid was sheared for 30 min and at higher shear rates, it was sheared for 2 min. The reason for longer shearing times at low shear rates was the longer time that it took for the sample to reach steady state. At high shear rates, in order to prevent shear heating, the sample was sheared for shorter periods of time. The apparent viscosities were measured for 3 independent batches of 40vol% GRADE B and PDMS (100 cSt) based MR fluids. The shear stresses at 0.1 and 100 s^{-1} were 17.6±6 and 190±13 Pa respectively and the viscosities were 199±52 and 1.9±0.3 Pa-s respectively. The apparent viscosity versus shear rate and the shear stress versus shear rate are presented in **Figure 4-31 and 4-32,** respectively. The wide scatter of the viscosity at the lower shear rate revealed that the sample had not reached the steady state. The shear stress, shear rate and viscosity values obtained from two different measurements by two different instruments were in good agreement. The comparison of the results from two instruments and geometries is presented in **Figure 4-33.**

The flow curves revealed shear thinning behavior in our MR fluids. One of the most empirical equations to represent non-Newtonian is given as [113]

$$\tau = K\dot{\gamma}^n \tag{4.13}$$

where τ is the stress, K is the consistency index and n is the flow index. For Newtonian fluids, n=1 and for shear thinning and thickening fluids, n<1, n>1 respectively. Due to the limitations of the instrument, we couldn't go to shear rates enough to reach a constant viscosity (Newtonian Plateau) value, in **Figure 4-31**, however, at high and low shear rates we observed the starting of the leveling out of the viscosity. This indicated that the material would eventually reach a

constant viscosity. The slope of log τ vs log $\dot{\gamma}$ curve between low and high shear rates gave the value of **n** as 0.13. Poslinski and co-workers [52] reported that the Newtonian plateau can disappear completely as the volume fraction of the solid particles increased.

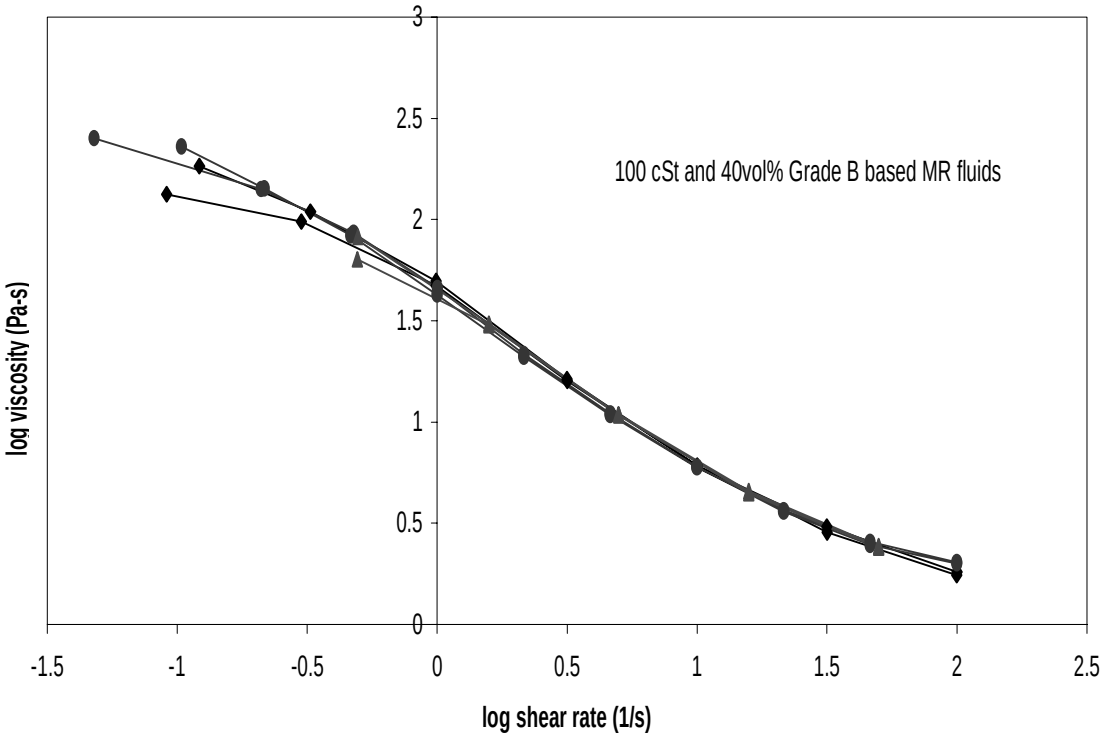

Figure 4. 31 Log apparent viscosity vs. log shear rate for 40 vol% GRADE B and 100 cSt PDMS based MR fluid measured in double concentric cylinder geometry in TA instruments

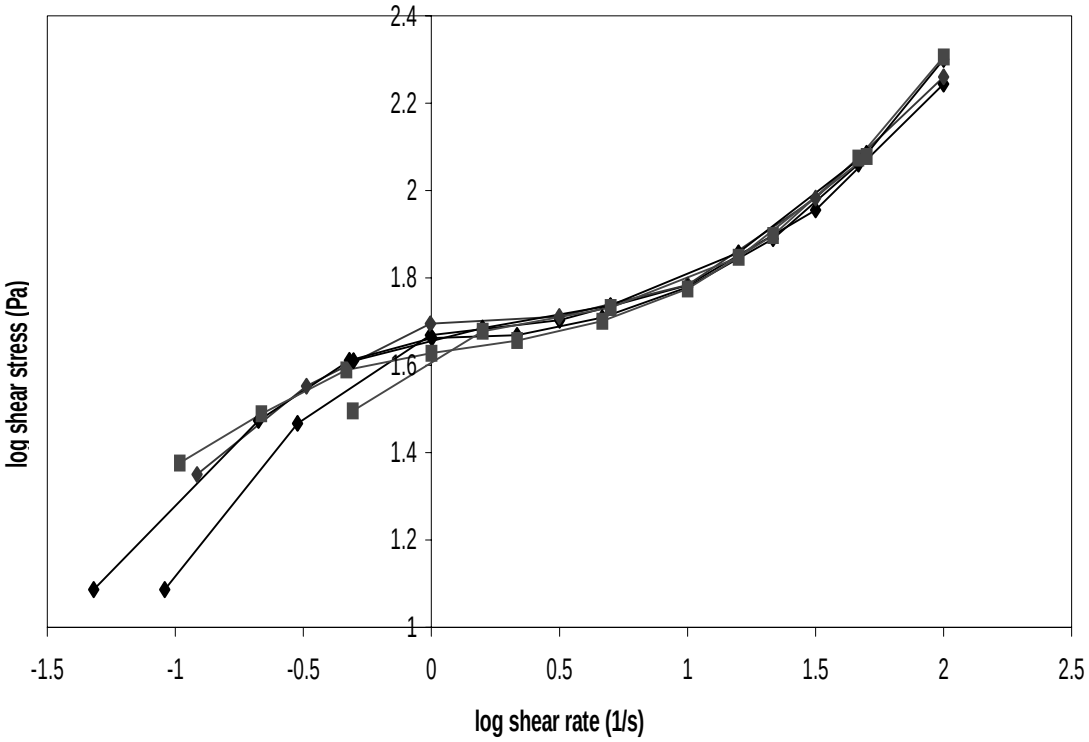

Figure 4. 32 Log shear stress vs. log shear rate for 40 vol % GRADE B and 100 cSt PDMS based MR fluid measured in double concentric cylinder geometry in TA instruments

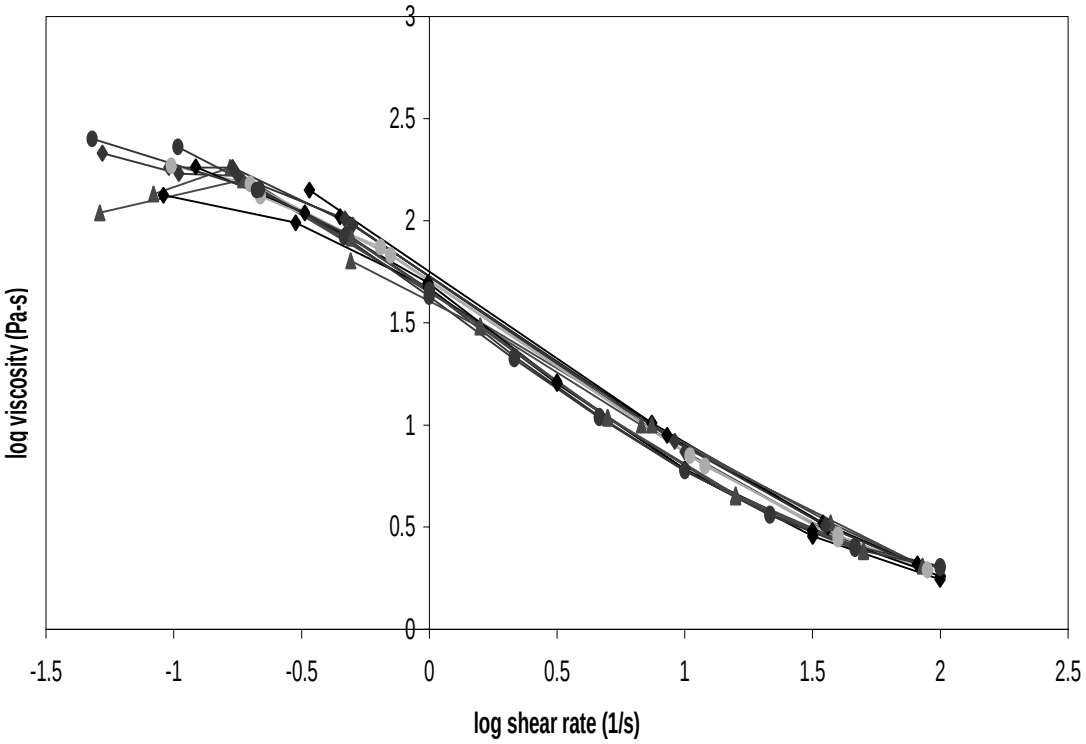

Figure 4. 33 Comparison of apparent viscosity vs. shear rate measurements for 40 vol % GRADE B and 100 cSt PDMS based MR fluid in different instruments and geometries (TA Instruments and MBTAC-IVb)

4.5.2.2 Creep and Recovery Measurements. The creep properties of MR fluids are important in terms of determining the thixotropic behavior of MR fluids and establishing the factors affecting the yielding of MR fluids. The creep and recovery measurements were performed on MR fluids prepared with 100 cSt PDMS, ISP GRADE B iron powder and SURFACTANT A. The non-colloidal (hydrodynamic interactions) and magnetic nature of the dispersed phase in MR fluids, make them quite complicated and difficult to be analyzed experimentally.

In the creep and recovery measurements that we performed, our purpose was to establish yield strain/yield stress and the relation between these two concepts. We also tried to establish how the material responded to various pre-shearing conditions. Recovery characteristics of MR fluids were also analyzed. In order to fulfill these purposes, we performed experiments on 5-6 different batches of the same kind of fluid as described in the first paragraph. We changed different variables, such as resting time, pre-shearing time, creep stresses.

4.5.2.2.1 Yield Strain. The yield strain of the MR fluids was determined by creep measurements where different stresses were applied and attained for some time. These measurements were performed by a TA instruments rheometer (Model 1000) on two different geometries, cone and plate and double concentric cylinder. Preshearing at 150 Pa for 5 minutes followed by 2 hours of resting was performed before the creep runs. **Figure 4-34** shows creep and recovery curves for 40 vol % GRADE B based MR fluid. The yield strain of the MR fluid was calculated from the linear compliance J versus time plot (**Figure 4-35**). The yielding was observed on the plot with a change in the slope of compliance versus time plot. Solving the equations of the slopes simultaneously gave us the compliance values at which the yielding occurred. By multiplying this value with the stress value gave the yielding value. The yield strains at 60, 40, 20, 10, and 5 Pa were calculated as ~1%. Figure 4-36 presents the yield strains at different creep stresses.

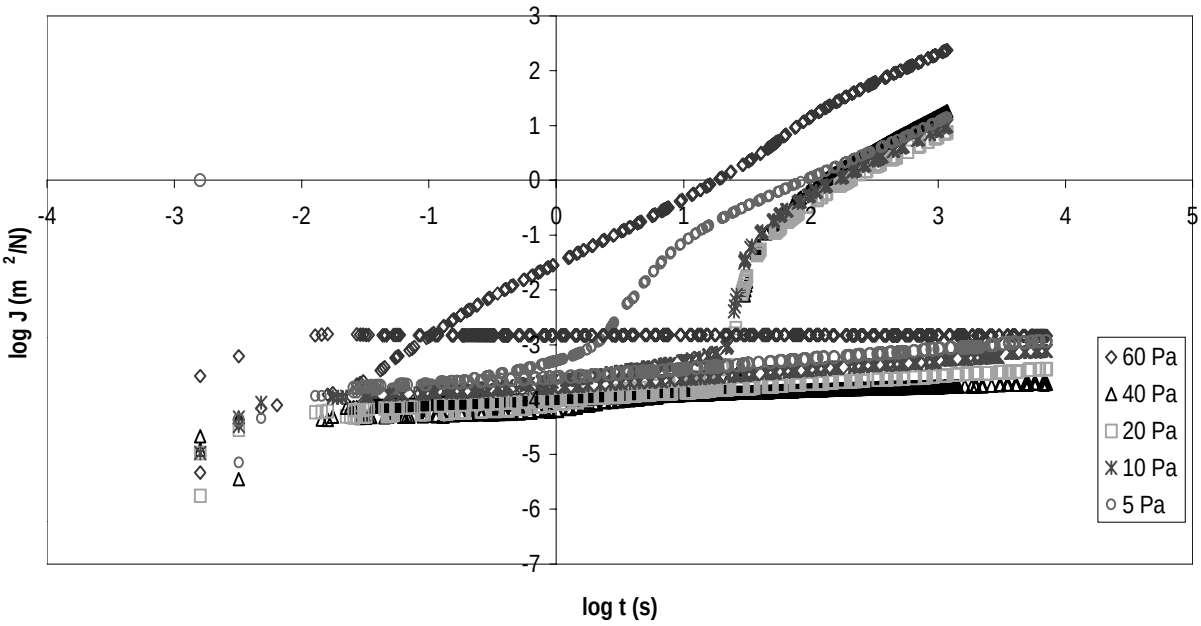

Figure 4. 34 Log compliance (J) vs. log ttime (t) for 40 vol% GRADE B and 100 cSt PDMS based MR fluid.

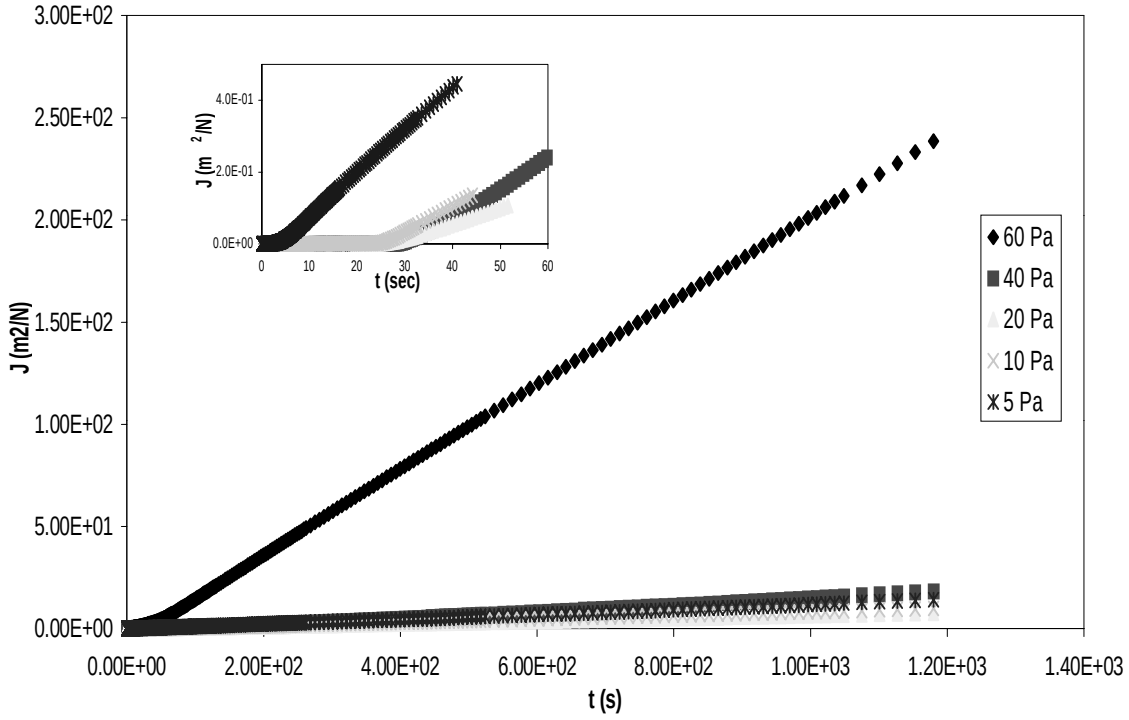

Figure 4. 35 Linear plot of Compliance vs. time for 40 vol% GRADE B and 100 cSt PDSM based MR fluid. (Linear plot for Figure 4-34).

As can be seen from **Figure 4-36**, the yield strains vary between 0.009 and 0.03. However, the majority of the yield strain values lie between 0.01 and 0.02. Weiss and co-workers [82] reported a yield strain of 0.8% at zero magnetic field and a magnetic field of 2000 Oe, for an MR fluid called MRX-I developed by Lord Corporation [27]. This was important because different mechanisms dominated the particle-particle interactions, such as magnetostatic interactions at off-state and particle polarization under a magnetic field. The volume percent of the magnetic phase was not mentioned. Li and co workers [84] investigated the yield strain of 15% Fe based MR fluid synthesized in Silicone oil and at a current of 0.8 A to induce magnetic field and they reported yield strain of 0.5%. On the contrary to Weiss et.al's work [82], the yield strain values that Li and co-workers [84]determined varied from 0.2-0.6% at different magnetic fields. The works by these two authors indicated yield strain values <1% which could hinder their efficiency in applications, especially in applications where pre-yield stability is required. MR fluids with higher levels of strain level will enhance the performance of these materials due to a strong network that would keep the particles dispersed in the liquid. If the network is weak and breaks at a smaller strain levels, then the particles can settle out.

Multiple yielding of our MR fluids was another interesting outcome of these experiments. Second yielding occurred at longer times and larger strains than did the first yielding of the MR fluid. **Figure 4-37** shows creep-recovery curves of MR fluid made of 40 vol% GRADE B in 100 cSt PDSM where the second yielding was circled. The second yielding varied between a yield strain value of 0.2 and 12.5 at stress levels between 40-110 Pa. The reason why our MR fluids showed multiple yielding hasn't been fully understood, however we believe that the smaller first yield strain occurred due to rolling of the particles over one another in order to start the MR fluid to flow which occurred after yielding whereas the second, larger yield strain occurred when

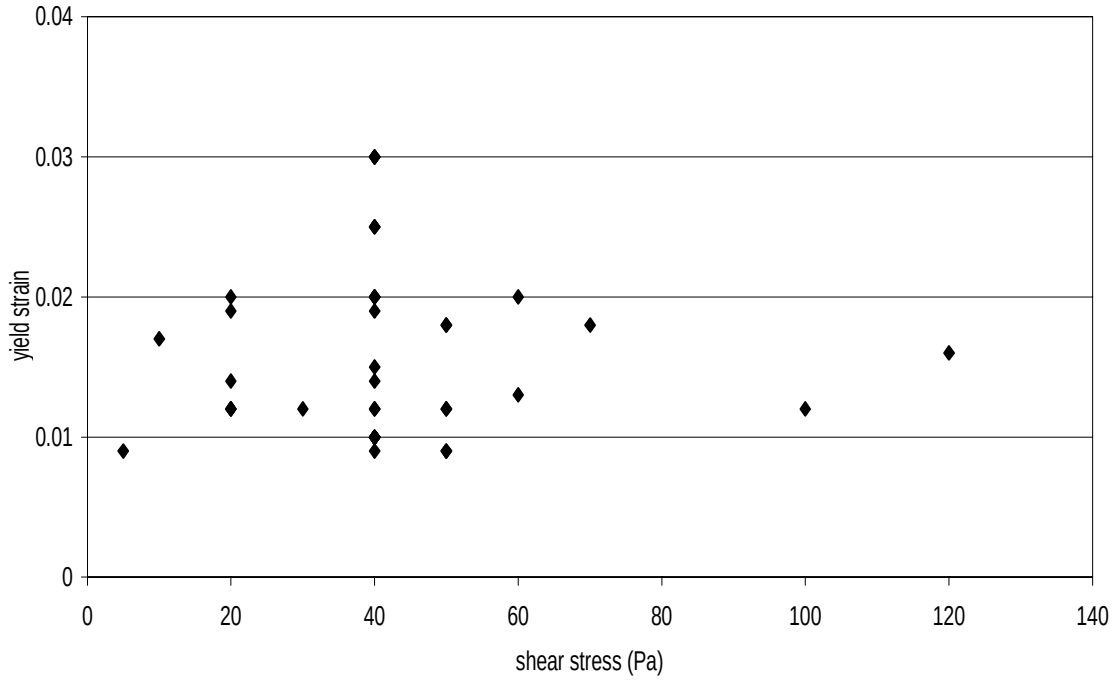

Figure 4. 36 Yield strain vs. shear stress for 40 vol% Grade B and 100 cSt PDMS based MR fluid.

agglomerates of iron particles started rolling over one another. The variation of the 2nd yield strain could be due to the size and distribution of the agglomerates. The second yielding could also occur due to breaking of the aggregates as well. This needs to be investigated in detail.

Although the first yield strains occurred around 0.01 – 0.02, the time to reach that yield point showed variations which could be attributed to the restructuring or breaking away of the network with resting time or shearing time. However, no specific pattern was observed in our preliminary measurements. This variation of the yielding times can be seen in **Figure 4-37.** Immediate yielding at 60 Pa after 2 hour resting occurred at 0.05 sec. As the stress got smaller (40 Pa) the yielding occurred at longer times (32 sec) which was expected. At 20 and 10 Pa stress level, the yielding almost occurred at the same time as 40 Pa. However, as the stress level went down to 5 Pa, the yielding occurred at a shorter time. This contradicted our expectations which was as the stress got smaller the yielding would occur at a longer time. This also showed that the strain history of the MR fluids could play an important role in reaching the yield point. Systematic experiments have to be conducted on the effect of resting periods on the rheological behavior of the MR fluids.

4.5.2.2.2 The Effect of Shearing Time on Yielding**.** One of the major contributions of this research was determining the behavior of the MR fluid under certain conditions such as pre-shearing. The pre-shearing is a crucial step because MR fluids are prone to sedimentation and separation of the liquid causing in-homogeneities in the MR fluid.

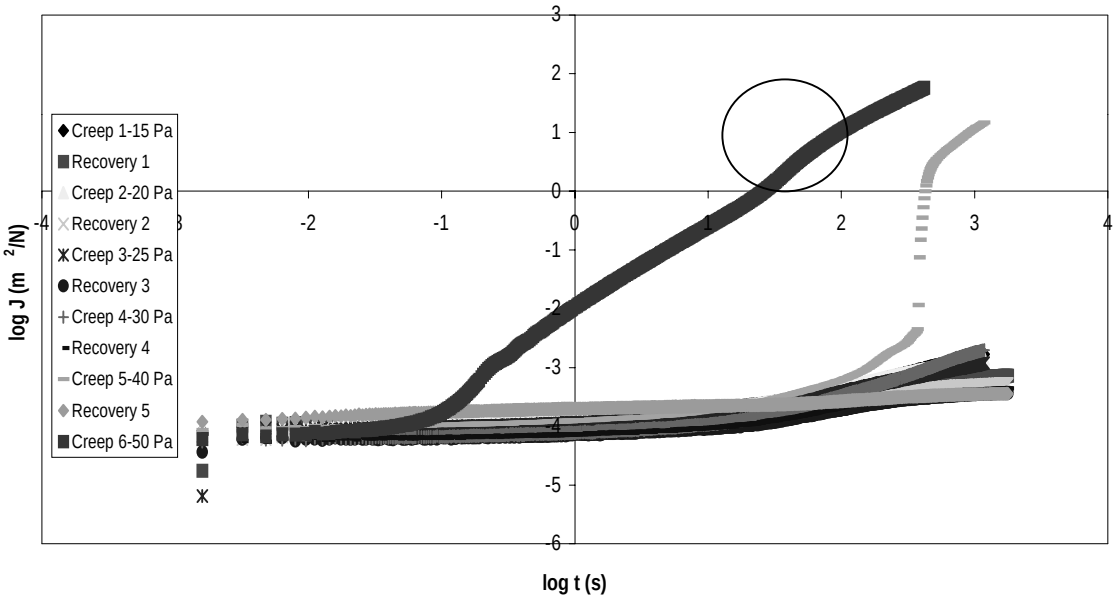

Figure 4. 37 Log compliance (J) vs. Log time (t) for 40 vol% GRADE B and 100 cSt PDMS based MR fluid showing second yield point. The second yielding is shown in circle.

MR fluid synthesized with 100 cSt PDMS and SURFACTANT A and 40 vol% GRADE B iron grade were pre-sheared at 110 Pa for 2 minutes and after each pre-shear, the MR fluid was rested for 1 minute before constant stress was suddenly imposed and the strain was recorded as a function of time. Different stress levels (33, 34, 35, 40 Pa) were imposed after 1 min. of resting time. **Figure 4-38** shows the creep compliance (J) versus time (t) plot. At the stress levels of 33, 34, and 35 Pa, MR fluid did not show any yielding in the time period that the stress was applied. However, yielding occurred at 40 Pa at 250 sec and at a yield strain of 0.025. These results showed that the state of the MR fluid at the end of 2 minutes of shearing was strong enough to withstand the yielding at lower stresses than 40 Pa in that given period of time. Although the creep strain seemed to reach the critical strain that was determined in the previous section, the material did not break away. This could be due to the time of shearing may not be enough to observe yielding or the stress level was just sufficient enough to keep the network at a specific state.

MR fluid was pre-sheared for different lengths of time before a constant stress was applied. The results are shown in **Figure 4-39**. After pre-shear at 110 Pa for 120, 300, 600, and 44460 sec, the MR fluid was exposed to 1 minute of resting followed by 35 Pa creep stress. No yielding was observed at 35 Pa after the pre-shear at 110 Pa was performed for 120 and 300 sec. However when the pre-shearing time increased to 600 sec, MR fluid yielded at around 1000 seconds and the overnight pre-shearing (44460 sec) resulted in yielding at a shorted time (~400 sec). When the material was sheared longer, it would homogenize gradually due to the non-homogeneous distribution of the stress in co-axial cylinder geometries. This could cause the MR fluid to be partially sheared and as the time of shearing was increased the sheared layer could decrease until it reached a size of the order of the several particle diameters [114]. One minute of

resting period applied after short periods of shearing might restructure the material quicker than the longer periods of shearing where the state of the fluid is more homogeneous and ruptured. This could cause the MR fluid to break away sooner after long periods of shearing. It is also possible that 1 minute of rest has little influence compared with the length scale of homogeneity and consequent effect on the strain required for rearrangement process.

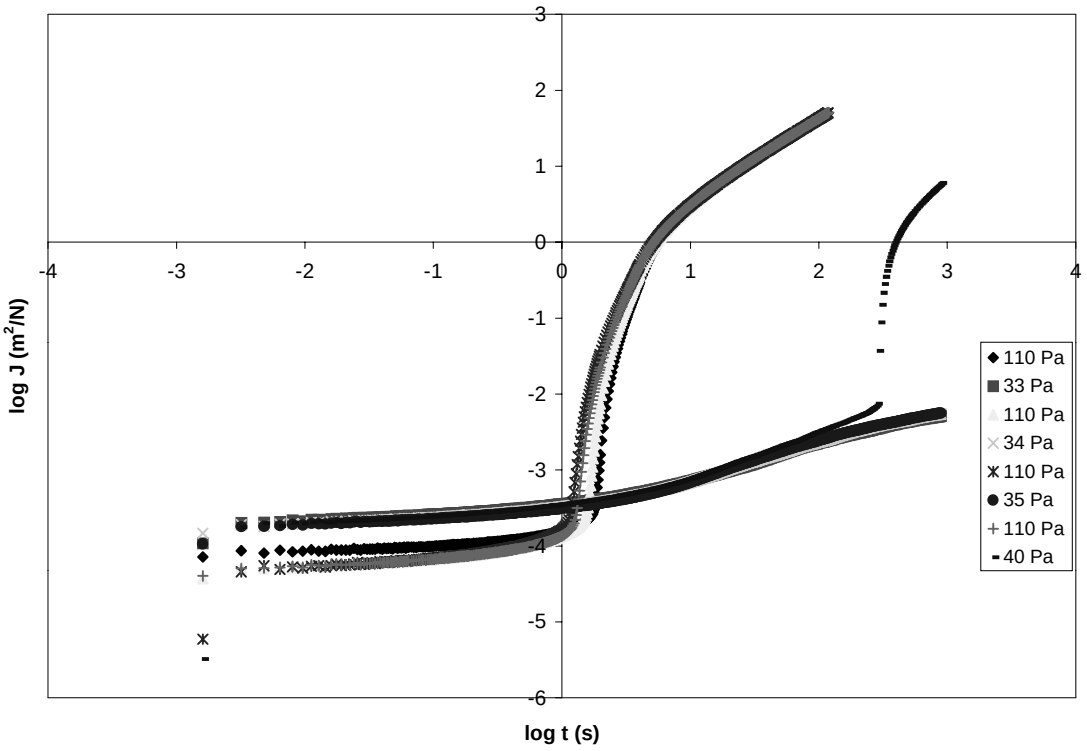

Figure 4. 38 Log compliance vs. log time showing the pre-shearing at 110 Pa for 2 minutes followed by various stress levels

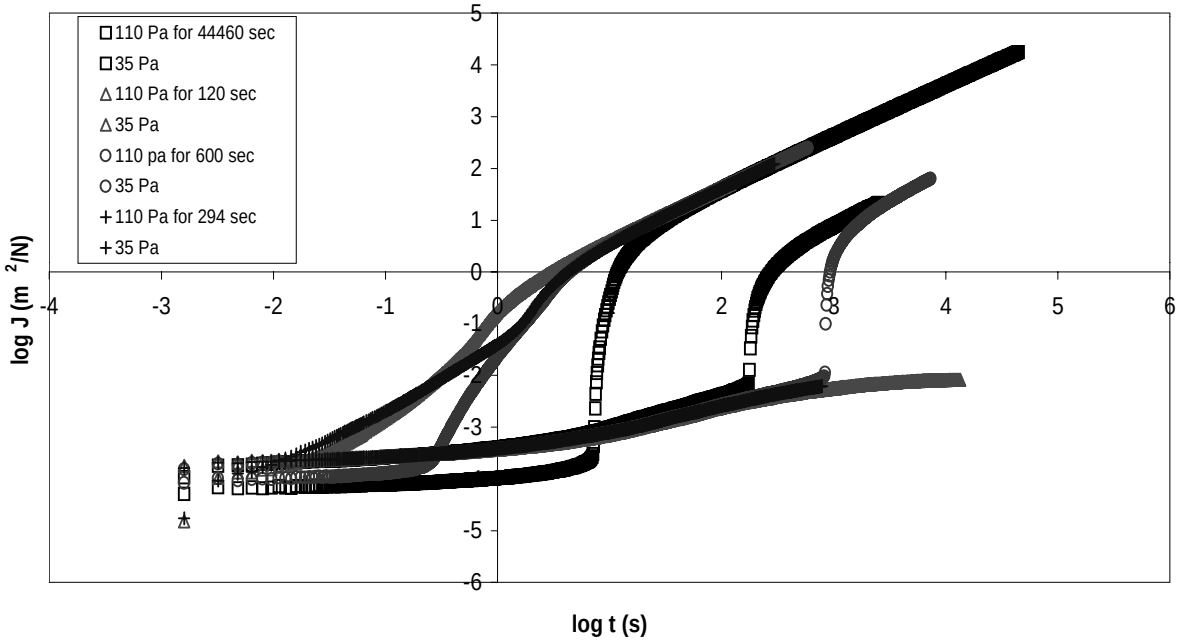

Figure 4. 39 Log compliance vs. log time plot showing the effect of various pre-shearing periods.

4.6 Durability of MR Fluids

4.6.1 On State Rheology of Heat Treated MR Fluids

MR fluids synthesized with 100 cSt PDMS, 40 vol% GRADE B Grade Fe powders and SURFACTANT A were exposed to a temperature of 175 ^{0}C for 24 hrs. The on state measurements performed on these samples exhibited no change in the yield stress in the heat treated MR fluids when compared to untreated MR fluids. The shear stress versus shear rate plot of 100 cSt based MR fluids before heat treatment is given in **Figure 4-40.** The yield stress of 100 cSt and 40 vol% GRADE B based MR fluid is 16.3 ± 0.4, 33.5 ± 0.5, 58.9 ± 0.8, 78.8 ± 2.4 kPa at flux densities of 0.2 ± 0.02, 0.39 ± 0.03, 0.59 ± 0.1, and 78.8 ± 0.1T. At higher flux densities the yield stress values were smaller than the yield stress values presented in **Section 4.5.1.** As we have mentioned before that the yield stress values in **Section 4.5.1** could be artificially higher due to evaporation of the carrier liquids, since 5 cSt and NPC-ST based MR fluids were used in those measurements. In a similar manner, these values might be artificially lower due to the extrusion of the fluid out of the gap at high shear rates.

The shear stress versus shear rate plot of the heat treated MR fluid presented in **Figure 4-41**. As can be seen from the plots, the yield stresses of the MR fluids before and after heat treatment were the same. In terms of magnetic properties of the dispersed phase, when the particles reach saturation, the yield stress is only a function of saturation magnetization (μ_0Ms) [68]. The yield stresses were 16 ± 1, 34 ± 1, 59 ± 1, and 79 ± 2 kPa at the flux densities of 0.24 ± 0.02, 0.40 ± 0.03, 0.60 ± 0.1, and 0.78 ± 0.1 T.

The heat treatment process of the MR fluids had no effect on the saturation magnetization of the magnetic particles, which indicated that iron particles were not oxidized by heating. This could be due to the already oxidized surfaces of iron particles and this oxide layer

may provide a self protection for further oxidation due to heat treatment [115]. Adsorption of the surfactant on the iron (Fe) particles may prevent the oxidation of these magnetic particles.

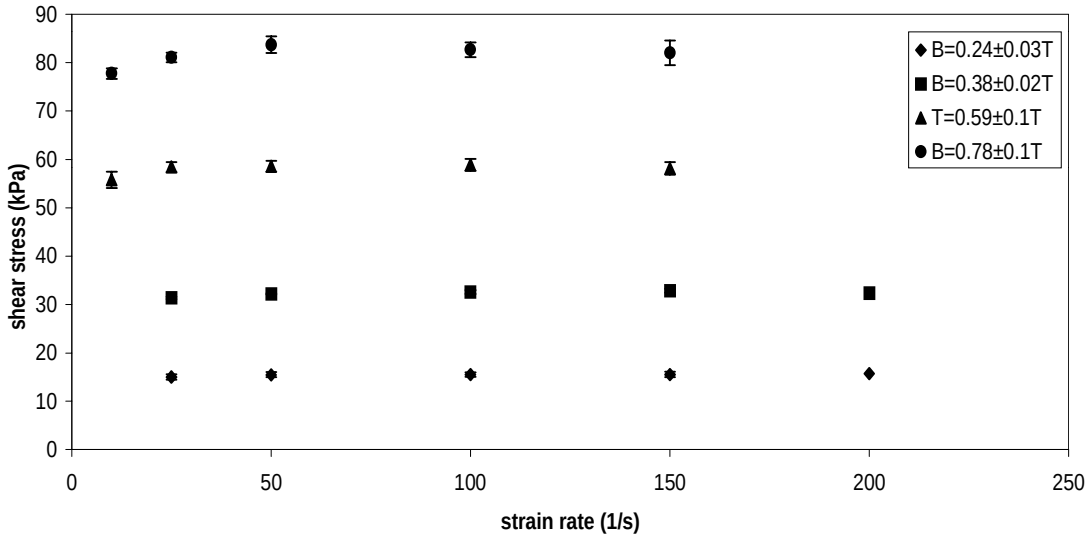

Figure 4. 40 Shear stress vs. strain rate for 40 vol% GRADE B and 100 cSt PDMS based MR fluid

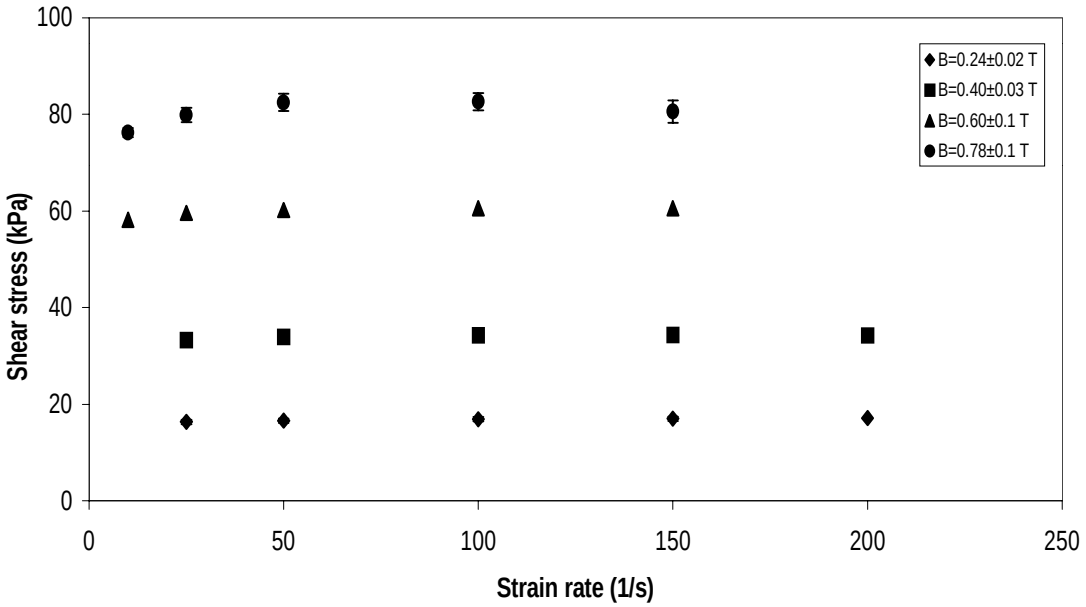

Figure 4. 41 Shear stress vs. strain rate for 40 vol% GRADE B and 100 cSt PDMS based MR fluid exposed to heat treatment @175 ^{0}C for 24 hours.

4.6.2 Off-State Rheology of Heat Treated MR Fluids

The off state rheological properties of the heat treated MR fluids were analyzed by TA rheometer. Double concentric cylinder was used in the measurements and it was operated at the constant shear rate mode at 25 ^{0}C. The shear rate was varied between 0.5-50 s^{-1}. The steady state flow curves were presented in **Figure 4-42**. Heat treated MR fluids exhibited shear thinning behavior between the shear rates of 0.5 and 15 s^{-1}. At high shear rates of 50 s^{-1}, the Newtonian plateau was observed at a viscosity level of 3.9 Pa-s for heat treated MR fluids. The increase in the viscosity of heat treated MR fluids may be due to the cross-linking of the PDMS at high temperatures. The density of the MR fluid was measured after heat treatment in order to ensure there is no evaporation of the liquid. The figure of merit for MR fluids is described as the ratio between the on state yield stress and the off state viscosity. Therefore, the MR effect can be reduced by exposing them to high temperatures for extended periods of time.

The rheological studies performed at high temperatures showed that MR fluids maintain the same yield stress at high temperatures. Bombard and co-workers reported that the temperatures between 10-60 ^{0}C did not seem to have a significant effect on the viscosity of the MR fluids under various applied magnetic fields [112]. The dependence of the off state viscosity on the temperature was not reported in their work. Kormann et al. reported that the viscosity of the MR fluids based on nano-sized particles measured at different temperatured decrease with temperature, independent of the applied magnetic field [109].

The creep and recovery measurements of the heat treated MR fluids revealed an increase in the yield strain. The yield strain values that were measured at constant stress mode of the rehometer by TA Instruments ranged from 0.13 to 0.195 at different stress values, such as 20, 30, 40, 50 Pa. The increase of the yield strain was about an order of magnitude greater than the yield

strain values of untreated MR fluids and this can be seen in **Figure 4-43**. This increase could be attributed to the cross-linking of the polymer or increasing of the aggregation of the iron particles.

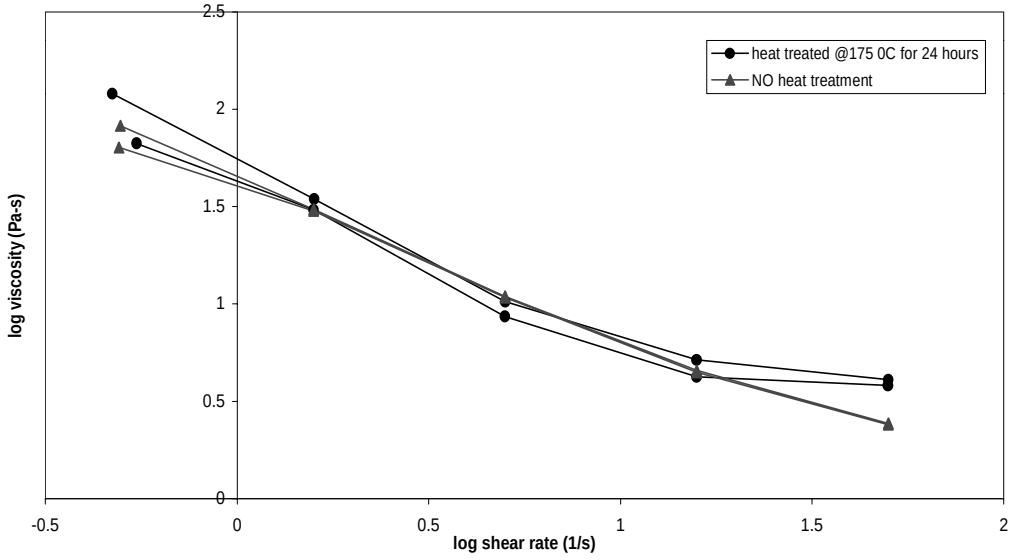

Figure 4. 42 Comparison of apparent viscosity of heat treated and regular MR fluid.

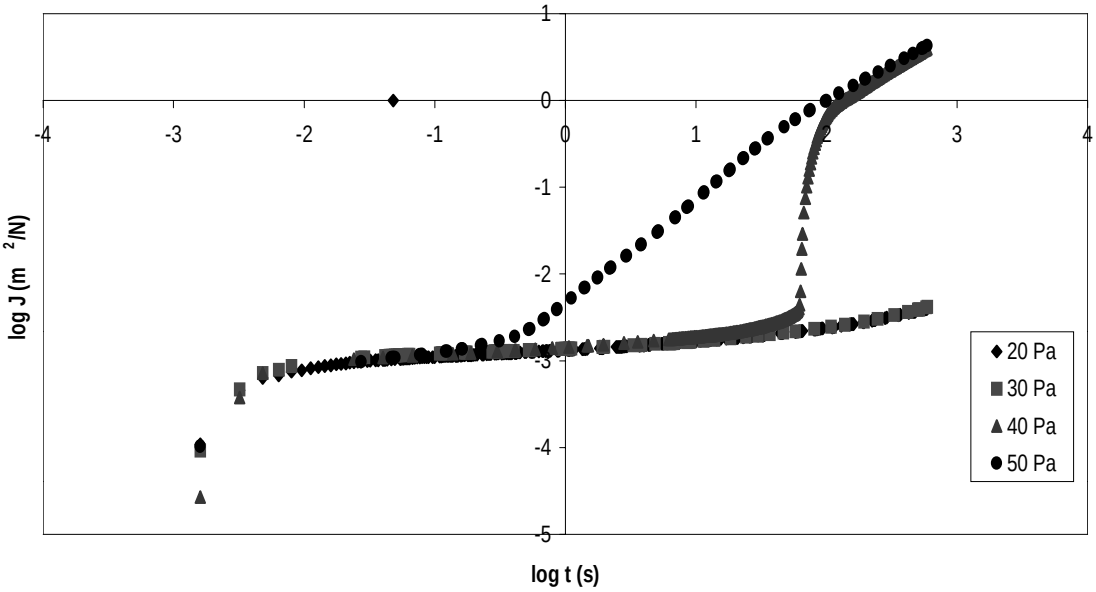

Figure 4. 43 Log compliance (J) vs. log time (t) for a heat treated MR fluid.

5.0 SUMMARY AND CONCLUSIONS

1. In this research MR fluids were synthesized using different grades of iron powder (GRADE A, GRADE B), PDMS, and SURFACTANT A. Glycol ether based MR fluids were also synthesized.

2. PDMS (100cST), SURFACTANT A, GRADE B based MR fluids and NPC-ST, SURFACTANT B and GRADE A based MR fluids exhibited the most stable and redispersible behavior. The difference in the redispersibility and stability of fluids with different grades of iron powder and carrier liquids and surfactants can be attributed to the interactions of the iron surface with different surfactants as well as the particle size differences.

3. The saturation magnetization ($\mu_0 M_s$) for GRADE A and GRADE B grades of iron powder was found to be 2.03 and 1.89T respectively. The coercivities of these powders were measured as 30.51 and 14.22 respectively whereas the coercivity of bulk iron is 1.01 Oe. A possible reason for the higher coercivity of the iron particles is the presence of impurities and defects in the particle. The lower coercivity of GRADE B which has more impurities than GRADE A could be attributed to the denser packing of the particles.

4. One of the most important results of this research was the influence of the remnant magnetization on the magnetic dipole-dipole interaction energy of 33 vol% iron, MnZn ferrite, and NiZn ferrite based MR fluids and hence on the redispersibility of MR fluids. The ratio between the magnetic dipole-dipole energies to the thermal energy (V_{mag}/k_BT) for 33 vol% iron, MnZn ferrite, NiZn ferrite based MR fluids were calculated as -161000, -6400 and -3900. The redispersibility of the MR fluids can be enhanced by using additives that would increase the interparticle distance.

5. The magnetic measurements followed by on state yield stress of MR fluids synthesize with different sized MR fluids (GRADE B : ~2 μm and GRADE A : ~7μm) showed that the decrease in the yield stress of GRADE B (102 ±2 kPa) at a magnetic induction of 0.8 T) based MR fluids was due to the lower levels of saturation magnetization ($\mu_0 M_s$ =1.89 T) of GRADE B grade iron powder.

6. The off state steady state flow measurements revealed a shear thinning behavior of MR fluids (40 vol% GRADE B in 100cSt PDMS with SURFACTANT A). The apparent viscosity of MR fluids at the lowest shear rate (0.01 s^{-1}) and highest shear rate (100 s^{-1}) was 199±52 and 1.9±0.3 Pa-s respectively. The measurements were conducted in two different rheometers and the close values of apparent viscosity values revealed that there was no slippage at the walls of the geometries (concentric cylinder and double concentric cylinder) used.

7. One of the most striking conclusions of this study was that the yield point of the MR fluid (40 vol% GRADE B in 100cSt PDMS with SURFACTANT A) was measured as a strain value of 1-2% at various creep stresses. Multiple yielding was also observed at higher yield strains.

8. The pre-shearing of MR fluids had a significant effect on the rheological properties of MR fluids. The longer the pre-shearing at 110 Pa, showed a yielding in the sample at shorter times at 35 Pa.

9. The heat treated MR fluids (@175 ^{0}C for 24 hrs) did not show any significant changes in the on state yield stress which could be attributed to the protective oxide layer which was already on the surface of the iron particles. This oxide layer prevented further oxidation of the iron particles.

10. The off state yield apparent viscosity of MR fluids showed increase in the highest strain rate that could be measured with the rheometer by TA instruments. The off state apparent viscosity was 3.9 Pa-s at 50 s^{-1} whereas for a regular MR fluid this value was ~2 Pa-s.

11. The strain increased 10 times (10%) for a heat treated MR fluid. This could be attributed to the cross linking of the PDMS.

6.0 SUGGESTIONS FOR FUTURE WORK

1. In depth analysis of the surface chemistry of iron particles is needed in order to understand the adsorption mechanism and the interaction between iron particles and the surfactants.

2. Off and on state dynamic measurements need to be performed systematically in order to have a better understanding of the rheological behavior of MR fluids.

3. Off state creep measurements need to be performed on the MR fluids in order to determine the effect of resting times and various pre-shear tress values on the yielding of the MR fluids.

4. The creep measurements have to be extended to on state measurements.

5. The effect of extensive amounts shearing on the durability of MR fluids is also needed to be investigated.

6. There is a need to develop a test procedure to measure the degree of redispersibility and caking of the MR fluids.

APPENDICES

APPENDIX A

(Conversion Factors for Magnetic Measurements)

Table A- 1 Conversion of magnetic units from CGS to SI

To convert the CGS value in	To the following in SI units	Multiply the CGS value by
Gausses	Webers/square meter	10^{-4}
Gausses	Tesla	10^{-4}
Gausses	Ampere-turns/meter	0.7958
Gilberts/cm	Ampere-turns/meter	79.58
Maxwells	Webers	10^{-8}
Oersteds	Ampere-turn/meter	79.58

Table A- 2 Conversion of magnetic units from SI to CGS

To convert the SI value in	To the following in CGS units	Multiply the SI value by
Webers/square meter	Gausses	10^4
Tesla	Gausses	10^4
Ampere-turns/meter	Gausses	1.257
Ampere-turns/meter	Gilberts/cm	0.01257
Webers	Maxwells	10^8
Ampere-turn/meter	Oersteds	0.01257

APPENDIX B

Viscosity-Unit Conversions

Table B- 1 Kinematic viscosity conversions

Kinematic Viscosity

multiply	by	to obtain
ft^2/sec	92903.04	centistokes
ft^2/sec	0.092903	m^2/sec
m^2/sec	10.7639	ft^2/sec
m^2/sec	1000000.0	centistokes
centistokes	0.000001	m^2/sec
centistokes	0.0000107639	ft^2/sec

Table B- 2 Dynamic viscosity

Absolute or Dynamic Viscosity

multiply	by	to obtain
lbf-sec/ft²	47880.26	Centipoises
lbf-sec/ft²	47.8803	Pascal-sec
centipoises	0.000102	kg-sec/m²
centipoises	0.00000208854	lbf-sec/ft²*
centipoises	0.001	Pascal-sec
Pascal-sec	0.0208854	lbf-sec/ft²
Pascal-sec	1000	centipoises

Table B- 3Conversion from Dynamic viscosity to Kinematic viscosity

Absolute to Kinematic Viscosity

Multiply	by	to obtain
centipoises	1/density (g/cm^3)	centistokes
centipoises	0.00067197/density (lb/ft^3)	ft^2/sec
lbf-sec/ft^2	32.174/density (lb/ft^3)	ft^2/sec
kg-sec/m^2	9.80665/density (kg/m^3)	m^2/sec
Pascal-sec	1000/density (g/cm^3)	centistokes

BIBLIOGRAPHY

BIBLIOGRAPHY

1. Rabinow, J., *The Magnetic Fluid Clutch.* AIEE Trans., 1948. **67**: p. 1308.

2. Rabinow, J., *Magnetic Fluid Torque and Force Transmitting Device*, in *U.S. Patent*. 1951: USA.

3. Kordonsky, W., O. Ashour, and C.A. Rogers, *Magnetorheological Fluids: Materials, Characterization, and Devices.* Journal of Intelligent Material Systems and Structures, 1996. **7**: p. 123-130.

4. Macosko, C.W., *Rheology: Principles, Measurements, and Applications*. 1994, New York: VCH Publishers, Inc.

5. Phulé, P.P., J.M. Ginder, and A.D. Jatkar. *Synthesis and Properties of Magnetorheological Fluids for Active Vibration Control*. in *Materials For Smart Systems II*. 1996. Boston, MA: Materials Research Society.

6. Weiss, K.D., et al., *High Strength Magneto- and Electro-rheological Fluids.* 1993: p. 425 - 430.

7. Havelka, K.O. and J.W. Pialet, *Electrorheological technology: The future is now*, in *Chemtech*. 1996. p. 36 -45.

8. Havelka, K.O. and J.W. Pialet, *Electroheologal technology: The future is now.* CHEMTECH, 1996. **26**(6): p. 36-45.

9. Filisko, F.E. *Rheological Properties and Models of Dry ER Materials*. in *Electrorheological Fluids*. 1991. Illinois, USA: World Scientific.

10. Auzans, E., et al., *Synthesis and Properties of Mn-Zn ferrite ferrofluids.* Journal of Materials Science, 1999. **34**: p. 1253-1260.

11. Berkovsky, B.M., V.F. Medvedev, and M.S. Krakov, *Magnetic Fluids: Engineering Applications*. 1993, New York: Oxford University Press.

12. Raj, K. and R. Moskowitz, *Commercial Applications of Ferrofluids.* Journal of Magnetism and Magnetic Materials, 1990. **85**: p. 233 - 245.

13. Gans, B.J.d., *Magnetorheology of an Inverse Ferrofluid*. 2000, University of Twente: Twente. p. 135.

14. Gans, B.J.d., et al., *Preparation and Magnetization of Silica Magnetic Inverse Ferrofluids.* Journal of Magnetism and Magnetic Materials.

15. Winslow, W.M., *Method and Means for Translating Electrical Impulses into Mechanical Force*, in *U.S Patent, 2417850*. 1947: USA.

16. Winslow, W.M., *Induced Fibration of Suspensions.* Journal of Applied Physics, 1949. **20**: p. 1137-1140.

17. Ginder, J.M., *Rheology Controlled by Magnetic Fields*, in *Encyclopedia of Applied Physics*, E. Immergut, Editor. 1996, VCH: New York. p. 487.

18. Carlson, J.D. and M.J. Charzan, *Magnetorheological fluid dampers*. 1994, Lord Corporation: United States.

19. Johnston, G.L., et al., *Passive Magnetorheological Clutch*. 1998, General Motors Corporation: USA.

20. Jolly*, et.al. Indirect measurements of microstructure development in magnetorheological fluids*. in *ER Fluids-MR Suspensions and Their Applications*. 1997. Japan.

21. Jolly, M.R., J.W. Bender, and C.J. D. *Properties and Applications of Commercial Magnetorheological Fluids*. in *SPIE 5th Annual Int. Symposium on Smart Structures and Materials*. 1998. San Diego.

22. Bolter, R., H. Janocha, and S. Hellbruck. *Design of Magnetorheological Fluid Actuators*. in *Actuator 96*. 1996. Bremen, Germany: AXON Technologie Consult GmbH.

23. Bolter, R. and H. Janocha. *Design Rules for MR Fluid Actuators in Different Working Modes*. in *Smart Structures and Materials 1997: Passive Damping and Isolation*. 1997. San Diego.

24. www.delphiautomotive.com.

25. Jacobs, S.D., et al., *MRF:Computer Controlled Optics Manufacturing.* The American Ceramic Society Bulletin, 1999(December): p. 42-48.

26. Kordonski, W. and S. Jacobs, *Model of Magnetorheological Finishing.* Journal of Intelligent Material Systems and Structures, 1996. **7**: p. 131-137.

27. www.lord.com.

28. Cullity, B.D., *Introduction to Magnetic Materials*. 1972, Reading, Mass.: Addison-Wesley Pub. Co.

29. Skomski, R. and J.M.D. Coey, *Permanent Magnetism*. Studies in Condensed Matter Physics, ed. J.A. Revill. 1999, London: Institute of Physics Publishing Ltd.

30. Chen, C.-w., *Magnetisn and Metallurgy of Soft Magnetic Materials*. 2 ed. 1986: Dover Publication.

31. Chikazumi, S., *The Physics of Magnetism*. 1964, New York: Wiley.

32. Rosensweig, R.E., *Ferrohydrodynamics*. 1985, New York: Dover Publications, Inc.

33. Chin, G.Y., *Magnetic Materials : An Overview*, in *Encyclopedia of Advanced Materials*.

34. Japka, J.E., *Microstructure and Properties of Carbonyl Iron Powder.* Journal of Metals, 1988(August): p. 18-21.

35. Japka, J.E., *Iron Powder for Metal Injection Molding.* the Internatioanl Journal of Powder Metallurgy, 1991. **27**(2): p. 107-114.

36. Bozorth, R.M., *Ferromagnetism*. 1978, New York: IEEE Press.

37. Carlson, J.D. and K.D. Weiss, *Magnetorheological Materials Based on Alloy Particles*, in *US Patent, 5382373*. 1995, Lord Corporation: USA.

38. Phulé, P.P., A.D. Jatkar, and J.M. Ginder. *Materials for Smart Systems, MRS Proceedings*. 1997.

39. Lemaire, E., G. Bossis, and Y. Grasselli, *Yield stress and structuration of magnetorheological suspensions.* Journal of Magnetism and Magnetic Materials, 1993. **122**: p. 51 - 52.

40. Phulé, P.P. and J.M. Ginder. *Synthesis and Properties of Novel Magnetorheological Fluids Having Improved Stability and Redispersibility*. in *6th International Conference on ER Fluids and MR Suspensions and Their Applications*. 1997. Yonezawa, Japan: World Scientific.

41. Nielsen, L.E., *Polymer Rheology*. 1977, New York: Marcel Dekker, Inc.

42. Barnes, H.A., *Shear-Thickening ("Dilatancy") in Suspensions of Nonaggregating Solid Particles Dispersed in Newtonian Liquids.* Journal of Rheology, 1989. **33**(2): p. 329 - 366.

43. Clarke, B., *Rheology of Coarse Settling Suspensions.* Trans. Instn. Chem. Engrs., 1967. **45**: p. 251-256.

44. Markovitz, H., *Polymer Rheology*. 1980, Carnegie Mellon University: Pittsburgh.

45. Braun, D.B. and M.R. Rosen, *Rheology Modifiers Handbook-Practical Use and Applications*. 2000, Norwich, New York: William Andrew Publishing.

46. Barnes, H.A., *Thixotropy-a review.* Journal of Non-Newtonian Fluid Mechanics, 1997. **70**: p. 1-33.

47. Navarrete, R.C., L.E. Scriven, and C.W. Macosko, *Rheology and Structure of Flocculated Iron Oxide Suspensions.* Journal of Colloid and Interface Science, 1996. **180**: p. 200-211.

48. Yang, M.-C., L.E. Scriven, and C.W. Macosko, *Some Rheological Measurements on Magnetic Iron Oxide Suspensions in Silicone Oli.* Journal of Rheology, 1986. **30**(5): p. 1015-1029.

49. Kanai, H. and T. Amari, *Negative Thixotropy in Ferric-Oxide Suspensions.* Rheologica Acta, 1995. **34**: p. 303-310.

50. Chong, J.S., E.B. Christiansen, and A.D. Baer, *Rheology of Concentrated Suspensions.* Journal of Applied Polymer Science, 1971. **15**: p. 2007-2021.

51. Krieger, I.M., *Flow Properties of Latex and Concentrated Solutions*, in *Surfaces and Coatings Related to Paper and Wood*, C. Skaar, Editor. 1967, Syracuse University Press: Syracuse. p. 25-51.

52. Poslinski, A.J., et al., *Rheological Behavior of Filled Polymeric Systems I. Yield Stress and Shear-Thinning Effects.* Journal of Rheology, 1988. **32**(7): p. 703-735.

53. Tsai, S.C., D. Botts, and J. Plouff, *Effects of Particle Properties on the Rheology of Concentrated Noncolloidal Suspensions.* Journal of Rheology, 1992. **36**: p. 1291.

54. Hoffman, R.L., *Factors Affecting the Viscosity of Unimodal and Multimodal Colloidal Dispersions.* Journal of Rheology, 1992. **36**: p. 947-965.

55. Chang, C. and R.L. Powell, *Effect of Particle Size Distributions on the Rheology of Concentrated Bimodal Suspensions.* Journal of Rheology, 1994. **38**(1): p. 85 - 98.

56. Greenwood, R., P.F. Luckham, and T. Gregory, *Minimising the viscosity of concentrated dipersions by using bimodal particle size distributions.* 1998.

57. Reed, J.S., *Principles of Ceramic Processing*. 2nd ed. 1995, New York, NY: John Wiley & Sons, Inc.

58. Ferry, J.D., *Viscoelastic Properties of Polymers*. 1961: John Wiley & Sons, Inc.

59. Otsubo, Y. and K. Edamura, *Creep Behavior of Electrorheological Fluids.* Journal of Rheology, 1994. **38**(6): p. 1721-1733.

60. Bonnecaze, R.T. and J.F. Brady, *Yield stresses in Electrorheological Fluids.* Journal of Rheology, 1992. **36**(1): p. 73 - 115.

61. Bossis, G. and E. Lemaire, *Yield Stresses in Magnetic Suspensions.* Journal of Rheology, 1991. **35**(7): p. 1345 - 1354.

62. Lemaire, E. and G. Bossis, *Yield Stress and Wall Effects in Magnetic Colloidal Suspensions.* Journal of Physics D, 1991. **24**: p. 1473-1477.

63. Shulman, Z.P., et al., *Structure, Physical Properties and Dynamics of Magnetorheological Suspensions.* Int. J. Multiphase Flow, 1986. **12**(6): p. 935-955.

64. Bossis, G., et al., *Yield stress in magnetorheological and electrorheological fluids: A comparison between microscopic and macroscopic structural models.* Journal of Rheology, 1997. **41**(3): p. 687 - 704.

65. Volkova, e.a. *Magnetorheology of Model Suspensions*. in *Er Fluids-MR Suspensions and Their Applications*. 1997. Japan.

66. Rosensweig, R.E., *On magnetorheology and electrorheology as states of unsymmetric stress.* Journal of Rheology, 1995. **39**(1): p. 179 - 192.

67. Laun, M., C. Kormann, and N. Willenbacher, *Rheometry on Magnetorheological Fluids.* Rheologica Acta, 1996. **35**(5): p. 417-431.

68. Ginder, J.M. and L.C. Davis, *Shear Stresses in Magnetorheological fluids: Role of Magnetic Saturation.* Applied Physics Letters, 1994. **65**(26): p. 3410 - 3412.

69. Ginder, J.M., L.C. Davis, and L.D. Elie. *Rheology of Magnetorheological Fluids: Models and Measurements*. in *5th International Conference on ER Fluids and MR Suspensions*. 1995: World Scientific.

70. Jolly, M.R., J.D. Carlson, and B.C. Munoz, *A model of the Behavior of Magnetorheological Materials.* Smart Materials and Structures, 1996. **5**: p. 607-614.

71. Barnes, H.A. and K. Walters, *The Yield Stress Mythh?* Rheologica Acta, 1985. **24**: p. 323-326.

72. Barnes, H.A., *The Yield Stress - a review - Everything Flows?* Journal of Non-Newtonian Fluid Mechanics, 1999. **81**: p. 133-178.

73. Plazek, D.J., W. Dannhauser, and J.D. Ferry, *Viscoelastic dispersion of Polydimethyl Siloxane in the Rubberlike Plateau Zone.* Journal of Colloid Science, 1961. **16**(2): p. 101-126.

74. Potanin, A.A., et al., *Rheological Probing of Structure and Pigment-Resin Interactions in Magnetic Paints.* Rheologica Acta, 1998. **37**: p. 89-96.

75. Foister, R.T., *Magnetorheological Fluids*, in *US Patent, 5667715*. 1997, General Motors Corporation: USA.

76. Ginder, J.M., *Behavior of Magnetorheological Fluids.* MRS Bulletin, 1998. **23**(8): p. 26-28.

77. Carlson, J.D. and K.D. Weiss, *A Growing Attraction to Magnetic Fluids.* Machine Design, 1994(August): p. 61-64.

78. Kordonski, W.I., S.R. Gorodkin, and Z.A. Novikova. *The Influence of Ferroparticle Concentration and Size on MR Fluid Properties*. in *ER Fluids-MR Suspensions and Their Applications*. 1997. Japan.

79. Shorey, A.B., et al., *Design and Testing of a New Magnetorheometer.* Review of Scientific Instruments, 1999. **70**(11): p. 4200-4206.

80. Chin, B.D., et al., *Rheological Properties and Dispersion Stability of Magnetorheological Suspensions.* Reologica Acta, 2001. **40**: p. 211-219.

81. Lemaire, E., et al., *Influence of the Particle Size on the Rheology of Magnetorheological Fluids.* Journal of Rheology, 1995. **39**(5): p. 1011 - 1020.

82. Weiss, K.D., J.D. Carlson, and D.A. Nixon, *Viscoelastic Properties of Magneto- and Electro-Rheological Fluids.* Journal of Intelligent Material Systems and Structures, 1994. **5**: p. 772-775.

83. Li, W.H., et al., *Experimental Investigation of Creep and Recovery Behaviors of Magnetorheological Fluids.* Materials Science and Engineering A - in press, 2001.

84. Li, W.H., G. Chen, and S.H. Yeo, *Viscoelastic Properties of MR fluids.* Smart Materials & Structures, 1999. **8**(4): p. 460-468.

85. Potanin, A.A. and R.J. Hirko, *Probing Magnetic Paints Through Magnetorheological and Susceptibility Measurements.* Journal of Rheology, 1998. **42**(5): p. 1249-1267.

86. Jolly, M.R. and J.D. Carlson. *Controllable Squeeze Film Damping using Magnetorheological Fluid*. in *ACTUATORS 96, 5th International Conference on New Actuators*. 1996. Brmen, Germany.

87. Janocha, H. and B. Rech. *Measurements of MR-Fluids using Rotational Viscometers*. in *Rheology 94*. 1994.

88. Yoshimura, A. and R.K. Prud'homme, *Wall Slip Corrections for Couette and Parallel Disk Viscometers.* Journal of Rheology, 1988. **32**(1): p. 53-67.

89. Gans, B.J.d., C. Blom, and J. Mellema. *The Development of Magnetorheometer and its Uses in Investigating Ferrofluids*. in *ER Fluids-MR Suspensions and Their Applications*. 1997. Japan.

90. Dang, A., L. Ooi, and J. Fales, *Yield Stress Measurements of Magnetorheological Fluids in Tubes.* Ind. Eng. Chem. Res., 2000. **39**: p. 2269-2274.

91. Acrivos, A., *Bingham Award Lecture: Shear-induced Particle Diffusion in Concentrated Suspensions of Noncolloidal Particles.* Journal of Rheology, 1995. **39**(5): p. 813-826.

92. Barnes, H.A., Journal of Non-Newtonian Fluid Mechanics, 1995. **56**: p. 221-251.

93. Hiemenz, P.C., *Principle of Colloid and Surface Chemistry*. Undergraduate Chemistry, ed. J.J. Lagowski. Vol. 4. 1986, New York: Marcel Dekker, Inc..

94. Rankin, P.J., A.T. Horvarth, and D.J. Klingenberg, *Magnetorheology in Viscoplastic Media.* Rheological Acta, 1999. **38**(471-477).

95. Svoboda , J., *Magnetic Flocculation and Treatment of Fine Weakly Magnetic Minerals.* IEEE Tran. on Magnetics, 1982. **Mag-18**(2): p. 796-801.

96. Chantrell, R.W., et al., *Agglomerate Formation in a Magnetic Fluid.* Journal of Applied Physics, 1982. **53**(3): p. 2742 - 2744.

97. Ozaki, M., et al., *Agglomeration in Colloidal Hematite Dispersions Due to Weak Magnetic Interactions.* Journal of Colloid and Interface Science, 1988. **126**(1): p. 212 - 219.

98. Ozaki, M., et al., *Reversible Ordered Agglomeration of Hematite Particles Due to Weak Magnetic Interactions.* Journal of Colloid and Interface Science, 1986. **113**(1): p. 76 - 80.

99. Rosensweig, R.E., *Magnetic Fluids: Phenomena and Process Applications.* Chemical Engineering Progress, 1989: p. 53-61.

100. Inoue, H., H. Fukke, and M. Katsumoto, *Effect of Polymer Adsorbed Layer on Magnetic Particle Dispersion.* IEEE Transactions on Magnetics, 1990. **26**(1): p. 75 - 76.

101. Foister, R.T., *Stabilized Magnetorheological Fluid Compositions*. 2000, General Motors Corporation: U.S. p. 9.

102. Homola, A.M., et al., *Novel Magnetic Dispersions Using Silica Stabilized Particles.* IEEE Transactions on Magnetics, 1986. **22**(5): p. 716 - 719.

103. Phulé, P.P., *Magnetorheological Fluid*, in *United States Patent*. 1999, University of Pittsburgh: USA.

104. Kordonsky, W.I. and S.A. Demchuck, *Additional Magnetic Dispersed Phase Improves the MR-Fluid Properties.* Journal of Intelligent Material Systems and Structures, 1996. **7**: p. 522-525.

105. Kormann, C., E. Schwab, and M. Laun, *Magnetorheological Fluid*. 1996, BASF Aktiengesellschaft: United States.

106. Halliday, D. and R. Resnick, *Fundamentals of Physics*. Third Edition Extended ed. 1988, New York: John Wiley and Sons, Inc.

107. Plazek, D.J., *Magnetic Bearing Torsional Creep Apparatus.* Journal of Polymer Science: Part A-2, 1968. **6**: p. 621-638.

108. Gorodkin, S.R., et al., *A Method and Device for Measurement of a Sedimentation Constant of Magnetorheological Fluids.* Review of Scientific Instruments, 2000. **71**(6): p. 2476-2480.

109. Kormann, C., M. Laun, and G. Klett. *Magnetorheological Fluids with Nano-sized Particles for Fast Damping Systems*. in *Actuator 94*. 1996. Ludwigshafen, Germany.

110. Toy, M.L., L.E. Scriven, and C.W. Macosko, *Nonhomogeneities in Couette Flow for Ferrite Suspensions.* Journal of Rheology, 1991. **35**(5): p. 887-899.

111. Gadala-Maria, F.a.A., A., *Shear-Induced Structure in a Concentrated Suspension of Solid Spheres.* Journal of Rheology, 1980. **24**(6): p. 799-814.

112. Bombard, A.J. and I. Joekes. *Temperature Effect on the Magnetorheological Properties of MRF-132LD Suspensions*. in *to be published in Electro-Rheological Fluids and Magneto-Rheological Suspensions*. 2001. Niece, France.

113. Markovitz, H., Lecture Notes, Carnegie Mellon University

114. Coussot, P., et al., *Viscosity Bifurcation in Thixotropic, Yielding Fluids.* Journal of Rheology, 2002. **46**(3): p. 573-589.

115. Kishimoto M., K.S., Amemiya M., *Morphology and magnetic properties of the iron oxide layer formed on iron acicular particles.* IEEE Transactions on Magnetics, 1986. 22(5): p. 732-734.